Design of Interference Canceller for Large Delay Spread Channel in Orthogonal Frequency Division Multiplexing Systems

A Dissertation
Presented in Partial Fulfillment of the Requirements
for the Degree of Doctor of Philosophy in Engineering
in the Graduate School of Keio University

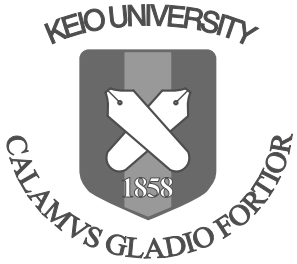

JunHwan Lee

Keio University
September 2009

Contents

List of Figures

List of Tables

Abstract

The introduction of OFDM technology has led to the dramatic transition from voice to multimedia service in applications such as digital television and audio broadcasting, wireless networking and broadband internet access ; IEEE 802.11a, g, n and HIPERLAN/2 for WLAN, DVB-H, T-DMB, and MediaFLO for the terrestrial mobile TV, 3gpp LTE/LTE-Adv. for the cellular communication, BWA, WiMAX for the fixed WMAN, MBWA, WiBro for the mobile WMAN, UWB (IEEE 802.15.3a) for WPAN and so on. Compared with single carrier scheme, the main characteristics of OFDM with a long symbol length inserted by a guard interval (GI) are the robustness to the wireless channel with a long multipath delay, and make it possible to implement an equalizer with a simple structure since the increased symbol duration satisfies the fading channel of each subcarrier to be flat. In addition, the flexible management of the subcarriers such as Adaptive Modulation and Coding (AMC) is attractive in OFDM. In particular, OFDM facilitates the design of single frequency network (SFN), where more than single base station can send the same signal simultaneously at the same frequency resulting in the macro diversity. In contrast to the above-mentioned advantages, the unacceptable performance degradation of OFDM is inevitable due to Doppler shift, frequency and time synchronization, high peak-to-average-power ratio (PARP). Among the impairments, particularly the large channel delay over GI causes an irreducible performance error bound due to inter-symbol interference (ISI) and inter-carrier interference (ICI). Even if the long GI and OFDM symbol length to cover the large channel delay can be a countermeasure, those are not the favorable solutions considering the frequency efficiency, power, and fast fading, respectively. Hence, the adoption of the interference canceller having immunity against ISI and ICI is needed to prevent the system performance from being degraded by those detrimental effects.

In this dissertation, we mainly focus on the equalizer design so called the interference canceller which is robust to the large delay spread channel whose multipath exceeds GI. The proposals in this thesis are twofold. One is the Canceller Operation Before Channel Decoding (COBD) and the other is the Canceller Operation After and Before Channel Decoding (COABD). Both cancellers are based on the Double Window Cancellation and Combining (DWCC) by taking a different look at the received OFDM symbol interfered by adjacent OFDM symbols, and also the intent of the proposed cancellers is to readily combine an entire OFDM symbol duration

delayed by multipath as a canceller processing window (PW).

In Chapter 1 the historical overview of OFDM technology and the trends of the forthcoming cellular based network are briefly introduced. In addition, the impairments, which severely degrade the performance in OFDM system, are also explained. In Chapter 2 the basic operations of OFDM including signal generation and signal detection are explained, and the motivation of this doctoral thesis is described by addressing the problems due to the impairments caused by the wireless channel.

In Chapter 2 the analysis on ISI and ICI under the assumed channel conditions is presented, and the characteristics of interferences are investigated. In addition, the criterion of designing the interference canceller is described with respect to the error performance, the computational complexity, and the latency. For the explanation of the algorithm features of the cancellers, the previously proposed cancellers are also discussed.

In Chapter 3 the two canceller algorithms of DWCC-I (Symbol-wise) and DWCC-II (Group-wise) based on double window cancellation and combining are introduced, and the characteristics of both schemes are also described. In the meantime, it is addressed how to apply channel equalizing methods in initial and iterative canceller operations. Finally, for the performance verification of the proposed schemes, each scheme is evaluated in the turbo coded OFDM for low (QPSK) and high level modulations (16QAM, 64QAM) and compared with the conventional canceller with respect to the bit error rate (BER) performance and computational complexity.

In Chapter 4 to cope with the drawback in DWCCs where the tentative symbol detection is still susceptible to deep fading, the COABD type of canceller, named TE-DWCC, is proposed. For the amelioration of the efficiency of TE-DWCC, the optimal incorporating method of DWCC and turbo equalization is investigated by varying the iterative cancellation procedure between DWCC and channel decoder and the decision feedback type such as hard decision feedback (HDF) or soft decision feedback (SDF). Finally, by changing interference level, code rate, and decision feedback type, the packet error performance (PER) of TE-DWCC is compared with the conventional canceller that adopts turbo equalization in the exponentially distributed slow fading channel.

Finally, Chapter 5 concludes the thesis.

Chapter 1

General Introduction

The principle of Orthogonal Frequency Division Multiplexing technology dates back nearly 50 years ago [1.1] [1.2] [1.3]. First promoted in the early 1990s for wireless LAN, OFDM is used in many wireless applications including Wi-Fi, digital radio, TV broadcasting, and nowadays it has become a powerful transmission technology to meet the current needs for QoS based multimedia services in wireless applications. In light of increasing bandwidth demands in future wireless service and satisfying high data rate services over 100 Mbps, it is no exaggeration to say that OFDM technology with high frequency efficiency in a severe wireless channel environment would be the promising technology in existing or forthcoming wireless applications [1.4] [1.5] [1.6].

1.1 General Overview on Wireless Communications

It was in 1887 that radio wave was first detected by Heinrich Hertz using a Spark Gap Transmitter. When he was asked about the impact it could have to the future, he claimed it would be of no importance. It was in 1893 when Nikola Tesla transmitted radio waves. In 1897 Gugleilmo Marconi was awarded patent for improving the transmission of electrical impulses. A year later, in 1898, Tesla awed the ignorant by demonstrating a remote-controlled boat which, his audience thought, was moved by his mind. Reginald Fessenden aired his voice through AM (amplitude modulation) which was heard over the North Atlantic in 1906. In 1913, Harold Arnold created the first amplifying vacuum tube which was used on long line transmission telephone lines. 1915 was when the first transatlantic transmission achieved by ATT from Arlington to Paris and the Eiffel Tower in France used to hold the receiving antenna. Shortwave radio was developed in 1921 and 10 years later, FM (frequency modulation) which was the key to transmit digital information across RF (radio frequency). In 1972, ethernet was created. In 1982, GSM group was formed to go digital on all its cellular systems. In 1989 GSM Technical details worked out and planned a narrowband time division multiple

access (TDMA). In 1990, L-band radio (digital radio) was demonstrated. The Global Positioning System (GPS) operates in the L-band. The first GSM specification was released. The first GSM call was made in Finland, March 1991 on the Radiolinja Network which was given GSM license in 1990. In April 1992, the first non-European network was launched in Australia. In 1997, IEEE 802.11 standard was created, also known as Wi-Fi. The Bluetooth Special Interest Group (SIG) was formed in September 1998 by IBM, Intel, Nokia, Ericsson and Toshiba. In 2000, the first consumer Bluetooth product was released by Ericsson. December 2001, WiMax was created. In 2004, WiMAX much more scalable than Wi-Fi. Today, 3.3 Billion subscriptions are connected worldwide with the GSM family of technologies - GSM, GPRS, EDGE and UMTS/HSPA [1.6] [1.7].

The rapid development of wireless communication technologies, as well as the market opportunities offered to operators by fast spectrum access regulations around the world requires a huge effort for the deployment of new wireless networks, the expansion of existing ones, and optimization of network resources. In particular, the effort on the swift transfer and share of the information has been unceasingly pursued through the variety of wired and wireless transmission media, and the recent developments of the wireless communication technologies and services are leading the rapid market expansion. After all, we can not imagine the world without communication. Cellular wireless networks such as 3G/4G and WLAN/WMAN play an important role in broadband communications and ubiquitous computing infrastructure. Cellular networks are the most promising technologies to provide wide area outdoor coverage as they have sophisticated mobility management and large coverage areas. Meanwhile, WLANs can complement 3G/4G cellular networks, as they can provide cheap high bit rate data services at hotspots. Finally, WMANs, known as WiMAX, mobile-WiMAX (WiBro) are expected to gain much interest for broadband fixed and mobile access [1.8] [1.9].

The first commercial cellular service, known as Nordic Mobile Telephone (NMT) was launched in 1981. In 1983, Advanced Mobile Phone System (AMPS) was commercialized in US and it ignited several other services all over the world. These have been called as the first generation (1G) system and the analog system since voice signal were modulated in an analog way. After then, the second generation (2G) system, based on the digital was emerged. The 2G system basically targeted for the voice service and partly supported the low rate data services. The representative 2G systems are GSM in Europe, and cdmaOne, IS-136 in America. Since 2G systems, the system providing the packet switched radio connection has appeared on the stage, and those were called as 2.5G systems. The current 3G system has been designed mainly for the multimedia services; WCDMA standardized by 3rd Generation Partnership Project (3GPP), cdma2000 evolved from cdmaOne, EDGE from TDMA and GSM. The 3G systems, known as IMT-2000 intended for global roaming and the data rate of 144 kbps and 2 Mbps in moving and fixed environment, respectively. In the meantime, for the incessant requirement of the wireless multimedia services similarly to wired broadband network, 3GPP has started the

Table 1.1: Spectral efficiencies for LTE-Advanced system.

	Downlink			Uplink	
	(bps/s/Hz/cell)			(bps/s/Hz/cell)	
Peak spectral efficiency	30			15	
Antenna configuration	2x2	4x2	4x4	1x2	2x4
Average spectral efficiency (case-1)	2.4	2.6	3.7	1.2	2.0
Cell edge user spectral efficiency	0.07	0.09	0.12	0.04	0.07

standard of 3G long-term evolution where mobile communication technology aims at low latency and high data rate with increased coverage. Accordingly, the 3G LTE has undertaken from the end of 2004 to now. In the meantime, the standard of 3G LTE-Advanced has started from the beginning of 2008. The requirements of LTE-Advanced, requested by most operators, are

- Lower CAPEX/OPEX
- Flexible and wider spectrum usage
- Performance target: NGMN recommendation
- Self Organizing/Optimizing Network (SON)
- Backward compatibility
- Enhanced cell average and cell edge performance

LTE-Advanced is one of powerful candidates for IMT-Advanced standard of ITU-R and is widely supported by many operators. The target for peak data rate is greater than 500 Mbps for uplink and 1Gbps for downlink, and 15 and 30 b/Hz/s for spectrum efficiency of uplink and downlink. For details, Table 1.1 summarizes the final system requirements for LTE-Advanced which was determined in June 2008 [1.10] [1.11] [1.12].

3G technologies are primarily based on the concept of the wide area network. Therefore, the large portions of the research focus on implementing the system that is faster, higher frequency efficiency, more capacity. Accordingly, the current network technology may not be sufficient to meet needs of future high-performance applications like multi-media, full-motion video, wireless teleconferencing. We need a network technology that extends 3G capacity by an order of magnitude. In addition, it should not be overlooked the interoperability across heterogeneous networks [1.13] [1.14].

1.2 Trends on OFDM Based 4G Mobile Wireless Communication

1.2.1 General Cellular Based 4G Activity

Since the current 3G wireless communication systems adopting single carrier transmission technology is hard to accommodate the high data rate transmission, Orthogonal Frequency Division Multiplexing (OFDM) technology rather insensitive to the wireless channel delay and impulse noise effect is paid much attention. In a wireless communication OFDM that simultaneously carries a number of subcarriers bearing low data rate data symbols is a promising transmission technology to increase capacity with a limited radio resource. Moreover, the advantages of OFDM can be found in a receiver structure, which can be implemented with a simple equalizer what so called one-tap frequency domain equalizer (FDE) by inserting a guard interval (GI) and in the flexible resource management of subcarriers with Adaptive Modulation and Coding (AMC), and so on. Owing to the abovementioned characteristics of OFDM, OFDM is considered as an appropriate transmission technology for broadband communications. In particular, the adoption of OFDM has been very attractive to the terrestrial broadcasting services known as Single Frequency Network (SFN) such as Integrated Services Digital Broadcasting (ISDB) in Japan [1.15], Digital Audio Broadcasting (DVB) and Digital Terrestrial Television Broadcasting (DTTB) in Europe [1.16], and is also a candidate to the cooperative communication field. Furthermore, it is also adopted for Wireless Local Area Network and Wideband Wireless Access Network (BWA); IEEE 802.11a/b/g/n for WLAN, BWA, MBWA, WiMAX, WiBro for BWA. Consequently, OFDM has become a key transmission technology in almost every wireless communication field [1.17] [1.18] [1.19].

The 4G technology preceded by 3G is defined as Systems Beyond IMT-2000 (SBI2K) by International Telecommunication Union (ITU) [1.20]. It should be possible for 4G to seamlessly incorporate PSTN, Satellite, Wireless LAN, and Internet Service and to support the increased transmission rate as much as tens or hundreds of achievable transmission rate in 3G. Accordingly, 4G technology premises the improved system design in the wireless communication environment by enabling the organic interoperability among mobile communication, wireless access, and wired broadband systems. However, 4G is not a totally separate system from the already existing communication systems. In other words, 4G is defined by ameliorated 3G being emphasized on the efficiency in every aspect such as resource utilization, system/service convergence. Figure 1.1 shows the evolution roadmap for the wireless communications [1.21], and Figure 1.2 shows the prospective scenario of 4G wireless communication networks where the multiple terminals such as cell phone, smart phones, PDA, PMP/Navigator, DMB, MP-3, Digital Camera, Game Devices coexist in multiple radios and multiple networks assuming the seamless

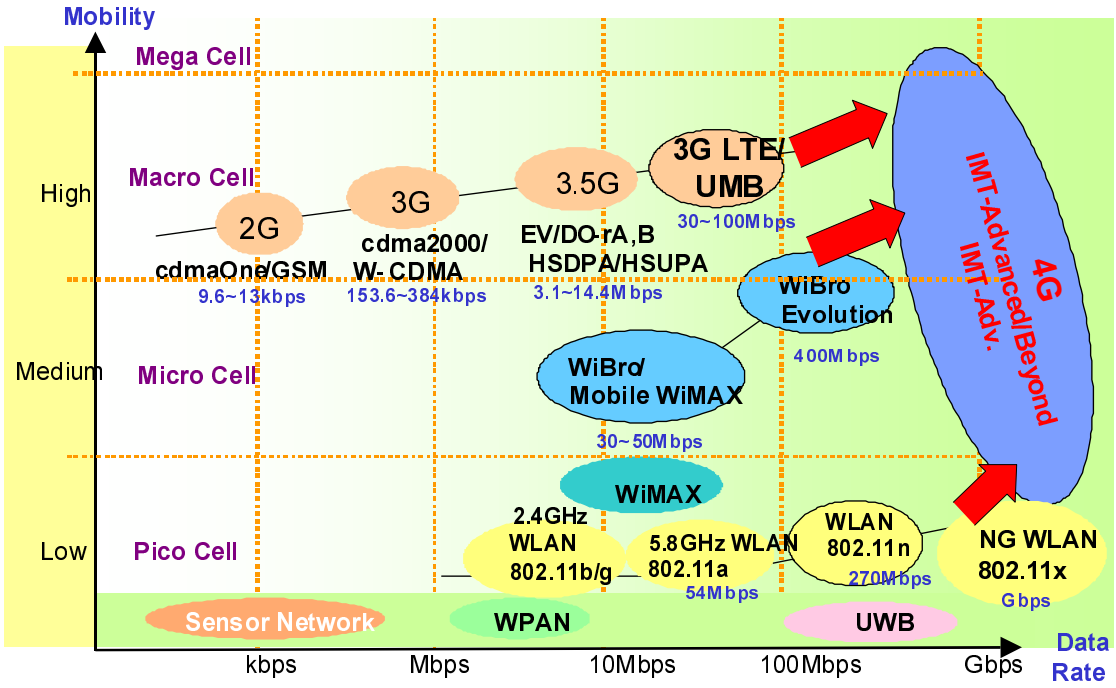

Figure 1.1: Roadmap for the evolving wireless communications.

mobility and ubiquitous access in all IP basis.

International Mobile Telecommunications-Advanced (IMT-Advanced) systems are mobile systems that include the new capabilities of IMT that go beyond those of IMT-2000. Such systems provide access to a wide range of telecommunication services including advanced mobile services, supported by mobile and fixed networks, which are increasingly packet-based. IMT-Advanced systems support low to high mobility applications and a wide range of data rates in accordance with user and service demands in multiple user environments. IMT Advanced also has capabilities for high-quality multimedia applications within a wide range of services and platforms providing a significant improvement in performance and quality of service. The key features of IMT-Advanced are:

- a high degree of commonality of functionality worldwide while retaining the flexibility to support a wide range of services and applications in a cost efficient manner
- compatibility of services within IMT and with fixed networks
- capability of interworking with other radio access systems
- high-quality mobile services

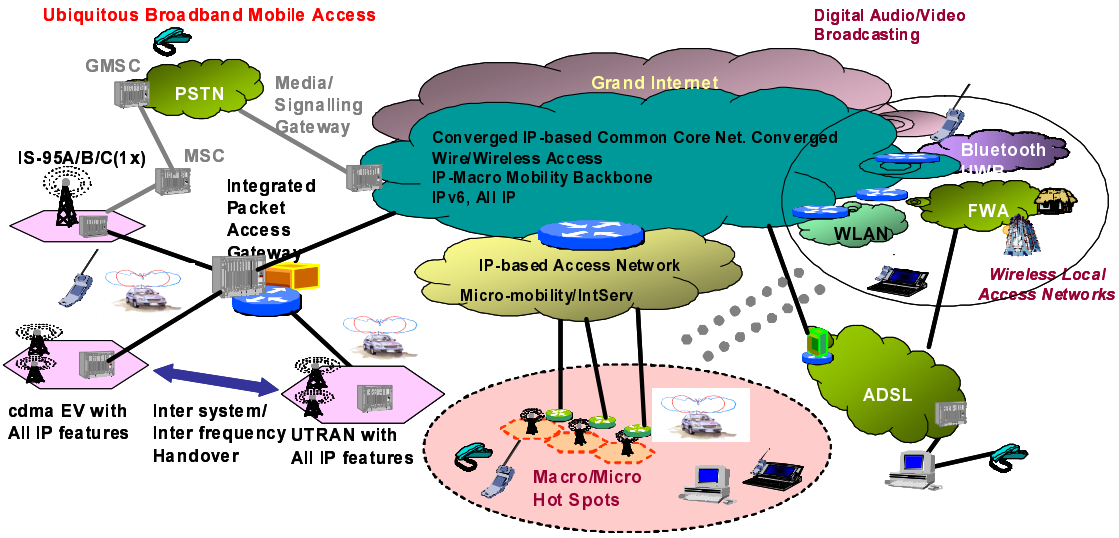

Figure 1.2: Multiple access environments: Heterogeneoity and Complexity-Ubiquity.

Table 1.2: Spectral efficiencies for IMT-Advanced system

	Downlink (bit/s/Hz/cell)	Uplink (bit/s/Hz/cell)
Peak spectral efficiency	15	6.75
Average spectral efficiency (Indoor/Microcellular/ Urban/High speed)	3 / 2.6 / 2.2 / 1.1	2.25 / 1.8 / 1.4 / 0.7
Cell edge user spectral efficiency (Indoor/Microcellular/ Urban/High speed)	0.1 / 0.075 / 0.06 / 0.04	0.07 / 0.05 / 0.03 / 0.015

- user equipment suitable for worldwide use
- user-friendly applications, services and equipment
- worldwide roaming capability
- enhanced peak data rates to support advanced services and applications (100 Mbit/s for high and 1 Gbit/s for low mobility were established as targets for research);

These features enable IMT-Advanced to address evolving user needs. The capabilities of IMT-Advanced systems are being continuously enhanced in line with user trends and technology developments. Consideration of every variation

to encompass all situations is therefore not possible; nonetheless the work of the ITU-R has been to determine a representative view of IMT-Advanced consistent with the process defined in Resolution ITU-R 57, "Principles for the process of development of IMT-Advanced" and the minimum requirements for cell average, peak, and cell edge user spectral efficiency are summarized in Table 1.2 [1.20].

1.2.2 New Paradigm for Cellular Based 4G Activity

The currently emerging new research trends in wireless communications are focusing on increasing capacity, constructing the human friendly communication networks, and compensating the reduced cell coverage due to the frequency policy. The following representative three issues toward the intelligent cellular based 4G activity are bringing the research paradigm change for the 4G wireless technologies.

1. Increased Power Consumption Due to the Frequency Shift

   The World Radio-communication Conference 2007 (WRC-07) concluded its deliberations with the adoption of an international treaty to meet the global demand for radio-frequency spectrum. Over 2800 delegates representing 164 Member States and 104 Observers attended the four-week Conference, marked by intense negotiations on the future of wireless communications. Rapid technological developments and growth in the information and communication technology (ICT) sector have fueled the demand for spectrum. The international treaty, known as Radio Regulations governing the use of the radio-frequency spectrum and satellite orbits were revised and updated by WRC-07 to achieve the global connectivity goals of the 21st Century. WRC-07 addressed some 30 agenda items related to almost all terrestrial and space radio services and applications. These included future generations of mobile telephony, aeronautical telemetry and telecommand systems, satellite services including meteorological applications, maritime distress and safety signals, digital broadcasting, and the use of radio in the prediction and detection of natural disasters. From the meeting four spectrum bands were determined as a candidate for use by International Mobile Telecommunications (IMT) [1.22].

   - 20 MHz band : 450 to 470 MHz
   - 108 MHz band : 698 to 806 MHz
   - 100 MHz band : 2.3 to 2.4 GHz
   - 200 MHz band : 3.4 to 3.6 GHz

   In the meantime, over a hundred of countries have expressed for the use of 3.4 GHz frequency band as IMT frequency band. As the carrier center

frequency is getting higher, the increased transmit power for high data rate transmission is required to retain the same cell coverage as the present cellular system. Otherwise, the present cell coverage should be reduced to support the same quality of service as in the present cellular network. After all, the change of fundamental paradigm for 4G network is necessary [1.23].

2. Increased Demands for Green Wireless Network

   The transmitted data traffic increases approximately by a factor of 10 every 5 years, which corresponds to an increase of the associated energy consumption by approximately 16 ~ 20 % per year. Currently, 3 % of the world-wide energy is consumed by Information, Communications Technology (ICT) infrastructure which causes about 2 % of the world-wide CO2 emissions (which is comparable to the world-wide CO2 emission by airplanes or one quarter of the world-wide CO2 emission by cars) [1.24]. As an example, in 2005 data centers consumed about 1.2 % of all electricity in the US at a cost of about $2.7 billion. Therefore, if this energy consumption is doubled every 5 years, serious problems will arise. Therefore, lowering energy consumption of future wireless radio systems is demanding greater attention. The activities for Green Radio are actively organized in Europe and the representative projects are VCE, Green Radio in Wireless at KTH, and Opera-Net projects [1.25] [1.26] [1.27]. Another challenge of future wireless radio systems is to globally reduce the electromagnetic radiation levels to have a better coexistence of wireless system, i.e., less interference as well as a reduced human exposure to radiations. In addition, there is also an effort to reduce CAPEX and OPEX since operator expectations to deliver mobile broadband internet experience to the user at a low CAPEX/OPEX, relying on flexible solutions to address a spectrum bands currently under identification.

3. Emphasis on User Centric System

   Instead of being only something that people use for task completion, communication technologies have become something that people live with, an integral part of everyone's life. In fact, their usage can not be separated from the rest of peoples' lives and examined under a microscope as an isolated object. So far, the designers of the new technology have not enough considered the world for which they are designing. Indeed, in a broader context, developing technology for technology is meaningless even for the telecom industries, since they will most likely not get paid back for their initial investments. Therefore, it appears more logical and less risky to set a goal to develop technology in order to provide new services to the user. In this aspect, the user is the main actor playing on the stage of the wireless world and he is unaware of and indifferent about the technology to use in order to get some desired service. Accordingly, understanding the user means understanding how he changes as the society around him changes

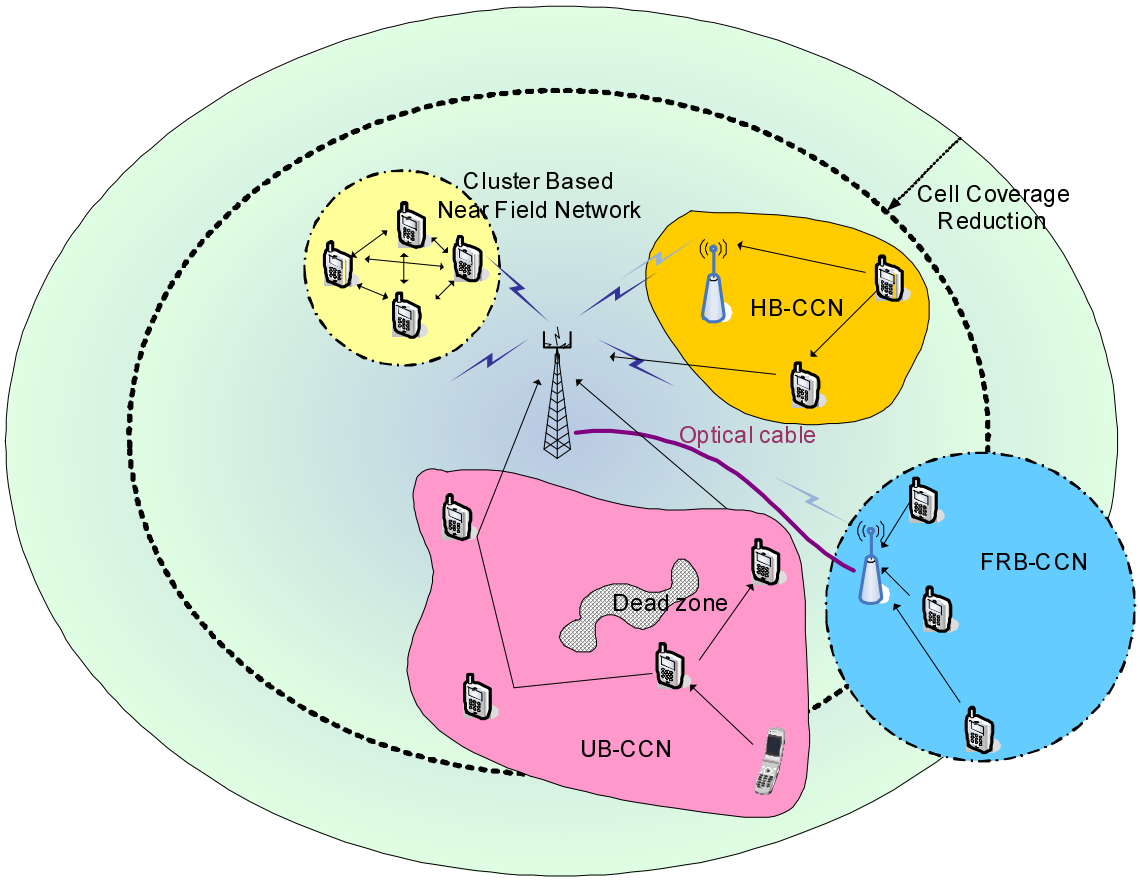

Figure 1.3: Conceptual drawing for cellular based heterogeneous cooperative communication networks.

in general, and specifically how he changes through the interaction with the products that are introduced. In particular, if technological developers start from understanding what human wants, they are more likely to accelerate evolutionary development of useful technology. Consequently, the previous concept for 4G emphasizing on techno-centric is moving toward user-centric concept. To implement the user-centric system, the key features of 4G should be re-evaluated in two-folds. The one is ”User Friendliness and User Personalization”, and the other is ”Network and Terminal Heterogeneity”, where ”User Friendliness” implies exemplifies and minimizes the interaction between applications and user thanks to the well designed transparency that allows the man and the machine to naturally interact, and ”User Personalization” refers to the way the user can configure the operational mode of his device and pre-select the content of the services chosen according to his preferences [1.28] [1.29] [1.30]. In regard of ”Network and Terminal Hetero-

geneity", the concept is not simply restricted to the vertical handover between different networks. In other words, in order for 4G to be a step ahead of 3G, it must not only provide higher data rates but also some clear and evident advantage in people's everyday life. Therefore, the success of 4G consists in the combination of network and terminal heterogeneity. Network heterogeneity guarantees ubiquitous connection and provision of common services to the user, ensuring at least the same level of Quality of Service (QoS) when passing from one network's support to another one. Moreover, due to the simultaneous availability of different networks, heterogeneous services are also provided to the user.

These needs create interdisciplinary research challenges including semiconductor technology, hardware, networks, services, and radio transmission, where schemes have to be designed that operate with a reduced transmit power and reduced radiations. To satisfy the above-mentioned needs, the current hot topics on wireless communication research considers the network configuration using the concept of the cooperative communication (CC) which has been introduced in 1971 by van der Meulen in [1.31] and a first rigorous information theoretical analysis of the relay channel has been exposed by Cover in [1.32]. The concept of CC is to look at all nodes in a cell as not a competitor but a cooperator. Depending on the cooperative network configuration, there can be three possible configurations of cooperative communication networks (CCN); Fixed relay based (FRB)-, User based (UB)-, and Hybrid based(HB)-CCNs. Figure 1.3 shows the conceptual network configuration of each cooperative communication network and it includes the envisaging cooperative network modes and the near field network in cellular based network environment. As the conventional cellular coverage is reduced by the frequency transition, it demands the new network topology by accommodating the relaying nodes instead of increasing the peak transmission power of eNB. The achievable power saving has been introduced by properly selecting the cooperative nodes [1.33] [1.34]. Besides, the one interesting point is the self organized cell, denoted by SOC in Figure 1.3, and the nodes belonging to SOC, similar to Peer-to-Peer network (P2P), can communicate each other by using a different network protocol like near field network protocols, and the research activities can be referred to [1.35].

The development of the future mobile eco-system, with the introduction of higher data rate radio access technology (RAT) can be approached in two distinct ways i.e. evolutionary and revolutionary ways. In the point of the pursuit of Green Network accompanying with the frequency policy change for 4G, the evolution towards 4G will encompass the introduction of new technology segments, including potential new releases of legacy radio access technologies or/and introduction of radically new radio access systems such as the conceptual drawing in Fig. 1.3.

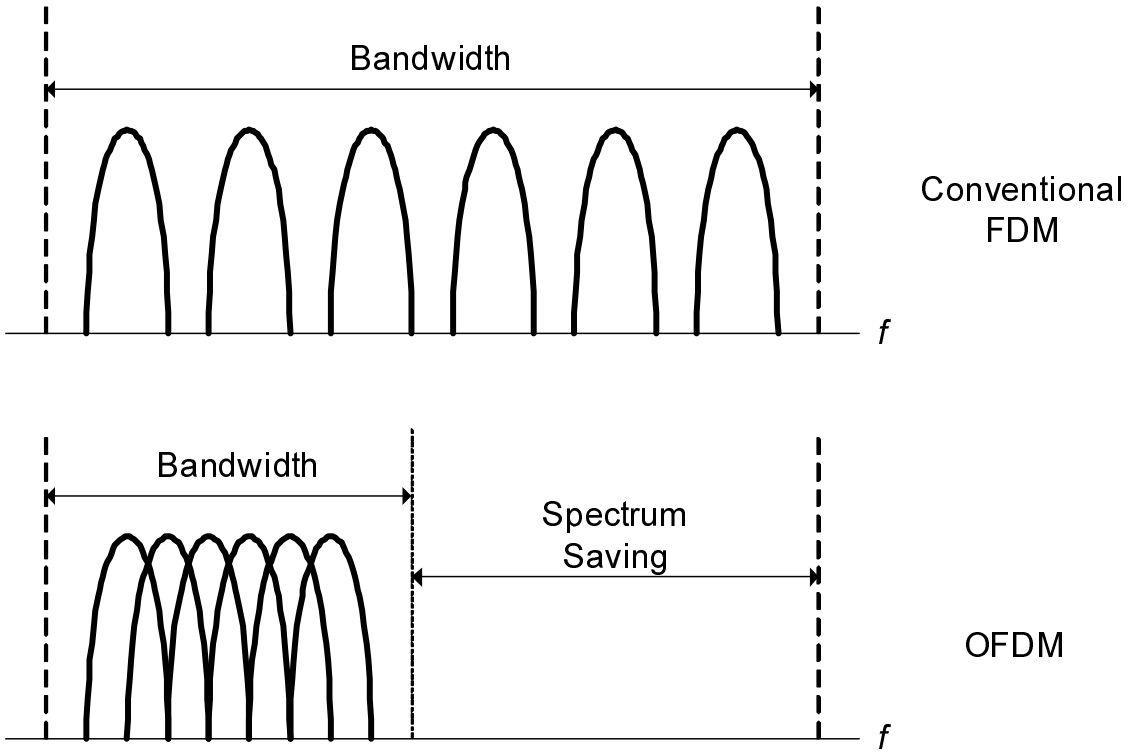

Figure 1.4: Spectrum saving in OFDM.

1.3 OFDM Technology

Orthogonal Frequency Division Multiplexing (OFDM) is well known for spectrum saving technology. As shown in Fig. 1.4 , OFDM over conventional FDM needs the reduced bandwidth for data transmission by using an orthogonal characteristic between subcarriers. This Chapter introduces the history of OFDM, and describes the baseband signal processing in both transmitter and receiver. Meanwhile, the impairments at OFDM system are addressed.

1.3.1 Brief History and Standard Activities

In mid-1960s the idea about parallel data transmission and frequency division multiplexing (FDM) was proposed, and OFDM technology was used in several high frequency military system [1.36]. In 1971 Weinstein and Ebert applied the Discrete Fourier Transform (DFT) to parallel data transmission system as part of modulation and demodulation process. In the 1980s OFDM was studied for high speed digital mobile communication and high-density recording.

In 1980 Hirosaki was firstly concerned about the impairments in OFDM system

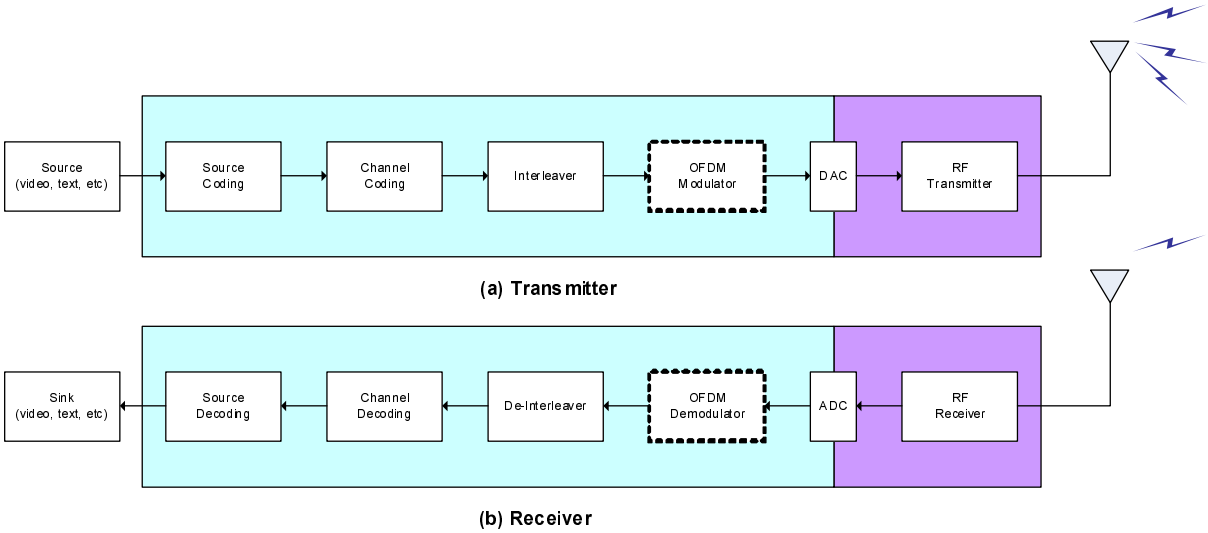

Figure 1.5: Block diagram of the coded OFDM.

and he suggested an equalization algorithm in order to suppress both inter-symbol and inter-carrier interferences caused by the channel impulse response or timing and frequency errors [1.37]. In addition, he also introduced the DFT-based implementation of Saltzburg's O-QAM OFDM system [1.38].

In the 1990s, OFDM was exploited for wideband data communications. In the following OFDM-based applications are listed.

- Mobile radio FM
- Fixed wired networks (HDSL, ADSL, VDSL)
- Digital audio broadcasting (DAB)
- Digital video broadcasting : DVB-C, DVB-S,
- High definition television (HDTV) terrestrial broadcasting : DMB (Korea), COFDM (Europe), 8-VSB (North America), BST-OFDM (Japan)
- Wireless Personal Area Network (PAN) : UWB, Bluetooth, BTSIG, MBOA, Wi-Media
- Wireless Local Area Network (LAN) : HiperLAN2 (Europe), IEEE 802.11a (US), IEEE 802.11g (US)
- Wireless Metropolitan Area Network (MAN) : WiMAX (US), WiBro (Korea), ETSI HiperMAN

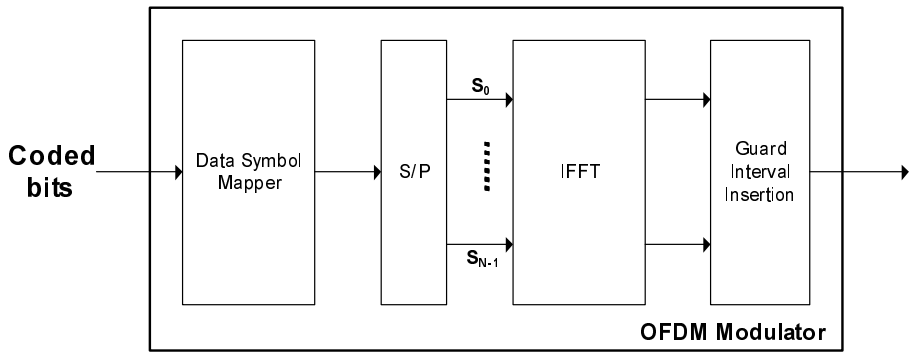

Figure 1.6: Block diagram of the OFDM modulator.

- Wide Area Network : 3GPP LTE, 3GPP LTE-Advanced, UMB

The standard activities in the list are still ongoing.

1.3.2 Baseband Signal Processing

Transmitter

The coded OFDM transmitter can be designed as shown in Fig. 1.5(a). The source bit stream is encoded by source coder for the efficiency, and the source coded bits are coded by channel encoder for the reliability. After encoding process, the coded bits are input to the OFDM modulator. The main operations in the OFDM modulator include data symbol mapping and subcarrier modulating parts. In Fig. 1.6 shows the detail operating blocks for the OFDM modulator.

The coded bits are firstly modulated by data symbol mapper, which can be lower (BSPK, QPSK) or higher modulation (16QAM, 64QAM). The serially aligned output from data symbol mapper is arranged in parallel by the S/P block. If the i^{th} data symbol vector, $\boldsymbol{S}_i$, is given through S/P block, the N-points IFFT of the channel coded i^{th} OFDM symbol vector can be expressed by (1.1).

$$x_{i,n} = \sqrt{\frac{1}{N}} \sum_{k=0}^{N-1} s_{i,k} \exp\left(j\frac{2\pi}{N}nk\right) \tag{1.1}$$

where $0 < n < N-1$. Here, the employment of IFFT implies Fig. 1.7, where the orthogonality between subcarriers follows the relationship of (1.2).

$$\frac{1}{T}\int_0^T \cos(2\pi nft)\cos(2\pi mft)\,dt = \begin{cases} m \neq n, & 0 \\ m{=}n, & 1 \end{cases} \tag{1.2}$$

Meanwhile, as an example of FFT engine, there is a reference for the performance and synthesis results in ASIC level that are dependent on the FFT size in

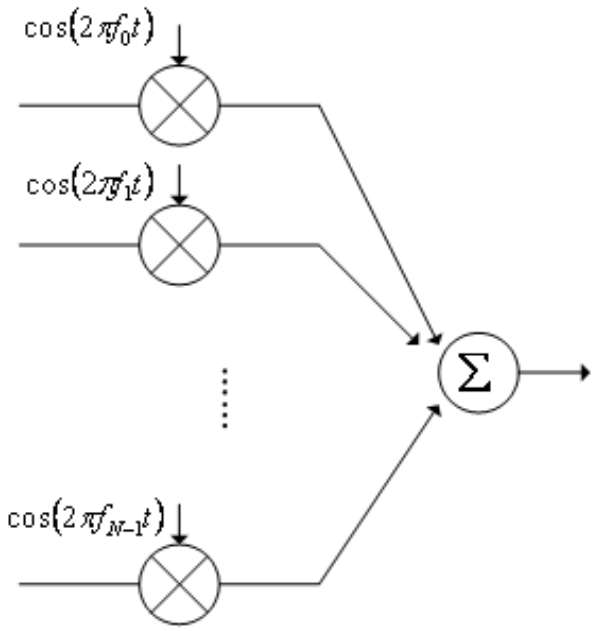

Figure 1.7: Concept of IFFT operation.

Table 1.3: Synthesis results for the FFT core.

FFT Length	With CBFP				
	128	256	512	1024	2048
Gate Count	43,727	44,957	50,105	61,767	67,344
RAM (bit)	6,124	10,592	17,504	41,848	71,544

WiBro communication system. The design of FFT processor listed in Tabs. 1.3 and 1.4 was targeted for WiBro testbed, where the CBFP stands for the "Convergent Block Floating Point" arithmetic that is compatible with the pipeline FFT structure. For more information on the status of the development of IFFT/FFT engines can be referred to [1.39].

Normally, DC does not carry data symbol because of dc offset, and the guard band to prevent the Adjacent Channel Interference (ACI) is considered. Finally, the guard interval (GI) is inserted and its duration depends on the cell radius which is directly related to the maximum wireless channel delay. The reason for inserting GI is to prevent the orthogonality from being destroyed by the wireless channel delay. The discrete IFFTed output is converted into analog with Digital-to-Analog Converter (DAC) and the converted signal is radiated through RF end.

Table 1.4: Performance results for the FFT core (∗Operating Condition: 2.5 V at 50 MHz, Input bit(12 bits), Output bit (16 bits), ∗Target Library: 0.25 um Standard Cell Library).

FFT Length		Latency	Max. Delay	Computation Time
with CBFP	128	186 cycles	11.4 ns	1.9 us
	256	315 cycles	11.4 ns	3.8 us
	512	574 cycles	11.4 ns	7.7 us
	1024	1,217 cycles	11.4 ns	15.4 us
	2048	2,244 cycles	11.4 ns	30.7 us

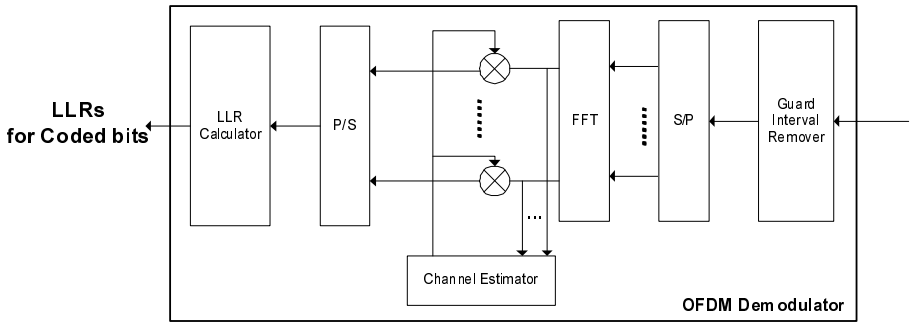

Figure 1.8: Block diagram of the OFDM demodulator.

Receiver

From Fig. 1.5(b), the main operation of OFDM receiver is performed in an OFDM demodulation block while the others oppositely correspond to the individual blocks at the transmitter. The OFDM demodulation block includes wireless channel estimation and channel compensation blocks as shown in Fig. 1.8. The channel estimation, as it implies, is to estimate the wireless channel variation which the transmit packet goes through. If the wireless channel is expressed by (1.3), taking FFT to (1.3) provides the channel distortion, $H_{i,k}$, in each subcarrier. Therefore, it is the channel compensation that is to eliminate the channel distortion with (1.4).

$$h_{i,n} = \sum_{l=0}^{L-1} \beta_{i,l} \delta(n-l) \tag{1.3}$$

$$H_{i,k} = \sum_{l=0}^{L-1} \beta_{i,l} \exp\left(-j2\pi lk/N\right) \tag{1.4}$$

In OFDM the effects of frequency-selective channel conditions, for example fading caused by multipath propagation, can be considered as constant (flat) over

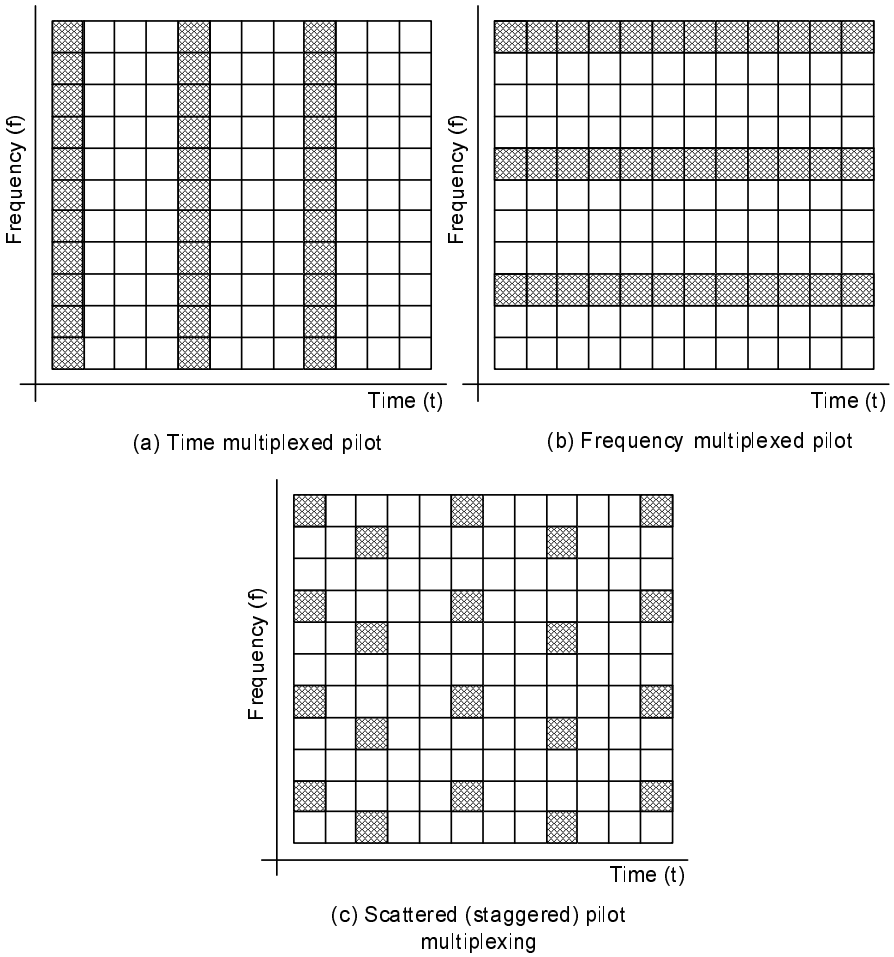

Figure 1.9: Pilot multiplexing methods depending on wireless channel environments.

an OFDM sub-channel if the sub-channel is sufficiently narrow-banded, i.e. if the number of sub-channels is sufficiently large. This makes equalization far simpler at the receiver in OFDM in comparison to conventional single-carrier modulation. The equalizer only has to multiply each detected sub-carrier (each Fourier coefficient) by a constant complex number, or a rarely changed value.

In general, the channel estimation is performed with the pilot symbols inserted in a packet, and there are time multiplexed, frequency-multiplexed, and scattered (staggered) pilot multiplexing methods as shown in Fig. 1.9. The individual multiplexing method depends on the characteristic of the wireless channel environments. In other words, time multiplexed pilot is suitable for the slowly fading channel with severe frequency selectivity, while frequency multiplexed pilot is suitable for rather fastly fading channel with less selectivity. Finally, scattered multiplexing is hybrid type of time and frequency multiplexing methods and normally

Figure 1.10: Wireless channel environment.

scattered multiplexing method is being adopted in broadcasting services [1.40].

1.4 Research Background

While the OFDM technology has the advantages of saving the spectrum and simplifying the receiver structure, the disadvantages of OFDM technology prevents the OFDM system from achieving the high data rate transmission through the efficient resource usage. In this subchapter the problems that OFDM systems are confronted with, are are illuminated, and finally the focused research topic in this thesis is described. Before proceeding the problem statements, the features of broadband wireless channel environment are briefly introduced since the wireless channel distortions are the key issues to be coped with.

1.4.1 Wireless Mobile Channel

The performance of mobile wireless communications is always hindered by the mobile radio channel between the transmitter and the receiver. Figure 1.10 shows the wireless communication link surrounded by the artificial or natural wireless channel environments. Since the radio wave experiences the reflection, diffraction, diffusion, and refraction by the obstacles surrounded by building, mountains, foliage, and so on, the transmit sinusoidal signals are constructively or destructively

summed at the receiver. In addition, the relative mobility between the transmitter and the receiver brings about the Doppler effect, which critically deteriorates the performance of OFDM systems. The Doppler frequency shift is caused by the mobile speed and the angle between the radio wave and mobile moving directions, and the Doppler shift, f_d, is calculated by (1.5).

$$f_d = \frac{\nu}{\lambda} \tag{1.5}$$

where ν and λ denote wavelength and velocity, respectively. In this wireless channel condition, the transmit signal is influenced by the small scale fading and the large scale fading. The former is the short term channel variation due to the constructive and destructive ways of the transmit signals, and the latter implies the long term channel variation such as pathloss and shadowing. In addition, the wireless channel is expressed by frequency selective and time selective channels depending on the propagation delay and the mobility where the each feature also defines the coherent frequency and coherent time, respectively. In other words, because the 'coherent' means 'constant', the coherent frequency and time implies the invariant frequency region and invariant time duration of the channel. Generally, the coherent frequency and time can be obtained by (1.6) and (1.7), respectively.

$$C_{freq} = \frac{1}{\alpha\sigma_\tau} \tag{1.6}$$

where σ_τ denotes the rms delay spread and α is approximately set to 50 at 0.9 of the frequency correlation.

$$C_{time} = \frac{1}{\beta f_d} \tag{1.7}$$

where f_d is Doppler frequency and β is the scaling parameter whose value is important parameter to decide the Transmit Time Interval (TTI) that is equal to the packet length. In Fig. the above-mentioned definitions are shown.

Standard Activities

There are several channel models introduced in standards bodies like 3GPP/3GPP2, IEEE 802.xx for various channel environments e.g. macrocellular, microcellular. In cellular standards a combined Spatial Channel Model (SCM) ad-hoc group from 3GPP and 3GPP2 has studied. The goal of this effort was to enable fair comparisons of multiple-antenna proposals and algorithms in standards. Unlikely the link-level simulation, the system-level simulation was the main concern, and the link-level parameters are only used for the calibration purpose. In the following the representative channel models are summarized.

- SCM : SCM is the output of joint 3GPP-3GPP2 SCM AHG, and is applicable to outdoor MIMO channel (CDMA) with 5 MHz BW at 2GHz. The model is Geometric or Ray-based mode based on stochastic modeling of scatters. The applicable scenarios are Suburban macro, Urban macro, Urban micro, and Urban micro in LOS condition. The used pathloss model is COST 231 Hata and COST 231 Walfish-Ikegami for Macro and Micro cells, respectively.

- SCME : SCME is the first channel model for B3G systems at WP5 WINNER project and it is the extension of 3GPP SCM. The channel model is applicable to the system operating at up to 100 MHz BW at 2 to 5 GHz and the pathloss model is COST 231 Walfish-Ikegami for all scenarios.

- WINNER-I : WINNER-I is generic channel model based on measurements and literature. The applicable scenarios are larger than those of SCM/SCME including indoor outdoor scenarios. The model can also be used for evaluating indoor and outdoor hotspot. The applicable systems are the same as SCME. The pathloss model uses measurement based models conducted in 5.2 GHz.

- WINNER-II: The WINNER-II is similar to WINNER-I while it includes further extended scenarios than those of WINNER-I.

For the details, refer to [1.41] for SCM, [1.42] for SCME, [1.43] for WINNER-I, [1.44] for WINNER-II.

1.4.2 Impairments in OFDM

The effects of common signal impairments using single-carrier modulation formats are generally well understood by system designers. The effects of these same impairments on an OFDM signal, however, can be quite different.

This simplest way to describe an OFDM signal is as a set of closely spaced frequency-division multiplexed (FDM) carriers. While this is a good starting point for those unfamiliar with the technology, it falls short as a model for analyzing the effects of signal impairments. The reason it falls short is that the carriers are more than closely spaced; they are heavily overlapped. In a perfect OFDM signal, the orthogonality property prevents interference between overlapping carriers. This is different form the FDM systems we are all familiar with. In FDM systems, any overlap in the spectrums of adjacent signals will result in interference. In OFDM systems, the carriers will interfere with each other only if there is a loss of orthogonality. So long as orthogonality can be maintained, the carriers can be heavily overlapped, allowing increased spectral efficiency.

The impairments in OFDM system are originated from frequency offset due to carrier mismatch and Doppler frequency shift, I/Q imbalance, and finally from the fast mobility and large channel delay spread.

IQ Imbalance

The RF transceiver using the direct conversion is the trend since the wireless communication devices are getting smaller and highly integrated. However, the direct conversion RF transceiver experiences the IQ imbalance that comes from the imperfection of the direct conversion. The gain mismatch might cause the I signal to be slightly smaller than the Q [1.45]. To better understand how gain imbalance will affect an OFDM signal, look at (1.8) describing each individual subcarrier.

$$C(t) = S_{k,m}(\exp^{2\Delta ft}) \tag{1.8}$$

In (1.8), $S_{k,m}$ is a complex number representing the location of the symbol within the constellation for the k^{th} subcarrier at the m^{th} symbol time. For exampble, if subcarrier k is BPSK modulated, then $S_{k,m}$ might take on values of $(\pm 1 + j0)$. The complex exponential portion of (1.8) represents the k^{th} subcarrier, which is amplitude-and phase-modulated by the data symbol, $S_{k,m}$. Using Euler's relation, (1.8) can be rewritten as (1.9).

$$C(t) = S_{k,m}(\cos(2\Delta ft) + j\sin(2\Delta ft))) \tag{1.9}$$

Adding the gain imbalance effect to (1.9) with the term β, the gain imbalanced transmit signal is given by (1.10).

$$C(t) = S_{k,m}((1+\beta)\cos(2\Delta ft) + j\sin(2\Delta ft))) \tag{1.10}$$

By rearranging (1.10), it can be rewritten as the sum of perfect signal and an error signal of (1.11).

$$C(t) = S_{k,m}(\exp^{2\Delta ft}) + (S_{k,m}\frac{\beta}{2})(\exp^{2\Delta ft} + \exp^{-2\Delta ft}) \tag{1.11}$$

From (1.11), a gain imbalance produces two error terms. The first term is the perfect term and the second error term is at the frequency of the $-k^{th}$ subcarrier. The phase and magnitude of the error terms are proportional to the symbol being transmitted on the k^{th} subcarrier. In other words, I/Q gain imbalance will result in each subcarrier being interfered with by its frequency mirror-image subcarrier. The delay mismatch between I and Q channels is a similar to a gain imbalance case.

Frequency Offset

In any coherent modulation format, it is critical that the receiver accurately tracks the transmitter frequency. Frequency is defined to be the derivative of the phase with respect to time, so frequency error can be described as a cumulative phase error that linearly increases or decreases with time depending on the sign of the frequency error. The frequency error is due to the oscillator mismatch and the fast mobility of the mobile station [1.46].

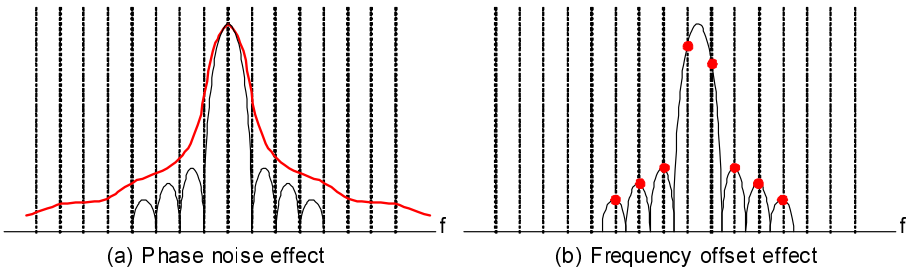

Figure 1.11: Intercarrier interference due to phase noise and frequency offset.

Under ideal conditions, each of the subcarriers in an OFDM signal is periodic within the FFT time buffer. This is critical if the subcarriers are to remain orthogonal and avoid mutual interference. A frequency error between the transmitter and the receiver will cause all of the subcarriers to have a non-integral number of cycles in the FFT interval, causing leakage. If the received OFDM symbol in time domain, $y(n)$, is converted into the frequency domain, the Y_k at the k^{th} subcarrier can be written by (1.12).

$$\begin{aligned} Y_k &= \sqrt{\frac{1}{N}}\sum_{n=0}^{N-1} y(n)\exp\left(-j\frac{2\pi}{N}nk\right) + W_k \\ &= \frac{1}{N}\sum_{n=0}^{N-1}\left[\sum_{k'=0}^{N-1} X(k')H(k')\exp\left(j\frac{2\pi}{N}n(k'+\varepsilon)\right)\right]\exp\left(-j\frac{2\pi}{N}nk\right) \\ &= \frac{1}{N}\sum_{n=0}^{N-1}\sum_{k'=0}^{N-1} X(k')H(k')\exp\left(j\frac{2\pi}{N}n(k'-k)\right)\exp\left(j\frac{2\pi}{N}n\varepsilon\right) \end{aligned} \tag{1.12}$$

where OFDM transmit signal and the wireless channel are $x(n) = \sum_{k=0}^{N-1} X(k)\exp\left(j\frac{2\pi}{N}nk\right)$ and $h_{i,n} = \sum_{l=0}^{L-1}\beta_l\delta(n-l)$, respectively. From (1.12), if k is equal to k',Y_k is given by (1.13), otherwise Y_k becomes (1.14).

$$\begin{aligned} Y_k &= X(k)H(k)\left[\frac{1}{N}\sum_{n=0}^{N-1}\exp\left(j\frac{2\pi}{N}n\varepsilon\right)\right] \\ &= X(k)H(k)\left[\frac{1}{N}\cdot\frac{1-\exp(j\frac{2\pi}{N}\varepsilon)^N}{1-\exp(j\frac{2\pi}{N}\varepsilon)}\right] \\ &= X(k)H(k)\frac{1}{N}\left[\frac{\exp(j\pi\varepsilon)\left(\exp(-j\pi\varepsilon)-\exp(j\pi\varepsilon)\right)}{\exp(j\frac{\pi\varepsilon}{N})\left(\exp(-j\frac{\pi\varepsilon}{N})-\exp(j\frac{\pi\varepsilon}{N})\right)}\right] \\ &= X(k)H(k)\left[\frac{1}{N}\cdot\frac{\exp(j\pi\varepsilon)}{\exp(j\frac{\pi\varepsilon}{N})}\cdot\frac{\sin(\pi\varepsilon)}{\sin(\frac{\pi\varepsilon}{N})}\right] \end{aligned} \tag{1.13}$$

$$Y_k = \frac{1}{N}\sum_{n=0}^{N-1}\sum_{\substack{k'=0\\k'\neq k}}^{N-1} X(k')H(k')\exp\left(j\frac{2\pi}{N}n(k'-k)\right)\exp\left(j\frac{2\pi}{N}n\varepsilon\right) \tag{1.14}$$

Both (1.13) and (1.14) imply the Common Phase Error (CPE) and the phase noise, respectively. Figure 1.11 shows the intercarrier interference due to phase noise and frequency error.

Peak to Average Power Ratio

If a signal is a sum of N signals each of maximum amplitude equal to 1 v, then it is conceivable that we could get a maximum amplitude of N that is all N signals addition at a moment at their maximum points. The PAPR is defined as (1.15).

$$PAPR = \frac{|x(n)|^2}{P_{avg}} \tag{1.15}$$

For an OFDM signal that has 1024 carriers, each with normalized power of 1 w, then the maximum PAPR can be as large as $10\log(1024)$ or 30 dB. This is at the example when all 1024 carriers combine at their maximum point, unlikely but possible. The rms PARP will be around half this number, namely 15 dB. The large amplitude variation increases in-band noise and increases BER when the signal has to go through amplifier non-linearities [1.47]. Large back-off is required in such cases. This makes use of OFDM just as problematic as multi-carrier FDM in high power amplifier applications such as satellite links.

Fast Mobility

Due to the fast mobility, the channel variation is incurred with an OFDM symbol. The channel variation with an OFDM symbol makes the channel estimate unreliable and causes ICI which results in the performance degradation [1.48]. In case that a mobile operating at 3.6 GHz of center frequency is moving at the speed of 200 km/h, the approximate coherent time is about 1.5 ms (Here, just assume the channel does not change within 1.5 ms). If TTI of the data packet is longer than the coherent time, the intercarrier interference between subcarriers occurs within an OFDM symbol. The detrimental effect by frequency offset is similar to the effect by fast mobility. As shown in Fig. 1.12, the faded OFDM symbol in time domain is equal to the convolution of the frequency converted time varying channel and OFDM symbol vector. As the slope due to channel variation is steeper with an OFDM symbol, the frequency domain channel variation gets broader which implies the increased intercarrier interference.

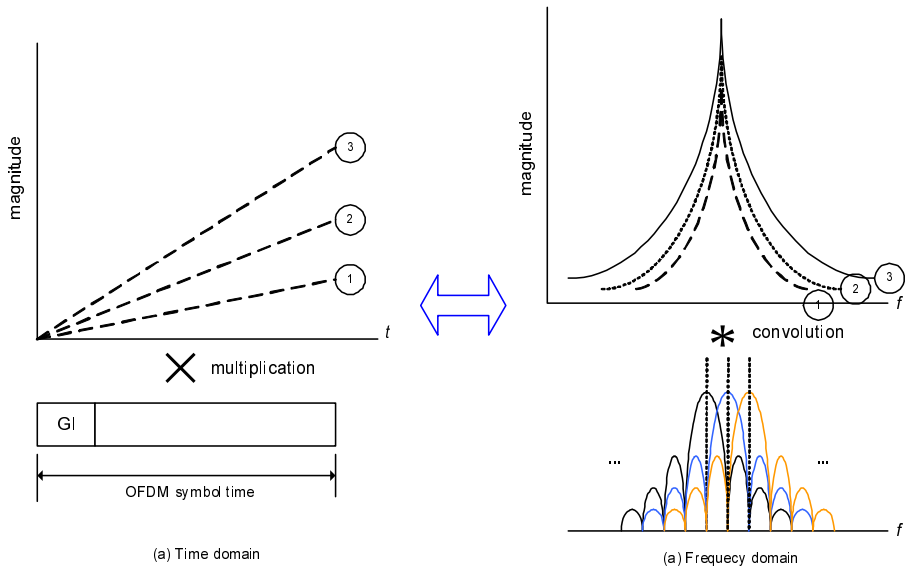

Figure 1.12: Equivalent model in time and frequency domain due to the fast fading within an OFDM symbol.

Timing Synchronization

Time synchronization error refers to the incorrect timing of OFDM symbols at the demodulator [1.49]. As shown in Fig. 1.13, the time synchronization error occurs when the misalignment of the FFT window is toward GI or away from GI. Both cases of misalignment result in erroneous effect on PSK modulated symbol detection.

The Case-I in Fig. 1.13 can be mathematically modeled by replacing $y(n)$ with $y(n+\epsilon)$ in (1.12), and results in (1.16).

$$\begin{aligned} Y_k &= \sqrt{\frac{1}{N}}\sum_{n=0}^{N-1} y(n+\epsilon)\exp\left(-j\frac{2\pi}{N}nk\right) + W_k \\ &= \frac{1}{N}\sum_{n=0}^{N-1}\left[\sum_{k'=0}^{N-1} X(k')H(k')\exp\left(j\frac{2\pi}{N}(n+\epsilon)k'\right)\right]\exp\left(-j\frac{2\pi}{N}nk\right) + W_k \\ &= \frac{1}{N}\sum_{n=0}^{N-1}\sum_{k'=0}^{N-1} X(k')H(k')\exp\left(j\frac{2\pi}{N}n(k'-k)\right)\exp\left(j\frac{2\pi}{N}\epsilon k'\right) + W_k \end{aligned} \tag{1.16}$$

where ϵ denotes the OFDM sample delay, and the frequency selective fading channel is assumed as in (1.12).

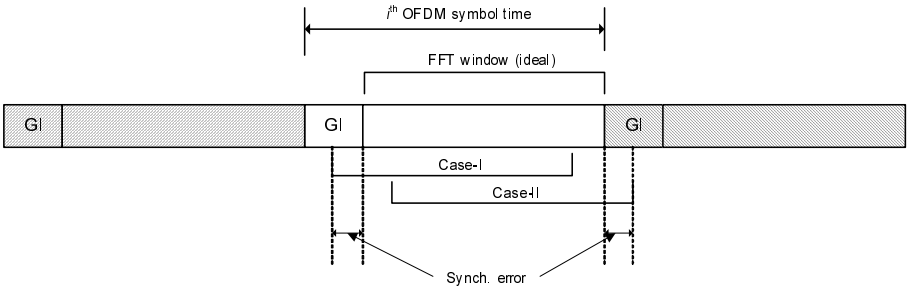

Figure 1.13: Symbol time synchronization error toward and away from GI.

From (1.16), if k is equal to $k^{'}$, Y_k is given by (1.17), otherwise Y_k becomes (1.18).

$$\begin{aligned} Y_k &= \frac{1}{N}\sum_{n=0}^{N-1} X(k)H(k)\exp\left(j\frac{2\pi}{N}\epsilon k\right) \\ &= X(k)H(k)\exp\left(j\frac{2\pi}{N}\epsilon k\right) \end{aligned} \tag{1.17}$$

$$\begin{aligned} Y_k &= \frac{1}{N}\sum_{n=0}^{N-1}\sum_{\substack{k'=0 \\ k'\neq k}}^{N-1} X(k')H(k')\exp\left(j\frac{2\pi}{N}n(k'-k)\right)\exp\left(j\frac{2\pi}{N}\epsilon k'\right) \\ &= 0 \end{aligned} \tag{1.18}$$

From the result, the wireless channel faded data symbols experience phase shift of (exp $j2\pi\epsilon k/N$). Even for a small window misalignment e.g. ϵ=0, the OFDM subcarriers at high frequency (for large k) experience large phase shifts causing PSK modulated data symbols to map into incorrect constellation points. In general, even though the phase shift in Case-I is compensated by normal channel estimation, it strongly depends on how pilot symbols are multiplexed within a packet.

The Case-II assumes the more critical time synchronization error since it also includes the adjacent symbol within the FFT window. The OFDM symbol, polluted by the adjacent symbol, faces with two types of interferences: One is intersymbol interference and the other is intercarrier interference. This analysis is very similar to the case of large channel delay exceeding the guard interval so that the analysis is prolonged to the following chapters.

Large Channel Delay

The guard interval insertion is applied in OFDM systems to prevent the interferences caused by radio propagation delay However, in mobile communication

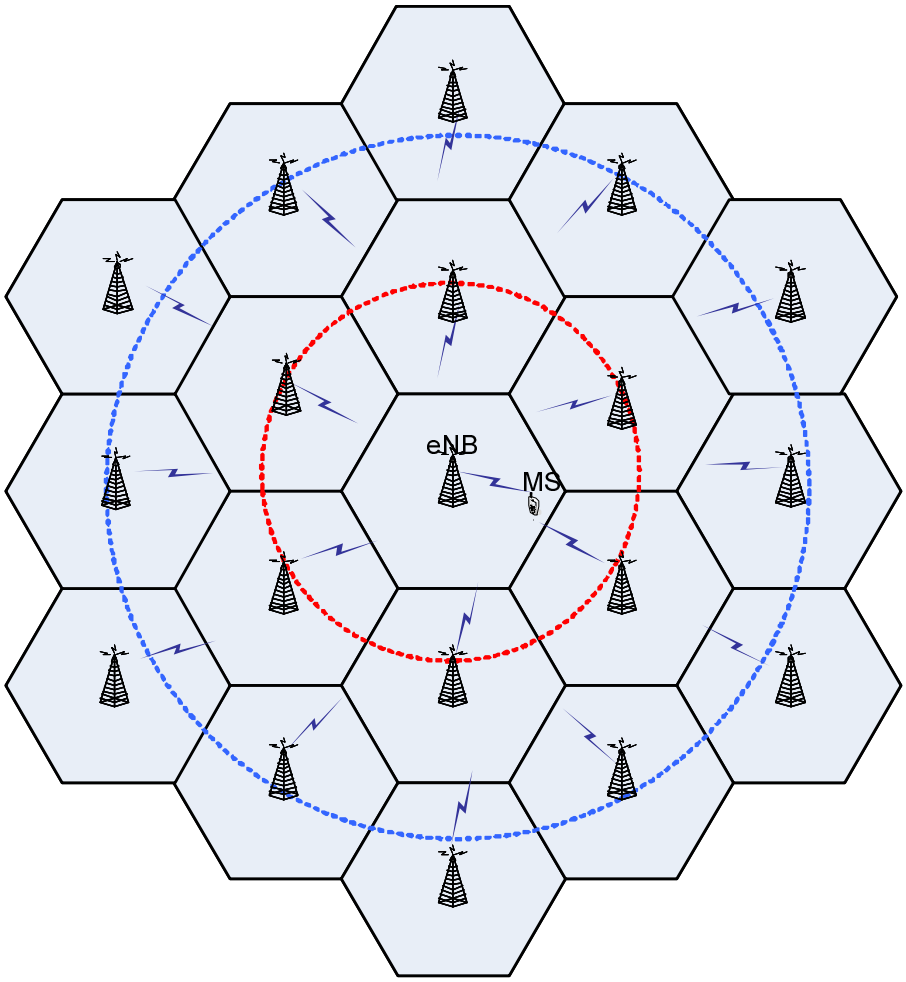

Figure 1.14: Single frequency network.

environments, some multipaths have longer delay than the guard interval occasionally. This phenomenon probably can be seen more often in Single Frequency Network (SNF) than in single cell network [1.50] [1.51]. Figure 1.14 shows SFN network where the base stations (eNB) located within 3-tier cell model broadcast the same information to mobile station (MS). The high signal to noise radio (SNR) in SFN can be achieved by enjoying a macro-diversity, but the large channel delay over GI is much probable resulting in intersymbol (ISI) and intercarrier interferences (ICI) as shown in Fig. 1.14. Even if the longer GI insertion can be a solution, it is also limited to the certain level because the increased GI is directly relevant to the losses of frequency efficiency and power. Therefore, the adoption of canceller is required to prevent the performance of OFDM system from being degraded due to ISI and ICI.

1.5 Purpose and Position of the Research

Up to now, there are several types of cancellers whose designs are generally classified into frequency domain canceller and time domain canceller with time domain or frequency domain wireless channel equalizer. In early 1990s the interference cancellers are based on the linear equalization per subcarrier in frequency domain and the role of power channel coder has been studied against ISI and ICI. In late 1990s the RISIC was firstly introduced. The important characteristic of RISIC can be found in ICI cancellation through cyclic reconstruction and it also makes use of the fast fourier transform (FFT) engine without demanding an additional processors in the interference cancellation. Accordingly, it is known as the simplest canceller ever known. From the introduction of RISIC, there have been proposed the variants of RISIC in early 2000s to improve the performance of RISIC. In summary, the previous cancellers until early 2000s have several problems such as convergence of equalizer tap weight, computational complexity due to the equalization per subcarrier, matrix inversion, and large deviation of the performance depending on the degree of the interferences.

Meanwhile, the turbo equalized canceller was introduced in 2003 by , and the canceller has overcome the performance limitation by including a guard interval and channel coding gain in the canceller operation. The canceller, however, includes the two defects. One is the heavy computational complexity due to ICI cancellation, and the other is the susceptibility to the degree of interferences.

In Fig. 1.15 it shows the overview on a research trend for the interference canceller, and the research purpose is summarized in Table 1.5. Meanwhile, the main focuses on designing the cancellers follow the issues, listed as below.

- Canceller Design Methodology (Frequency Domain Canceller or Time Domain Canceller)
- How to Suppress ISI and ICI
- How to Select Canceller Processing Window
- How to Include Guard Interval in Canceller Operation
- How to Equalize the Channel Distortion (Time Domain and Frequency Domain Equalizers)
- How to Incorporate the Proposed Canceller with Channel Decoder
- Considerations of Performance, Computational Complexity and Latency

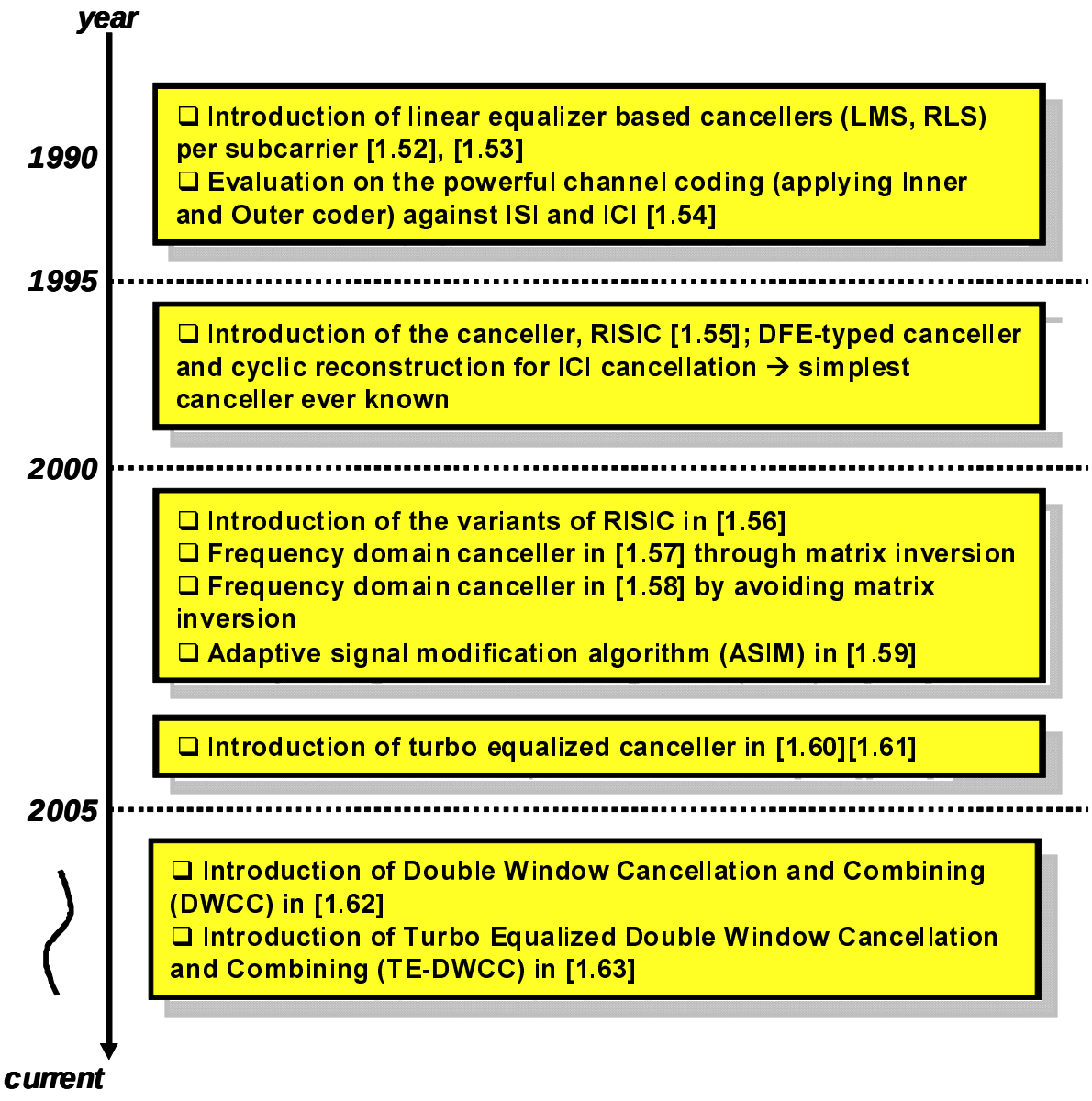

Figure 1.15: Research position on the interference canceller.

Table 1.5: Outline of the proposed approaches.

Chapter 3	Purpose	Improve the reliability of the symbol replicas in DFE, while the processing window length for the interference cancellation extends to the entire OFDM symbol duration.
	Research Issue	Conventional cancellers operating with an iterative DFE are susceptible to the frequency selectivity and the degree of interference.
	Proposed Scheme	By applying the double window cancellation and combining (DWCC) to the interfered OFDM symbols, two different COBD type of cancellers are proposed.
	Achievement	Becomes possible to readily include a guard interval and enjoy an additional *SINR* gain. Results in more robust canceller against large channel delay by making the symbol replicas more reliable.
Chapter 4	Purpose	Improve the reliability of the symbol replicas in DFE by applying turbo equalization, and find the optimal combining method between canceller engine and channel decoder without sacrifice of too much computational complexity.
	Research Issue	There are two available gains from the canceller engine and the channel decoder and the gains could depend on how to combine canceller engine and channel decoder.
	Proposed Scheme	By optimally incorporating the channel decoding gain into DWCC, TE-DWCC with hard decision feedback is proposed.
	Achievement	Found the optimal processing procedure and the compatibility with decision feedback type. In addition, TE-DWCC is not severely affected by code rate, compared with conventional turbo equalized canceller.

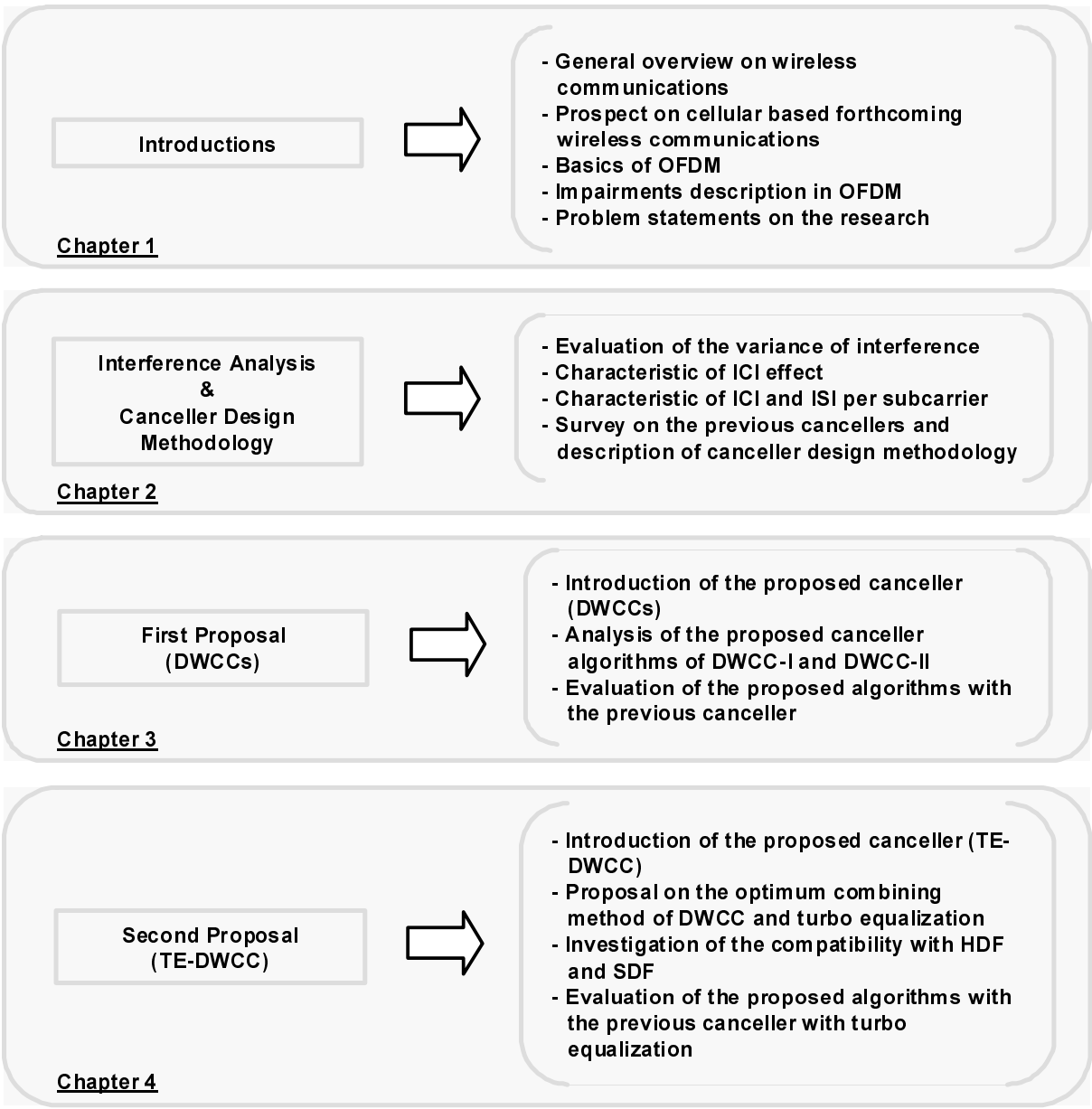

Figure 1.16: Overall configuration of the dissertation.

1.6 Configuration of the Dissertation

The dissertation is organized as follows. Chapter 1 includes the general overview on the wireless communication systems, and predicts the forthcoming cellular based wireless communication. Additionally, the basics on the OFDM technology and research background about the interference canceller are also included.

In Chapter 2 the analysis results of the interferences (ISI and ICI) due to large channel delay spread exceeding a guard interval are investigated, and the interference canceller design methodology is explained by presenting the several types of the previous cancellers with a processing window length of N-FFT. Finally, the advantage and disadvantage of the turbo equalized canceller are mentioned.

Chapter 3 proposes how to suppress ISI and ICI in considerations of how to select a canceller processing window, how to include a guard interval, and finally how to apply channel equalization method. In regards of those requirements, the two proposed schemes of DWCC-I (Symbol-wise) and DWCC-II (Group-wise) are introduced including the concept of double window cancellation and combining (DWCC), and the immunity to ISI and ICI in both schemes are analyzed through the computer simulations. For the evalution of the algorithms, each scheme is evaluated in the turbo coded OFDM for low (QPSK) and high level modulation (16QAM, 64QAM) under the minimum and non-minimum phase wireless channel models, and compared with the conventional canceller with respect to the performance and computational complexity.

In Chapter 4 the optimal combining of DWCC and turbo equalization (TE), named TE-DWCC, is introduced by investigating the iterative canceller procedure between DWCC and channel decoder and the compatibility with the decision feedback types such as hard decision feedback (HDF) and soft decision feedback (SDF). Finally, the performances of TE-DWCC is compared with the conventional turbo equalized canceller by varying the interference level, code rate, and decision feedback type in the exponentially distributed slow fading channels.

Finally, this thesis ends with the concluding remarks in Chapter 5.

1.7 References

[1.1] R. R. Mosier and R. G. Clabaugh, “Kineplex, a bandwidth efficient binary transmission system,“ AIEE Trans. Commun. Electro., vol. 76, pp. 723–728, Jan. 1958.

[1.2] C. G. Porter, “Error distribution and diversity performance of a frequency differential PSK HF modem,” IEEE Trans. Commun., vol. COM-16, pp. 567–575, Aug. 1968.

[1.3] M. S. Zimmerman and A. L. Kirsch,”The AN/GSC-10 (KATHRYN) variable rate data modem for HF radio,” IEEE Trans. Commun., vol. COM-15, pp. 197–205, Apr. 1967.

[1.4] IEEE 802.11-VHT SG, http://www.ieee802.org/11/Reports/vht-update.htm.

[1.5] IEEE 802.16 Task Group m (TGm), http://wirelessman.org/tgm/.

[1.6] 3GPP Standard for Mobile Broadband, http://www.3gpp.org/.

[1.7] History of GSM and GSMA, http://www.gsmworld.com/about-us/history.htm.

[1.8] K. Tachikawa, "A Perspective on the evolution of mobile communications," IEEE Commun. Mag., vol. 41, no. 10, pp. 66–73, 2003.

[1.9] J. Govil, "4G mobile communication systems:Turns, Trends and Transition," IEEE Convergence Info. Technol. (ICCIT), pp. 13–18, Nov. 2007.

[1.10] Dahlman. E, 3G evolution : HSPA and LTE for mobile broadband. Oxford ; Burlington, MA, Elsevier Academic Press, 2007.

[1.11] Lescuyer. P and T. Lucidarme, Evolved packet system (EPS) : the LTE and SAE evolution of 3G UMTS. Chichester, West Sussex, England ; Hoboken, NJ, J. Wiley Sons.

[1.12] 3GPP TS 39.913 v8.0.0, "Requirements for further advancements for E-UTRA," June 2008.

[1.13] UMA Overview, http://www.umatechnology.org/overview/index.htm.

[1.14] V. Gupta, M. G. Williams, DJ. Johnston, S. McCann, P. Barber, Y. Ohba, "IEEE 802.21 Overview of standard for media independent handover services," IEEE P802.21 Tutorial, July 2006.

[1.15] www.dibeg.org.

[1.16] ITU-DTTB Tutorial, http://happy.emu.id.au/lab/tut/dttb/dttbtuti.htm.

[1.17] IEEE Standard 802.16e-2005, "IEEE Standard for local and metropolitan area networks part 16: Air interface for fixed broadband wireless access systems - amendment2: Physical and medium access control layers for combined fixed and mobile operation in licensed bands and corrigendum 1," Feb. 2006.

[1.18] P802.16 Rev.2/D3, "Draft standard for local and metropolitan area networks part 16: Air interface for Broadband Wireless Access systems," Feb. 2008.

[1.19] WLAN Medium Access Control (MAC) and Physical Layer (PHY) Specification, ANSI/IEEE 802.11, 1999.

[1.20] WP5D, "Requirements related to technical performance for IMT-Advanced radio interface(s)," Aug. 2008.

[1.21] http://www.rrl.go.kr/book/document/view.jsp?dc_*seq*=575, 2007.

[1.22] Darlene A. Drazenovich, "WRC-07 Summary and WRC-11 Preview", May 2008.

[1.23] F. Adachi, "Wireless Challenge : From Wireless Voice to Wireless Video," May 2008.

[1.24] http://www.emobility.eu.org/WorkingGroups/Broadband/Broadband-for-Europe.html.

[1.25] S. McLaughlin, "Green Radio: The key issues," Mobile VCE, 2008.

[1.26] France Telecom RD and Regis Esnault, "OPERA-NTE," CELTIC, Jan. 2007.

[1.27] http://www.wireless.kth.se/projects/GREEN/index.php.

[1.28] S. Frattasi et al., "Defining 4G technology from the user's perspective," IEEE Proc. Network, vol. 20, no. 1, pp. 35–41, Feb. 2006.

[1.29] S. Frattasi et al., "Designing socially robust 4G wireless services," IEEE Technol. and Society Mag., vol. 25, no. 2, pp. 51–64, Summer 2006.

[1.30] U. Javaid et al., "A novel dimension of cooperation in 4G," IEEE Technol. and Society Mag., vol. 27, no. 1, pp. 29–40, Spring 2008.

[1.31] E. van der Meulen, "Three-terminal communication channels," Adv. Appl. Prob., vol. 3, pp. 120–154, 1971.

[1.32] T. Cover and A. el Gamal, "Capacity theorems for the relay channel," IEEE Trans. on Inform. Theory, vol. IT-25, no. 5, pp. 572–584, Sept. 1979.

[1.33] T. Himsoon et al., "Lifetime maximization via cooperative nodes and relay deployment in wireless networks," IEEE Journal on Sel. Areas in Commun., vol. 25, no. 2, Feb. 2007.

[1.34] H. Adam, C. Bettstetter, and S. M. Senouci, "Adaptive relay selection in cooperative wireless networks," IEEE Proc. PIMRC., Sept. 2008.

[1.35] L. Militano, F.H.P. Fitzek, A. Iera, and A. Molinaro, "On the beneficial effects of cooperative wireless peer to peer networking," Tyrrhenian International Workshop On Digital Commun., 2007.

[1.36] Richarad van Nee and Ramjee Prasad, OFDM wireless multimedia communication, Artech House Boston London, 2000.

[1.37] B. Hirosaki, "An analysis of automatic equalizers for orthogonally multiplexed QAM system," IEEE Trans. Commun., vol. 28, no. 1, pp. 73–83, Jan. 1980.

[1.38] B. Hirosaki, "An orthogonally multiplexed QAM system using the discrete fourier transform," IEEE Trans. Commun., vol. 29, no. 7, July 1981.

[1.39] http://nova.stanford.edu/ bbaas/fftinfo.html.

[1.40] G. Faria, "The evolutions of the digital broadcast landscape," Networked and Electron. Media (NEM) Summit, Oct. 2008.

[1.41] 3GPP TR 25.996 v6.1.0, "Spatial channel model for Multiple Input Multiple Output (MIMO) Simulations," Sept. 2003.

[1.42] D.S. Baum, J. Hansen, and J Salo, "An interim channel model for beyond-3G systems: extending the 3GPP spatial channel model(SCM)," IEEE Proc. Vehicular Technol., vol. 5, pp. 3132–3136, June 2005.

[1.43] IST-2003-507581-WINNER, "Final Report on Link Level and System Level Channel Models," Nov. 2005.

[1.44] IST-4-027756-WINNER II, "WINNER II Channel Models," Sept. 2007.

[1.45] A. Tarighat and A.H. Sayed, "MIMO OFDM receivers for systems with IQ imbalances," IEEE Trans. on Signal Processing, vol. 53, no. 9, Sept. 2005.

[1.46] B. Cutler, "Effects of physical layer impairments on OFDM systems," www.rfdesign.com, May 2002.

[1.47] C. Langton, "Orthogonal Frequency Division Multiplexing (OFDM)," www.complextoreal.com, 2004.

[1.48] J. Ahn and H.S. Leel, "Frequency domain equalization of OFDM signals over frequency nonselective rayleigh fading channels," Electron. Lett., vol. 29, no. 16, Aug. 1993.

[1.49] Y. Mostofi and D.C. Cox, "Mathematical analysis of the impact of timing synchronization errors on the performance of an OFDM system," IEEE Trans. on Commun., vol. 54, no. 2, Feb. 2006.

[1.50] G. Guerra et al., "Field measurement based characterization of the wideband urban multipath channel for portable DTV reception in single frequency networks," IEEE Trans. on Broadcasting, vol. 51, no. 2, June 2005.

[1.51] L. Zhang, L. Gui, Y. Qiao, and W. Zhang, "Obtaining diversity gain for DTV by using MIMO structure in SFN," IEEE Trans. on Broadcasting, vol. 50, no. 1, March 2004.

[1.52] M. Itami, H. Takano, H. Ohta, and K. Itoh, "A method of equalization of OFDM signal with inter-symbol and inter-channel interferences," IEEE Proc. ICCS, vol. 1, pp. 109–113, pp. 14-18, Nov. 1994.

[1.53] G. Santella, "OFDM with guard interval and sub-channel equalization in a 2-resolution transmission scheme for digital television broadcasting," IEEE Proc. ICC, vol. 1, pp. 374–380, May 1994.

[1.54] E. Viterbo, and K. Fazel, "How to combat long echoes in OFDM transmission schemes: Sub-channel equalization or more powerful channel coding," IEEE Proc. GLOBECOM, vol. 3, pp. 2069–2074, Nov. 1995.

[1.55] D. Kim and G.L. Stber, "Residual ISI cancellation for OFDM with applications to HDTV broadcasting," IEEE J. Sel. Areas Commun., vol. 16, no. 8, pp. 1590–1599, Oct. 1998.

[1.56] C. J. Park, and G. H. Im, "Efficient cyclic prefix reconstruction for coded OFDM systems," IEEE Commun. Lett., vol. 8, no. 5, pp. 274–276, May 2004.

[1.57] H. J. Yu, M. S. Kim, T. H. Jeon, and S. K. Lee, "Equalization scheme for OFDM systems in long delay spread channels," IEEE Proc. PIMRC, vol. 2, pp. 1297–1301, Sept. 2004.

[1.58] W. Zhong, and Z. Mao, "Tentative decision based low complexity equalization for OFDM systems with insufficient cyclic prefix," IEEE Proc. ICICS, pp. 116–119, Sept. 2005.

[1.59] M. Uesugi, "An interference cancellation scheme for OFDM using adaptive algorithm," IEICE Trans. Commun., vol. E86-B, no. 11, pp. 3182–3191, Nov. 2003.

[1.60] S. Suyama, S. Suzuki, and K. Fukawa, "An OFDM receiver employing turbo equalization for multipath environments with delay spread greater than the guard interval," IEEE Proc. Vehicular Technol., vol. 1, pp. 632–636, Apr. 2003.

[1.61] Y. Sagae, S. Suyama, H. Suzuki, and K. Fukawa, "An OFDM turbo equalizer for scattered pilot signals in multipath environments with delay difference greater than guard interval," IEEE Proc. Vehicular Technol., vol. 1, pp. 425–429, May 2004.

[1.62] J. H. Lee, Y. Kishiyama, T. Ohtsuki, and M. Nakagawa, "Double window cancellation and combining for OFDM in time-invariant large delay spread channel," IEICE Trans. Fundamentals, vol. E90-A, no. 10, pp. 2066–2078, Oct. 2007.

[1.63] J. H. Lee, T. Ohtsuki, and M. Nakagawa, "Turbo equalized double window cancellation and combining robust to large delay spread channel," IEICE Trans. on Commun., vol. E92-B, no. 2, pp. 517–526, Feb. 2009.

Chapter 2

Interference Analysis and Canceller Design Methodology

This Chapter starts with the analysis on intersymbol interference (ISI) and intercarrier interference (ICI) caused by the large channel delay spread over guard interval (GI) [2.1]– [2.8]. The analysis is given by matrix expressions and the variances of ISI and ICI are calculated by using the bias function which is well known analysis function, proposed by [2.9]. In addition, the analysis result is proved by comparing with the simulation result.

There are several types of cancellers whose canceller operation is performed in frequency domain and time domain with frequency or time domain channel equalization. For simplicity, both schemes of time domain and frequency domain cancellers are named as TDC and FDC hereafter, while FDE and TDE are the abbreviated terms for frequency and domain time domain equalization, respectively [2.10]– [2.18]. By considering the canceller design methodology, the characteristics of the cancellers are presented.

Finally, the representative cancellers, which have been surveyed so far, are presented, and their algorithm features are investigated. From that, the advantages and the disadvantages of the previous cancellers are characterized.

2.1 Analysis of Interference

2.1.1 Theoretical Analysis

The channel coded and interleaved bits in the transmitter are modulated by symbol mapper and then the i^{th} modulated data symbol vector, $\mathbf{s}_i = s_0, s_1, \cdots, s_{N-1}$, is are modulated by subcarriers through N-IFFT operation , which results in $x(n)$ of (2.1).

$$\mathbf{x}_i = \mathbf{F}\mathbf{s}_i \tag{2.1}$$

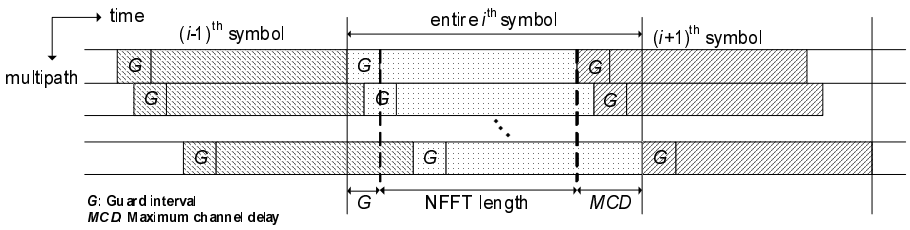

Figure 2.1: Received OFDM symbols interfered by adjacent symbols due to multipath exceeding the guard interval.

where $\mathbf{F}$ is $(N + GI) \times N$ IFFT matrix and the (k, m) entry of the $\mathbf{F}$ matrix can be calculated by (2.2)

$$\mathbf{F}_{(k,m)} = \frac{1}{\sqrt{N}} \exp\left(j\frac{2\pi}{N}(m - GI)k\right) \tag{2.2}$$

The i^{th} OFDM symbol in time domain, $\mathbf{x}_i$ goes through the wireless channel and the additive white Gaussian noise (AWGN) is added at the receiver. Figure 2.1 shows the delayed version of the transmit signal at the receiver. The received i^{th} OFDM symbol, $\mathbf{r}_i$, experienced by the wireless channel, $h_i(n)$ where $h_i(n) = \sum_{l=0}^{L-1} \beta_{i,l}\delta(n - l)$, is expressed by

$$\mathbf{r}_i = \mathbf{H}_i\mathbf{x}_i + \mathbf{n}_i \tag{2.3}$$

where $N \times N$ circular channel matrix, $\mathbf{H}_i$ is expressed by

$$\mathbf{H}_i = \begin{bmatrix} \beta_0 & 0\cdots & \beta_{L-1} & \cdots & \beta_1 \\ \beta_1 & \beta_0 & 0 & \ddots & \beta_2 \\ \vdots & \vdots & \vdots & \vdots & \vdots \\ \beta_{L-1} & \ddots & \beta_0 & \ddots & 0 \\ \vdots & \vdots & \vdots & \vdots & \vdots \\ 0 & \cdots & \beta_{L-1} & \cdots & \beta_0 \end{bmatrix} \tag{2.4}$$

and $\mathbf{n}_i$ is the noise vector with the variance of σ^2.

When the maximum channel delay, (MCD), is N >MCD>GI, the received signal, $\mathbf{r}_i$ interfered by the $(i-1)^{th}$ symbol can be redefined as

$$\mathbf{r}_i = \mathbf{H}_i^{isi}\mathbf{x}_{i-1} + \mathbf{H}_i^{ici}\mathbf{x}_i + \mathbf{n}_i \tag{2.5}$$

where $\mathbf{H}_i^{isi}$ and $\mathbf{H}_i^{ici}$ denote ISI and ICI channel matrices of the $(i-1)^{th}$ and i^{th} symbols in the i^{th} OFDM symbol, respectively. Therefore, the circular channel matrix, $\mathbf{H}_i$ is decomposed into ISI and ICI channel matrices in the following.

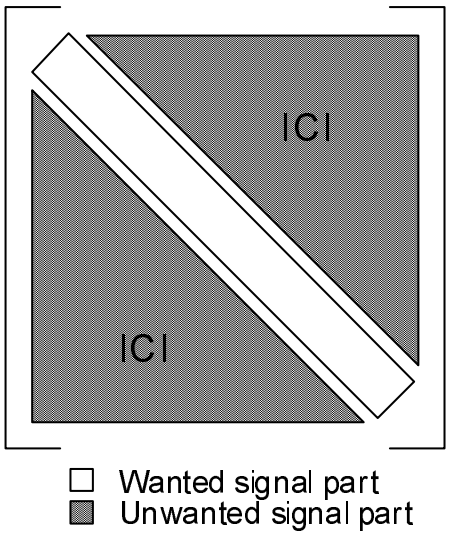

Figure 2.2: Bias function model.

$$\mathbf{H}_i^{isi} = \begin{bmatrix} 0 & \cdots & \beta_{L-1} & \cdots & \beta_{K+1} \\ 0 & \ddots & \ddots & \ddots & \vdots \\ 0 & \ddots & \ddots & \ddots & \beta_{L-1} \\ \vdots & \vdots & \vdots & \vdots & \vdots \\ 0 & \cdots & \cdots & \cdots & 0 \end{bmatrix} \tag{2.6}$$

$$\mathbf{H}_i^{ici} = \begin{bmatrix} \beta_0 & 0\cdots & \beta_K & \cdots & \beta_1 \\ \beta_1 & \beta_0 & \ddots & \ddots & \vdots \\ 0 & \ddots & \beta_0 & \ddots & \beta_{L-1} \\ \vdots & \vdots & \vdots & \vdots & \vdots \\ 0 & \cdots & \beta_{L-1} & \cdots & \beta_0 \end{bmatrix} \tag{2.7}$$

where K denotes the largest number of the multipath index that is smaller than GI. Taking N-FFT to (2.5), the result is expressed by

$$\mathbf{R}_i = \mathbf{F}^{-1}\mathbf{H}_i^{isi}\mathbf{x}_{i-1} + \mathbf{F}^{-1}\mathbf{H}_i^{ici}\mathbf{F}\mathbf{s}_i + \mathbf{F}^{-1}\mathbf{n}_i \tag{2.8}$$

Ignoring the thermal noise, the first and second terms of (2.8) imply ISI and ICI, while $\mathbf{F}^{-1}\mathbf{H}_i^{ici}\mathbf{F}$ of the second term can be divided into unwanted and wanted signal parts. Those are shown in Fig , where the hatched areas are due to the destruction of the orthogonality.

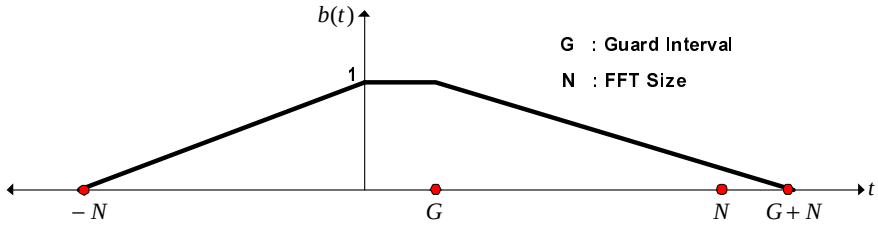

Figure 2.3: Bias function model.

Bias Function

Including the terms for both ISI and ICI, the paper in [2.5] derived the accurate useful power and interference power based on a continuous time power delay profile. In a finite discrete impulse response channel model, the expressions in [2.5] reduce to the same signal and interference power that was proposed by [2.9], where the concept of the bias function is introduced. The bias function is useful tool to calculate the useful signal power and interference power when the wireless channel is time and frequency selective channel, so called as doubly selective channel.

The OFDM symbol interval is NT where N is the FFT length in OFDM samples and T is the sample interval in seconds. If the guard interval length is $\triangle$ seconds, the total OFDM symbol time is $NT + \triangle$. The bias function b(t) is shown in Fig. 2.3. Depending on the wireless channel delay along the t-axis in Fig. 2.3, the function, $b(t)$ is defined as below.

$$b(\tau) = \begin{cases} 0 & (\text{if } \tau < -NT) \\ (NT+\tau)/NT & (\text{if } -NT \leq \tau < 0) \\ 1 & (\text{if } 0 \leq \tau < \triangle) \\ (NT-(\tau - G))/NT & (\text{if } \triangle \leq \tau < NT + \triangle) \\ 0 & (\text{if } NT+\triangle \leq \tau) \end{cases} \tag{2.9}$$

According to the definition of the bias function, when the multipath channel delay (τ_l) is set, the bias function can evaluate the received multipath effect to the total received power. By using $b(t)$, the total received power, P_s can be expressed by (2.10).

$$P_S = \sum_{l=0}^{L-1} b(\tau_l)^2 E\left[|\alpha_l|^2\right] \tag{2.10}$$

where $E\left[|\alpha_l|^2\right]$ is the average power per multipath, and the transmit signal power is assumed to be '1'. Accordingly, if there is no interference within the FFT symbol

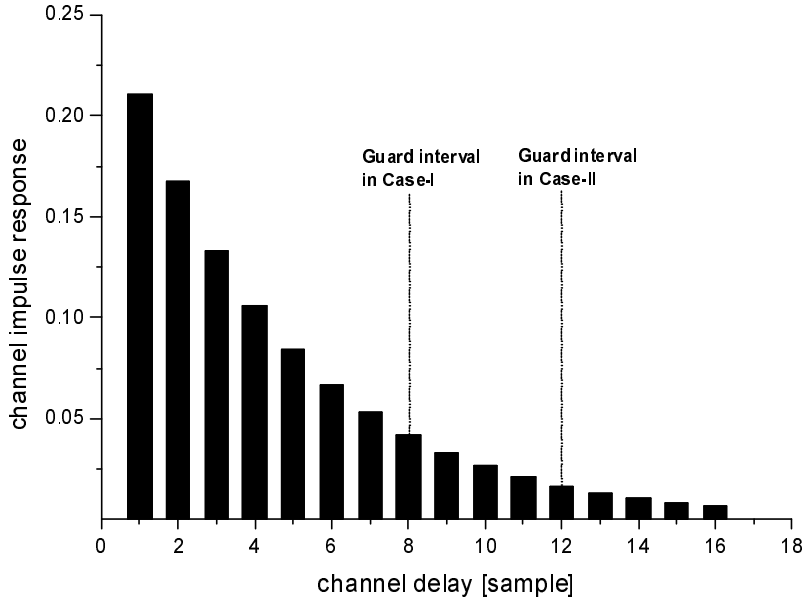

Figure 2.4: Assumed channel model.

interval, the total received power, P_T becomes (2.11)because the bias function, $b(t)$, is equal to '1'.

$$P_T = \sum_{l=0}^{L-1} E\left[|\alpha_l|^2\right] \tag{2.11}$$

On the other hand, if there exists an interference, the interference power, P_I, can be found by subtracting (2.10) from (2.11) and results in.

$$\begin{aligned} P_I &= P_T - P_S \\ &= \sum_{l=0}^{L-1} E\left[|\alpha_l|^2\right] - \sum_{l=0}^{L-1} b(\tau_l)^2 E\left[|\alpha_l|^2\right] \\ &= \sum_{l=0}^{L-1} (1 - b(\tau_l)^2) E\left[|\alpha_l|^2\right] \end{aligned} \tag{2.12}$$

From Fig. 2.2, the interference occurs where $\triangle \leq \tau_l < N + \triangle$, so (2.12) can be rewritten as in (2.13) by replacing the bias function with the value defined in (2.9).

$$P_I = \sum_{l=0}^{L-1} \left(\frac{\tau_l - G}{N}\right)\left(1 + \frac{N + G - \tau_l}{N}\right) E\left[|\alpha_l|^2\right] \tag{2.13}$$

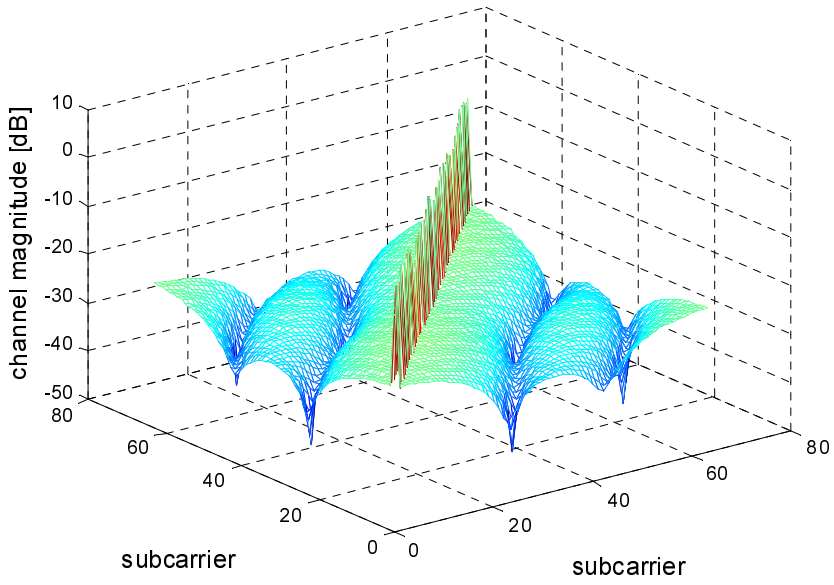

Figure 2.5: ICI effect for Case-I.

Finally, the interference power of (2.12) is further divided into ISI and ICI powers, P_{ISI} and P_{ICI} and each term is given by (2.14) and (2.15), respectively.

$$P_{ISI} = \sum_{l=0}^{L-1} \left(\frac{\tau_l - G}{N} \right) E\left[|\alpha_l|^2 \right] \tag{2.14}$$

$$P_{ICI} = \sum_{l=0}^{L-1} \left(\frac{\tau_l - G}{N} \right) \left(\frac{N + G - \tau_l}{N} \right) E\left[|\alpha_l|^2 \right] \tag{2.15}$$

When the FFT length is comparatively larger than the channel delay, P_{ICI} becomes P_{ISI}. After all, the interference power is obtained approximately by (2.16).

$$P_I \approx 2P_{ISI} \tag{2.16}$$

To evaluate the effect of the intercarrier interference, Figs. 2.5 and 2.6 are simulated under the wireless channel condition of Fig. 2.4, where the number of multipath is 16. For the simulation, it is also assumed that the size of N-FFT is 64, and OFDM sample delay between multipath is one sample delay. Both Case-I and Case-II experience ISI and ICI with the lack of guard interval whose the lengths for Case-I and Case-II are set to 12 and 8, respectively. By comparing both of Figs. 2.5 and 2.6, it can be seen that the shorter guard interval length is, the severer interference occurs and also every data symbol is strongly affected by the adjacent symbols.

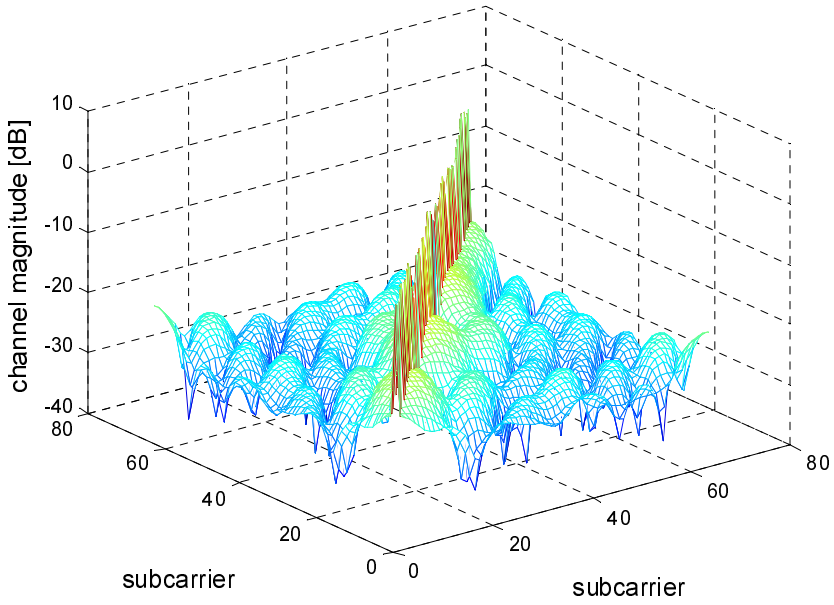

Figure 2.6: ICI effect for Case-II.

2.1.2 Evaluation of Interferences

For the detail understanding of the interference effects, this sub-chapter investigates the variance of the interferences of ISI and ICI in different delay spread channels, where PDB implies the **P**ower difference between multipath in **dB** scale as shown in Fig. 2.7. As PDB decreases, the interference increases and deteriorates the system performance. In addition, the characteristics of the interferences are evaluated in frequency domain. For the evaluation, it is assumed that the OFDM symbols are 64 points with 16 samples of guard interval and the multipath tap delay is 2 OFDM samples interval, and the interference level is controlled by the PDB.

Figure 2.8 includes the variances of the interferences by simulation and analysis, respectively, where the analysis results are calculated by using (2.14) and (2.15). As can be seen, the interference levels are exponentially increasing depending on the corresponding interference level. For example, if *SNR* is assumed to be 20 dB under 1.4 dB of PDB where the transmit signal power is '1', the SNR loss approximately amounts to 3 dB since the variance of interferences is about 0.01 at a given interference level. Therefore, it is concluded that the performance of OFDM system is limited by the large channel delay spread over guard interval.

From Fig 2.9 the distribution of interference variances across subcarriers are almost white, similarly to white thermal noise. Accordingly, the powerful channel

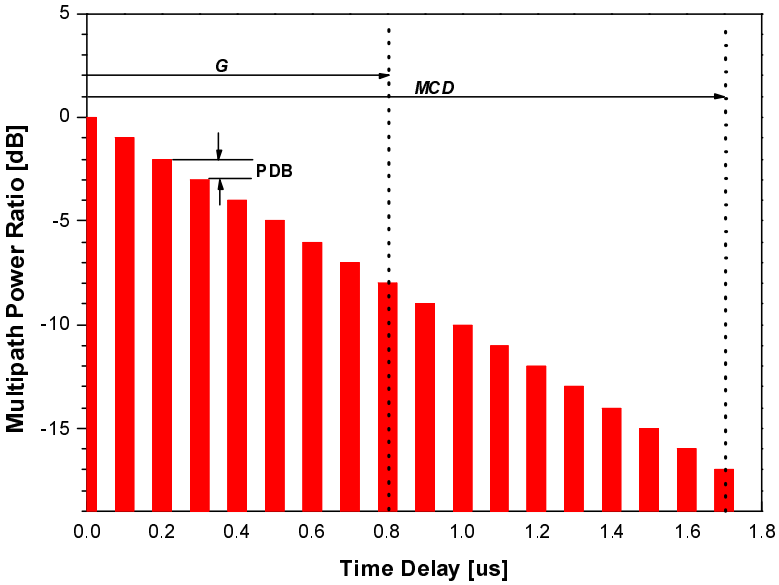

Figure 2.7: Multipath channel model.

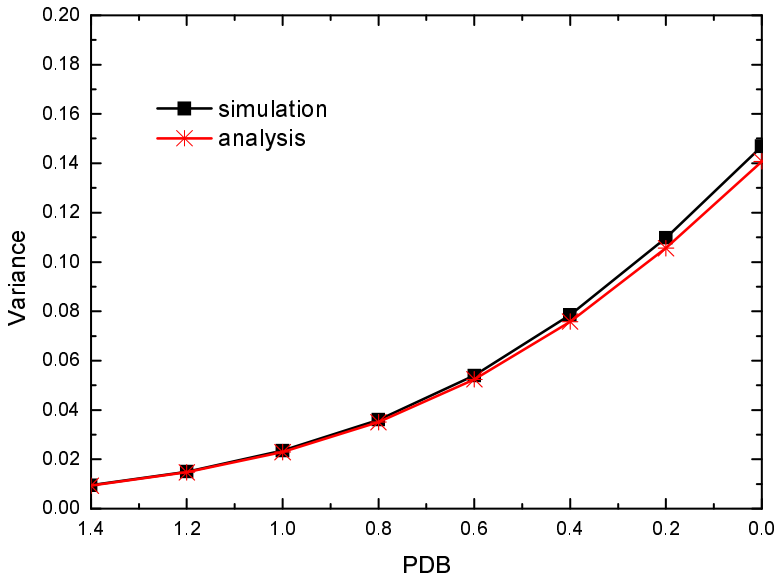

Figure 2.8: Variances of interferences in different delay spread channels, controlled by PDB.

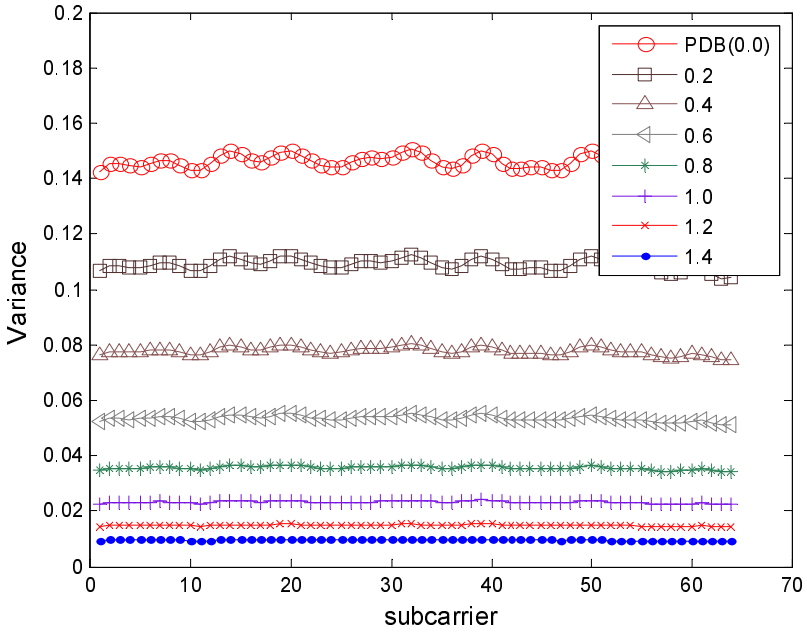

Figure 2.9: Distribution of interference variance across subcarriers.

coder/decoder itself could play an important role as an interference canceller [2.19]. In the following chapters, however, the only channel coder without adopting an interference canceller can not be an effective solution to mitigate the interferences.

2.2 Canceller Design Methodology

The technologies of the interference canceller up to date have the characteristics, individually, and the design methods of the their own way have been being progressed rather than considering the performance comparison among them. In other words, it is overlooked that the design of the interference canceller should be emphasized on three criteria as described in this part.

In this chapter, the requirements in the interference canceller design are actually formulated, and it is intended to mention about the concrete canceller design methodology which is satiable to the requirements. The representative criteria in the interference canceller design can be summarized in performance, latency, and hardware complexity.

Firstly, as to the performance point of view, the interference canceller should be robust regardless of the degree of interference whether it is small or large. Moreover, the interference canceller should not also be sensitive to the wireless channel environment whose channel characteristic is a severe frequency selective channel.

As to a reason, the performance of the interference canceller exploiting the decision feedback (DF) with the temporary symbol decision is dominated by the D/U ratio (Desired and Undesired Signal) and the frequency selectivity. In general, the operation of the previously proposed cancellers up to now are based on the iterative decision feedback. In the meantime for the sacrifice of the computational complexity, the interference cancellers could include the guard interval length to enjoy a more gain in the canceller operation. Although the concept of GI inclusion in the cancellation can bring the improved reliability, its operational feature, especially how to combine a GI, affects the degree of computational complexity and the performance.

Secondly, the interference canceller should consider the hardware complexity since the main advantage of OFDM, i.e., simple receiver structure, should not be ignored. Accordingly, there can be two factors determining the hardware complexity. One depends on whether the canceller operation is performed in time domain (TD) or frequency domain (FD), and the other is how to equalize the wireless channel distortion under the existence of the interference. For the wireless channel equalization it can also be performed in time domain or frequency domain, respectively.

Thirdly, the interference canceller should not overlook the latency, which is also related to the computational complexity by which the packet delay is determined. In other words, it is favorable that the canceller had better not take the matrix inverse operation as best as possible because the computational complexity is critical, especially in the large size of N-FFTed OFDM system. Meanwhile, the latency is accentuated in the canceller employing the turbo equalization. Even though the performance of the canceller can be more resistant not only to the small D/U environment but also to the frequency selective channel, the computational complexity in the turbo equalized is largely affected by how to incorporate the channel coding gain.

By now, there are several approaches in designing the interference canceller. According to canceller operation, the previous cancellers can be classified into time domain and frequency domain canceller, and those cancellers are adopting the channel equalization in time domain and frequency domain. Most of the cancellers are based on the decision feedback for ISI cancellation, while several different approaches are applied for ICI cancellation. In the following sub-chapters those cancellers are introduced and explained with respect to their features.

2.2.1 Interference Cancellation

When the wireless channel delay exceeds the guard interval, there occur two detrimental effects such as intersymbol (ISI) and intercarrier interference (ICI). The ISI is due to the adjacent OFDM symbol, while ICI is caused by the destruction of the orthogonality among subcarriers.

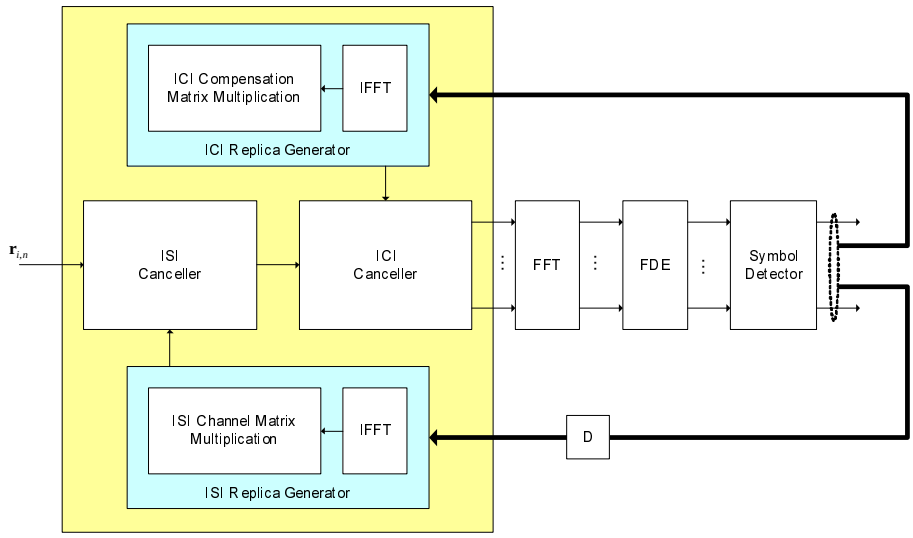

Figure 2.10: Interference canceller operation in TDC.

TDC

The TDC stands for time domain canceller where the signal processing to suppress ISI and ICI is performed in time domain. In other words, the interference cancellation is performed before FFT operation at the receiver. If the receiver could estimate the wireless channel impulse response (WCIR), it means the receiver is to know about the interfered and non-interfered signal parts. The operation of TDC is shown in Fig. 2.10, where ISI and ICI cancellations are all performed in time domain. If the current input of i^{th} OFDM symbol interfered by the $(i-1)^{th}$ OFDM symbol comes into the canceller, ISI is firstly subtracted by using a ISI channel matrix and the $(i-1)^{th}$ OFDM symbol replica. Both ISI channel matrix and the symbol replica are constructed by the WCIR information and tentative symbol decision. After that, ICI cancellation is performed. The representative TDC is found in [2.20], where the canceller is known as RISIC. The operation of RISIC is simplified as shown in Fig. 2.11 and the operation procedures are as follows.

Step-1 The i^{th} symbol interfered by the $(i-1)^{th}$ symbol is received.

Step-2 The i^{th} symbol with the FFT length is taken at the received packet.

Step-3 The ISI cancellation with the previously detected $(i-1)^{th}$ symbol is performed.

Step-4 One-tap FDE to the output of Step-3 is executed, and the tentative symbol detection to the equalized output is performed.

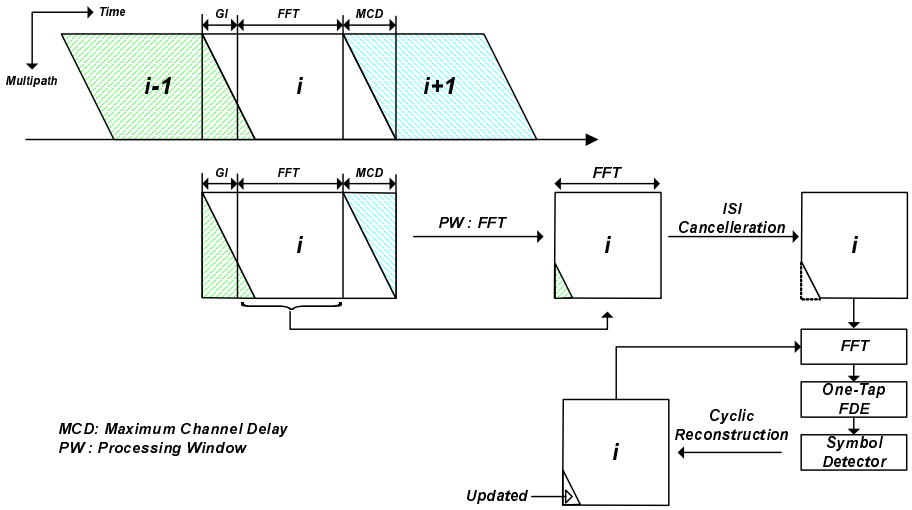

Figure 2.11: Block diagram of the RISIC operation.

Step-5 The detected i^{th} symbol in Step-4 is fed back and the cyclic reconstruction is performed through the convolution of the ISI channel matrix. This is repeated until iteration ends.

The main signal processing in RISIC consists of ISI cancellation and cyclic reconstruction for ICI cancellation. As the characteristics of RISIC, the scheme can be implemented with a rather simple hardware, but the performance is degraded in a severe frequency selective channel, where the symbols experiencing deep fading could be wrongly determined and lead to the unreliable decision feedback operation. In terms of the computational complexity, TDC demands two times of IFFT operation for every iteration compared to the normal operation in OFDM receiver. The concept of ICI cancellation in RISIC is to keep the sinusoidal continuity in the interfered OFDM symbol region in time domain. Consequently, this ICI cancellation method does not require a heavy burden for designing the interference canceller with respect to the computational complexity and hardware complexity. Otherwise, other complex equalization techniques are applied and it causes the interference canceller to be complex.

FDC

Unlike the canceller operation in TDC, the canceller operation in FDC is performed in frequency domain. For the cancellation of ISI the operation is very similar to that of time domain operation. In other words, the cancellation to ISI can be done by using (2.8) and ISI replica.

$$\mathbf{R}_i^{ICI} = \mathbf{R}_i - \mathbf{F}^{-1}\mathbf{H}_i^{isi}\mathbf{x}_{i-1} \tag{2.17}$$

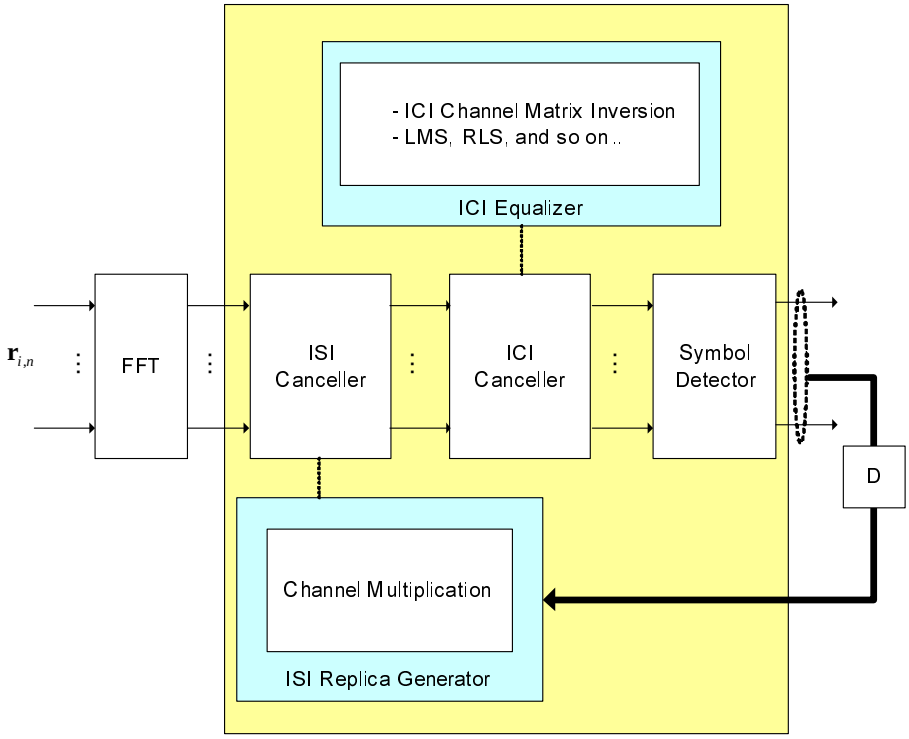

Figure 2.12: Interference canceller operation in FDC.

Compared with ISI cancellation in time domain, ISI cancellation in frequency domain does not bring a benefit of the computational complexity. Even though the IFFT operation to data symbols is avoided, the overall complexity is almost equal in both cases.

In regarding ICI cancellation to (2.17), there can be several approaches. As shown in ICI equalizer of Fig. 2.12, ICI cancellation can be considered as twofold. One is to use the inversion of ICI channel matrix, where it is constructed by $\mathbf{F}^{-1}\mathbf{H}_i^{ici}\mathbf{F}$. If ICI channel matrix is obtained, ICI cancellation is performed to (2.17) by multiplying an inverse matrix of ICI channel matrix.

$$\hat{\mathbf{R}}_i = \frac{\mathbf{R}_i^{ICI}}{\mathbf{F}^{-1}\mathbf{H}_i^{ici}\mathbf{F}} \tag{2.18}$$

This type of ICI cancellation does not require iterative canceller operation, but it largely depends on the composition of the precise ICI channel matrix, and the matrix inversion demands a heavy computational complexity, particularly in OFDM system with the large size of FFT operation. For more information the operation procedure can be referred to [2.21]. The other ICI equalizers can be found in [2.22], where ICI cancellation is to apply the windowing and the maximum likelihood sequence estimation (MLSE). Considering Figs. 2.5 and 2.6, since ICI components

at the k^{th} subcarrier are largely caused by the adjacent subcarriers, the MLSE can be performed with the reduced transmitted signal candidates. However, the operation could not be applicable to high level modulations such as 16QAM and 64QAM because of the increased computational complexity. For other ICI cancellation methods, they utilize the linear equalization per subcarrier such as LMS and those cancellers can be referred to [2.23].

In summary, the computational complexity of ISI cancellation in both TDC and FDC is almost same, but ICI cancellation in TDC demands less computational complexities than that of FDC because ICI cancellation in FDC is performed per subcarrier or it requires the inverse matrix operation. In terms of the performance, TDC is rather more sensitive to the large interference and the frequency selectivity than FDC since it depends on the tentative symbol replicas. Consequently, it is expected that the advantage and disadvantage in both TDC and FDC could depend on the detrimental parasitic effects rather than on the performance and computational complexity. As an example of the detrimental parasitic effects, the sensitivity of the performance degradation due to wrongly composed channel matrix can be exemplified.

2.2.2 Channel Equalization

For channel compensation in the interference canceller, there are two types of frequency domain and time domain equalization. The operation of FDE is the same as that of the conventional OFDM receiver, whereas the operation of TDE is based on the estimated channel impulse response (CIR) [2.2] [2.6] [2.11].

FDE

As in the conventional OFDM receiver, the channel compensation in FDE is performed with the diagonalized channel coefficients which imply the frequency selective characteristics of the subcarriers. Owing to the guard interval insertion, the channel at the receiver can be expressed by circular matrix. From (2.1) the N-FFT points of the i^{th} transmitted OFDM signal experiencing the wireless channel is given by

$$\mathbf{r}_i = \mathbf{H}_i\mathbf{F}\mathbf{s}_i + \mathbf{n}_i \tag{2.19}$$

where the IFFT matrix, $\mathbf{F}$, becomes $N \times N$ matrix by removing the guard interval, and the channel matrix is $N \times N$ circular matrix. For the channel equalization, the FFT to (2.19) becomes

$$\begin{aligned} \mathbf{F}^{-1}(\mathbf{r}_i) &= \mathbf{F}^{-1}(\mathbf{H}_i\mathbf{F}_i\mathbf{s}_i + \mathbf{n}_i) \\ &= \mathbf{F}^{-1}\mathbf{H}_i\mathbf{F}\mathbf{s}_i + \mathbf{F}^{-1}\mathbf{n}_i \\ &= \mathbf{D}_i\mathbf{s}_i + \mathbf{N}_i \end{aligned} \tag{2.20}$$

where the FFT matrix is the Hermitian of the IFFT matrix. The $N \times N$ diagonal matrix, $\mathbf{D}_i$ has the elements of $d_k = \sum_{l=0}^{L-1} h_l \exp(-j\frac{2\pi kl}{N})$, where $k = 0, 1, \ldots, N-1$. As a result, the equalization to (2.20) can be simply performed with one-tap frequency domain equalizer (FDE) to compensate for the channel distortion per subcarrier.

TDE

After ISI cancellation to the interfered i^{th} received OFDM signal of (2.5) is performed, the resulting signal can be rewritten by (2.21).

$$\begin{aligned} \mathbf{r}_i^{ICI} &= \mathbf{r}_i - \mathbf{H}_{i-1}^{isi}\mathbf{F}\mathbf{s}_{i-1} \\ &= \mathbf{H}_i^{ici}\mathbf{F}\mathbf{s}_i + \underbrace{\mathbf{n}_i^{res,isi} + \mathbf{n}_i} \\ &= \mathbf{T}_i^{ici}\mathbf{s}_i + \mathbf{n}_{i,tot} \end{aligned} \tag{2.21}$$

where the matrix, $\mathbf{H}_i^{ici}$ is ICI channel matrix, and $\mathbf{n}_i^{res,isi}$ denotes the residual ISI at the i^{th} symbol. When the i^{th} OFDM symbol vector is transmitted, the transfer functions that the i^{th} OFDM symbol vector experiences before FFT operation of the receiver are IFFT and wireless channel. Accordingly, it is concluded that TDE is how to compensate both transfer functions.

As an initial equalizer to ISI free symbol block of (2.21), there are several time domain equalizers such as zero forcing (TDE-ZF), maximal ratio combining (TDE-MRC), or minimum mean square error combining (TDE-MMSEC). First of all, the TDE-ZF equalization matrix is obtained by taking an inverse of the estimated channel matrix, $\widetilde{\mathbf{T}}_i^{ici}$ so that the TDE-ZF to (2.21) gives the i^{th} equalized symbol vector, $\widetilde{\mathbf{s}}_{i,ZF}$ in

$$\widetilde{\mathbf{s}}_{i,ZF} = \mathbf{s}_i + \frac{\mathbf{n}_{i,tot}}{\widetilde{\mathbf{T}}_i^{ici}} \tag{2.22}$$

The TDE-ZF requires an inverse matrix and the second term of (2.22) brings about the noise amplification in the deep faded sub-carriers.

The TDE-MRC equalization matrix is found by the Hermitian of the $\widetilde{\mathbf{T}}_i^{ici}$. By applying the TDE-MRC to (2.21), the equalized symbol vector becomes

$$\widetilde{\mathbf{s}}_{i,MRC} = \left(\widetilde{\mathbf{T}}_i^{ici}\right)^H \mathbf{T}_i^{ici}\mathbf{s}_i + \left(\widetilde{\mathbf{T}}_i^{ici}\right)^H \mathbf{n}_{i,tot} \tag{2.23}$$

Unlike TDE-ZF, it does not need an inverse channel matrix and there is no noise amplification. However, the result of $(\widetilde{\mathbf{T}}_i^{ici})^H\mathbf{T}_i^{ici}$ is not diagonalized due to the destruction of the orthogonality between the IFFT and FFT matrices so that the interference among the sub-carriers exists. Finally, the TDE-MMSEC equalization matrix can be calculated by finding a matrix, $\mathbf{W}$ that minimizes the cost function ($\mathbf{J}$), $\mathbf{J} = E\left\{|\mathbf{W}\mathbf{r}_i - \mathbf{d}_i|^2\right\}$ where $\mathbf{d}_i$ is the reference. The equalization matrix, $\mathbf{W}$ can be

found in

$$\mathbf{W} = \frac{(\widetilde{\mathbf{T}}_i^{ici})^H}{\left((\widetilde{\mathbf{T}}_i^{ici})^H \mathbf{T}_i^{ici} + \widetilde{\sigma}^2 \mathbf{I}\right)} \tag{2.24}$$

where $\mathbf{I}$ denotes the $N \times N$ identity matrix. The $\widetilde{\sigma}^2$ is the estimated noise variance that is assumed as common to all the subcarriers, and can be calculated by

$$\widetilde{\sigma}^2 = E\left\{|\mathbf{r}_i^{ICI} - \widetilde{\mathbf{T}}_i^{ici}\widehat{\mathbf{s}}_i|^2\right\} \tag{2.25}$$

However, the i^{th} detected symbol vector, $\widehat{\mathbf{s}}_i$ is not available in the initial processing. Therefore, the TDE-MMSEC can be applicable in the iterative processing. Even if the $\widehat{\mathbf{s}}_i$ is known in the initial symbol detection, the TDE-MMSEC in the single antenna receiver does supply a negligible diversity gain, particularly in a time-invariant wireless channel. By applying (2.24) to (2.21), the equalized symbol vector can be detected in

$$\widetilde{\mathbf{s}}_{i,MMSEC} = \frac{(\widetilde{\mathbf{T}}_i^{ici})^H \mathbf{T}_i^{ici}\mathbf{s}_i + (\widetilde{\mathbf{T}}_i^{ici})^H \mathbf{n}_{i,tot}}{\left((\widetilde{\mathbf{T}}_i^{ici})^H \mathbf{T}_i^{ici} + \widetilde{\sigma}^2 \mathbf{I}\right)} \tag{2.26}$$

The TDE-MMSEC equalizer can achieve the best performance by avoiding the noise amplification at the sacrifice of the computational complexity such as the matrix inversion and the noise power estimation. However, the matrix inversion in OFDM with a large FFT size costs too much computational complexity ($\mathbf{O}(N^3)$), and also it is not easy to estimate the noise power since the detected symbol vector is not available in the initial processing. Although the theoretical noise power estimation can be applied, its estimation results would not be reliable. As a result, the TDE-MRC is a candidate which can be well balanced with the performance and the computational complexity.

2.3 Representative Previous Cancellers Including GI

As explained in the previous sub-chapter, the interference canceller can be designed in time domain and frequency domain. Moreover, the interference cancellers can be further classified depending on the selection of the canceller processing window and the adoption of turbo equalization [2.24]− [2.27]. Up until now, most of the previously proposed interference cancellers take a processing window size of N-FFT length, and the canceller operation is very susceptible to the large interference and severe frequency selectivity because the canceller operation is based on the decision feedback of the tentatively determined symbol replicas.

In this sub-chapter, the canceller that adopts turbo equalization and takes the extended processing window is described. In general, the interference canceller takes the canceller processing window of N-FFT size, i.e., the canceller operates

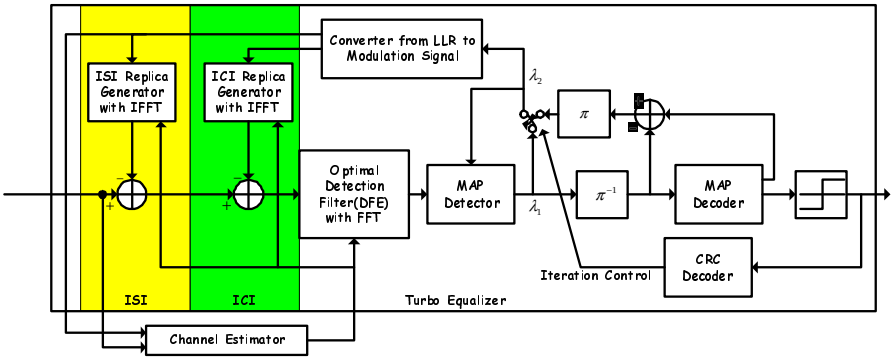

Figure 2.13: Turbo equalized canceller proposed in [2.24].

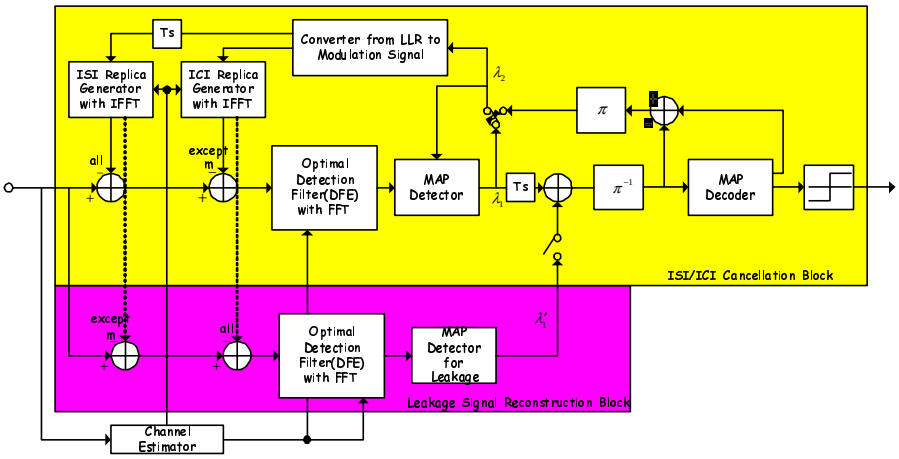

Figure 2.14: Turbo equalized canceller proposed in [2.25].

after removing the guard interval that is normally inserted about 20% of the OFDM symbol duration. Accordingly, the canceller with the extended processing window can enjoy the gain by including the loss of guard interval. As for the adoption of turbo equalization, the canceller operation without a help of channel coding gain is always exposed to the unreliable decision feedback in frequency selective channel since the decision of the symbol replica is executed in the frequency domain. At the sacrifice of the computational complexity and latency, the turbo equalized canceller with the extended processing window is a countermeasure against the large interference and severe frequency selectivity.

2.3.1 Turbo Equalized Canceller

The previous turbo equalized canceller takes the different processing window. The processing window for each case is referred to Fig. 2.1, where the cancellers in [2.24] and [2.25] takes the processing window of '$N+G$' and '$N+G+L$', respectively. The

canceller operations of both schemes are shown in Figs. 2.13and 2.14. The basic canceller operation is similar in both schemes, but the difference can be found in the leakage signal reconstruction in Fig. 2.14, where the block combines the i^{th} OFDM symbol smeared into the $(i+1)^{th}$ OFDM symbol. In other words, the canceller in [2.25] takes the entire symbol duration of the targeted OFDM symbol. The turbo equalized canceller operation begins when CRC from the normal receiver operation fails. In the first iteration the canceller starts with the map decoder outputs. The channel matrix for the entire i^{th} OFDM symbol can be divided into three parts. Each part is expressed by (2.27), (2.28), and (2.29), provided that the estimated channel coefficient is denoted by β_l.

$$\mathbf{H}_{ICI} = \begin{bmatrix} \beta_0 & 0 & \cdots & \cdots & 0 \\ \vdots & \ddots & \ddots & \ddots & \vdots \\ \beta_L & \cdots & \beta_0 & \cdots & 0 \\ \vdots & \vdots & \vdots & \vdots & \vdots \\ 0 & \cdots & \cdots & \cdots & \beta_L \end{bmatrix} \tag{2.27}$$

$$\mathbf{H}_{pre} = \begin{bmatrix} 0 & \beta_L & \cdots & \cdots & \beta_1 \\ \vdots & \ddots & \ddots & \ddots & \vdots \\ 0 & \cdots & 0 & \ddots & \vdots \\ \vdots & \vdots & \vdots & \vdots & \beta_L \\ 0 & \cdots & \cdots & \cdots & 0 \end{bmatrix} \tag{2.28}$$

$$\mathbf{H}_{post} = \begin{bmatrix} 0 & 0 & \cdots & \cdots & 0 \\ \beta_0 & \ddots & \ddots & \ddots & \vdots \\ \vdots & \ddots & \cdots & \cdots & 0 \\ \vdots & \ddots & \vdots & \vdots & \vdots \\ \beta_{L-1} & \cdots & \beta_0 & \cdots & 0 \end{bmatrix} \tag{2.29}$$

where L denotes the index of the maximum channel delay. The first part of $\mathbf{H}_{ICI}$ is $[(N+G+L)\times(N+G)]$ ICI channel matrix for the delayed version of the i^{th} OFDM symbol, the second part of $\mathbf{H}_{pre}$ is $[(N+G+L)\times(N+G)]$ channel matrix from the $(i-1)^{th}$ OFDM symbol, and the third part of $\mathbf{H}_{post}$ is also $[(N+G+L)\times(N+G)]$ channel matrix from the $(i+1)^{th}$ OFDM symbol. Therefore, the entire i^{th} OFDM symbol is written by

$$\mathbf{r}_i = \mathbf{H}_c\mathbf{s}_i + \mathbf{H}_{-1}\mathbf{s}_{i-1} + \mathbf{H}_{+1}\mathbf{s}_{i+1} + \mathbf{n}_i \tag{2.30}$$

where $\mathbf{H}_c = \mathbf{H}_{ICI}\mathbf{F}$, $\mathbf{H}_{-1} = \mathbf{H}_{pre}\mathbf{F}$, $\mathbf{H}_{+1} = \mathbf{H}_{post}\mathbf{F}$ with $[(N+G)\times N]$ IFFT matrix, $\mathbf{F}$.

When it comes to the size of channel matrices, the size of channel matrices in [2.24] is reduced to $[(N+G)\times N]$ since the canceller of [2.24] does not include

the leakage signal part into the $(i+1)^{th}$. Considering that, the processing window can be given by

$$\mathbf{r'}_i = \hat{\mathbf{H}}_c \mathbf{s}_i + \hat{\mathbf{H}}_{-1} \mathbf{s}_{i-1} + \mathbf{n}_i \tag{2.31}$$

Given the $(i-1)^{th}$ symbol replica, ISI cancellation is performed to (2.31). Likewise, ISI cancellation in [2.25] is performed with the $(i-1)^{th}$ and $(i+1)^{th}$ symbols.

For ICI cancellation, the cancellers subsequently subtract ICI replica from the output of ISI cancellation. The operation of ICI cancellation is expressed by (2.32).

$$\mathbf{r}_i(k) = \mathbf{r}_{c,i} - \hat{\mathbf{H}}'_c \hat{\mathbf{s}}_i(k) \tag{2.32}$$

where $\hat{\mathbf{s}}_i(k) = [\hat{s}_{i,0} \cdots \hat{s}_{i,k-1}\ 0\ \hat{s}_{i,k+1} \cdots \hat{s}_{i,N-1}]$. Since ICI is caused by the adjacent data symbols, ICI cancellation for data symbol at the k^{th} subcarrier is to eliminate all data symbols except k^{th} data symbol. In a similar way, ICI cancellation is performed for the other data symbols.

After finishing ISI and ICI cancellation for the k^{th} subcarrier, the time domain signal of k^{th} data symbol perturbed by the channel is equalized with the optimal detection filter. The optimal detection filter applies TDE-MMSE to the output of (2.32), and its operation is given by (2.33).

$$\begin{aligned} \tilde{s}_i(k) &= \mathbf{w}_k^H \mathbf{r}_i(k) \\ &= \frac{\hat{\mathbf{h}}_k^H}{\hat{\mathbf{h}}_k^H \hat{\mathbf{h}}_k + \hat{\sigma}_k^2} \mathbf{r}_i(k) \end{aligned} \tag{2.33}$$

where $\hat{\mathbf{h}}_k$ is the k^{th} column vector of $\hat{\mathbf{H}}'_c$ or $\hat{\mathbf{H}}_c$. As mentioned in the previous sub-chapter, the application of TDE-MMSE in single antenna system does provide negligible benefit under the time-invariant channel environment. After all, the TDE-MRC with ICI channel matrix is suitable as a channel equalization filter.

The above-mentioned turbo equalized cancellers supported by the inclusion of guard interval and channel coding gain could be robust to the large interference and frequency selective channel. However, the disadvantages of the cancellers can be found in the performance and computational complexity. The cancellers can improve the performance by the decision feedback of the decoded bits and also combines the entire symbol duration. However, there can be found two defects in the cancellers. One is the computational complexity in ICI cancellation, and the other is the positive feedback, possibly incurred by including the non-interfered part of a received symbol as a processing window. Besides, the performance of the cancellers is subject to the channel coding rate. Therefore, it is very challenging work of how to incorporate the interference canceller and turbo equalization.

2.4 References

[2.1] S. Chen, and C. Zhu, "ICI and ISI analysis and mitigation for OFDM systems with insufficient cyclic prefix in time-varying channels," IEEE Trans. Consumer Electron., vol. 50, no. 1, pp. 78–83, Feb. 2004.

[2.2] S. Chen, and T. Yao, "FEQ for OFDM systems with insufficient CP," IEEE Proc. PIMRC, vol. 1, pp. 550–553, Sept. 2003.

[2.3] R. Baldemair, and P. Frenger, "A time-domain equalizer minimizing intersymbol and intercarrier interference in DMT systems," IEEE Proc. GLOBECOM, vol. 1, pp. 381–385, Nov. 2001.

[2.4] J. L. Seoane, and S. K. Wilson, "Analysis of intertone and interblock interference in OFDM when the length of the cyclic prefix is shorter than the length of the impulse response of the channel," IEEE Proc. GLOBECOM, vol. 1, pp. 32–36, Nov. 1997.

[2.5] V. D. Nguyen, and H. Kuchenbecker, "Intercarrier and intersymbol interference analysis of OFDM systems on time-invariant channels," IEEE Proc. PIMRC, vol. 4, pp. 1482–1487, Sept. 2002.

[2.6] M. Batariere, K. Baum, and T. P. Krauss, "Cyclic prefix length analysis for 4G OFDM systems, "IEEE Trans. Vehicular. Technol., vol. 1, pp. 543–547, Sept. 2004.

[2.7] L. Sun, and A. Sano, "OFDM Receiver for long multipath interferences via frequency-domain identification approach," IEEE Proc. SPAWC, pp. 1–5, June 2007.

[2.8] O. Landau, and A. J. Weiss, "OFDM guard interval : analysis and observations," IEEE Proc. ICASSP, vol. 3. pp. III-93–III96, Apr. 2007.

[2.9] H. Steendam, and M. Moeneclaey, "Analysis and optimization of the performance of OFDM on frequency-selective time selective fading channels," IEEE Trans. on Commun., vol. 47, no. 12, pp. 1811–1819, Dec. 1999.

[2.10] Y. Sun, and L. Tong, "Channel equalization for wireless OFDM systems with ICI and ISI," IEEE Proc. ICC, vol. 1, pp. 182–186, June 1999.

[2.11] Y. Sun, and L. Tong, "Channel equalization using one-tap DFE for wireless OFDM systems with ICI and ISI," IEEE Proc. SPAWC, pp. 146–149, May 1999.

[2.12] Y. Wang, H. M. Chen, Y. L. Jin, and Z. Wu, "Design of a novel frequency domain equalizer for OFDM systems," IEEE Proc. WiCOM, pp. 365–368, Sept. 2007.

[2.13] J. Zhu, W. Ser, and A. Nehorai, "Channel equalization for DMT with insufficient cyclic prefix," Intl. Conf. on Signals, Systems and Computers, vol. 2, pp. 951–955, Nov. 2000.

[2.14] A. F. Molisch, M. Toeltsch, and S. Vermani, "Iterative methods for cancellation of intercarrier interference in OFDM systems," IEEE Trans. on Vehicular Technol., vol. 56, no. 4, pp. 2158–2167, July 2007.

[2.15] L. Zhao, and B. Yang, and A. Men, "A new equalization scheme for OFDM systems with insufficient guard interval," IEEE Proc. WiCOM, pp. 1-4, Oct. 2008.

[2.16] C. Wang, and Z. Zhou, "A new detection algorithm for OFDM system without cyclic prefix," Proc. of the IEEE 6th Circuits and Systems Symposium on Emerging Technol., vol. 2, pp. 453–456, June 2004.

[2.17] S. Kunaruttanapruk, and S. Jitapunkul, "The novel decision feedback equalizer for OFDM system with insufficient cyclic prefix," Communication Networks and Services Research, pp. 19–24, May 2004.

[2.18] T. Karp, M. J. Wolf, S. Trautmann, and N. J. Fliege, "Zero-forcing frequency domain equalization for DMT systems with insufficient guard interval," IEEE Proc. ICASSP, vol. 4, pp. IV221–IV224, Apr. 2003.

[2.19] E. Viterbo, and K. Fazel, "How to combat long echoes in OFDM transmission schemes: Sub-channel equalization or more powerful channel coding," IEEE Proc. GLOBECOM, vol. 3, pp. 2069–2074, Nov. 1995.

[2.20] D. Kim and G.L. Stber, "Residual ISI cancellation for OFDM with applications to HDTV broadcasting," IEEE J. Sel. Areas Commun., vol. 16, no. 8, pp. 1590–1599, Oct. 1998.

[2.21] H. J. Yu, M. S. Kim, T. H. Jeon, and S. K. Lee, "Equalization scheme for OFDM systems in long delay spread channels," IEEE Proc. PIMRC, vol. 2, pp. 1297–1301, Sept. 2004.

[2.22] S. Suyama, M. Ito, H. Suzuki, and K. Fukawa, "A scattered pilot OFDM receiver with equalization for multipath environments with delay differenece greater than guard interval," IEICE Trans. Commun., vol. E86-B, no. 1, Jan. 2003.

[2.23] M. Itami, H. Takano, H. Ohta, and K. Itoh, "A method of equalization of OFDM signal with inter-symbol and inter-channel interferences," IEEE Proc. ICCS, vol. 1, pp. 109–113, pp. 14-18, Nov. 1994.

[2.24] S. Suyama, S. Suzuki, and K. Fukawa, "An OFDM receiver employing turbo equalization for multipath environments with delay spread greater than the guard interval," IEEE Proc. Vehicular Technol., vol. 1, pp. 632–636, Apr. 2003.

[2.25] Y. Sagae, S. Suyama, H. Suzuki, and K. Fukawa, "An OFDM turbo equalizer for scattered pilot signals in multipath environments with delay difference greater than guard interval," IEEE Proc. Vehicular Technol., vol. 1, pp. 425–429, May 2004.

[2.26] M. Grossmann, M. Schneider, R. S. Thoma, "Turbo equalization for MIMO-OFDM transmission with insufficient guard interval," 2006 International Zurich Seminar on Commun., pp. 114-117, 2006.

[2.27] M. Torabi, M. R. Soleymani, "Turbo coded OFDM for wireless local area networks," IEEE Proc. CCECE, vol. 3, pp. 1363–1367, May 2002.

Chapter 3

Interference Canceller Based on Double Window Cancellation and Combining

In a slowly fading wireless channel, the multipath that exceeds the cyclic prefix (CP) or the guard interval (GI) causes orthogonal frequency division multiplexing (OFDM) systems to hardly achieve high data rate transmission due to the inter-symbol interference (ISI) and the inter-carrier interference (ICI). In this proposal the new canceller scheme, named as Double Window Cancellation and Combining (DWCC) is proposed. It includes the entire symbol interval, delayed by multipath as a signal processing window and intends to improve the performance by combining the double windows that can be formed by the pre- and post-ISI cancellation and reconstruction to the received OFDM symbol interfered by the multipath exceeding the guard interval. The proposed scheme has two algorithm structures of the DWCC-I and -II which are distinguished by the operational sequence (Symbol-wise or Group-wise) to the OFDM symbols of the received packet and by the selection of the processing window in the iterative decision feedback processing. Since the performance of the canceller is dependant on the equalization, particularly on the initial equalization, the proposed schemes operate with the time and frequency domain equalizer in the initial and the iterative symbol detection, respectively. For the verification of the proposed schemes, each scheme is evaluated in turbo coded OFDM for low (QPSK) and high level modulation systems (16QAM, 64QAM), and compared with the conventional canceller with respect to the performance and computational complexity. As a result, the proposed schemes do not have an error floor even for 64QAM in a severe frequency selective slow fading channel.

3.1 Background of Proposal

To achieve the demand of the high data rate services, the orthogonal frequency division multiplexing (OFDM) was introduced as a candidate of transmission modulation. The main characteristics of OFDM with a long symbol length inserted by GI are the robustness to the wireless channel with a long multipath delay, and make it possible to implement an equalizer with a simple structure since the increased symbol duration satisfies the fading channel of each subcarrier to be flat. In addition, the flexible management of the subcarriers such as Adaptive Modulation and Coding (AMC) per subcarrier is the advantage of OFDM [3.1] [3.2]. In particular, the adoption of OFDM has been very attractive to the terrestrial broadcasting known as single frequency network (SFN) such as Integrated Services Digital Broadcasting (ISDB) in Japan [3.3], Digital Audio Broadcasting (DVB) and Digital Terrestrial Television Broadcasting (DTTB) in Europe [3.4]. The high signal to noise ratio (SNR) in the SFN can be achieved by combining all the same information from the base stations, but the large channel delay over GI is inevitable which results in ISI and ICI [3.5]. Even if the enough GI duration in OFDM system can be a solution, it is limited to the certain level because the increased GI is directly related to the losses of the frequency efficiency and the power. Accordingly, the efficient canceller is required.

The cancellers ever known can be grouped into the time domain canceller (TDC) and the frequency domain canceller (FDC) with time domain or frequency domain equalization. In brevity, the TDC-TDE denotes the time domain cancellation with time domain equalization. The representative TDC-FDE has been proposed in [3.6], called as the residual ISI cancellation (RISIC) which is the simplest canceller ever known. Even though the system is simple with one-tap frequency domain equalizer (FDE), it is very sensitive to the severe frequency selective channel, and also it has a power loss by removing GI. Meanwhile, the TDC-TDE was introduced in [3.7] and [3.8], where the canceller adopts the turbo equalization. Unlike RISIC, it can improve the performance by the decision feedback of the decoded bits and also combines the entire symbol duration. However, the computational complexity, particularly in OFDM with a large FFT size must be a burden due to the symbol detection per subcarrier. For more information on other types of cancellers can be also found in [3.9]– [3.16]. The canceller in this paper is based on the Double Window Cancellation and Combining (DWCC). The proposed schemes intend to combine the extended processing window. In other words, the processing window includes the GI and the delayed signal part of the symbol. As proposed in [3.7] and [3.8], it is not an easy task to combine the extended processing window since the extended processing window can not be directly processed with the Fast Fourier Transform (FFT) so that the canceller demands the heavy computational complexity for the symbol detection. In contrast, the proposed system does not require the ICI cancellation per subcarrier to combine the extended processing window by taking a different look at the received symbol that can be composed of the double windows.

The double windows are constructed by the pre- and post-ISI cancellation by reconstructing the extended processing window. The double windows look like cyclically shifted overlapped windows so that the non-overlapped signal part of the double windows can lead to the noise suppression by combining. The noise in the non-overlapped signal part of the double windows includes the uncorrelated residual ISI, ICI, and the receiver thermal noise.

Meanwhile, the proposed schemes have two different algorithm structures of DWCC-I and -II. Both schemes are distinguished by the operational sequence and by the selection of the processing window in the iterative processing. The former is the symbol-wise canceller, and takes the FFT length for the processing window in iteration, while the latter is the group-wise canceller with the extended processing window length in iteration. As the operational characteristic, DWCC-I pursues the SNR gain after iteration, while DWCC-II pursues the SNR gain during iteration. In addition, the proposed schemes apply a time domain matched filter (TDE-MRC) and frequency domain equalizer (One-Tap FDE) in the initial and the iterative processing, respectively. For the performance evaluation of the proposed schemes, DWCC is simulated in turbo coded OFDM for low and high level modulations. In addition, it is shown that the turbo channel coding itself can play a role as a canceller in low level modulation (QPSK).

3.2 Extended Processing Window Combining Approaches

In consideration of the performance improvement of the canceller operation, there are several ways of extending a processing window to the entire symbol duration. Similarly to turbo equalized canceller introduced in Chap. 2, the canceller operated by subtraction based ICI cancellation can extend a processing window at the sacrifice of the computational complexity. Instead, the following two approaches are also a way to readily extend a processing window with less burden of the computational complexity since it does not demand ICI cancellation per subcarrier, and the characteristic of each approach is investigated here.

3.2.1 Combining Approach - I

In Fig. 3.1 the i^{th} received symbol is shown where N-FFT = 16, GI = 4, and MCD = 7. The entire i^{th} symbol is interfered by the $(i-1)^{th}$ and $(i+1)^{th}$ symbols, respectively, so the i^{th} received symbol, $\mathbf{r}_{i,ext}$ can be defined by (3.1).

$$\mathbf{r}_{i,ext} = \mathbf{H}_i^{ici}\mathbf{x}_i + \mathbf{H}_{i-1}^{isi}\mathbf{x}_{i-1} + \mathbf{H}_{i+1}^{isi}\mathbf{x}_{i+1} + \mathbf{n}_i \tag{3.1}$$

where $\mathbf{x}_i$ is the IFFTed output of the i^{th} modulated symbol vector, and $\mathbf{H}_i^{ici}$, $\mathbf{H}_{i-1}^{isi}$, and $\mathbf{H}_{i+1}^{isi}$ are defined by (2.27), (2.28), and (2.29), respectively. After the pre- and post-ISI are cancelled out with the replicas of the $(i-1)^{th}$ and $(i+1)^{th}$ symbols, the

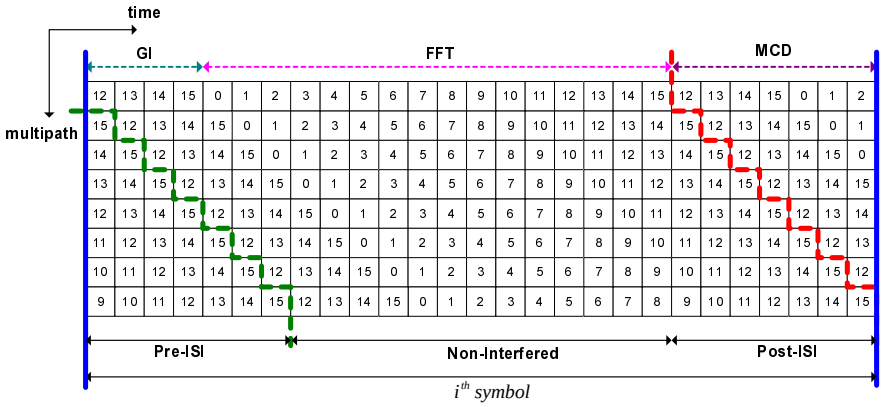

Figure 3.1: i^{th} symbol block interfered by pre- and post-symbol of $(i-1)^{th}$ and $(i+1)^{th}$.

result can be shown in Fig. 3.2. If the delayed signal part smeared into the $(i+1)^{th}$ symbol is moved into the front as shown in Fig. 3.2, the i^{th} symbol is recomposed as shown in Fig. 3.3. As a result, (3.1) can be reexpressed by

$$\mathbf{r}_{i,ext} = \mathbf{H}_i\mathbf{x}_i + \mathbf{n}_{i-1}^{res,isi} + \mathbf{n}_{i+1}^{res,isi} + \mathbf{n}_i \tag{3.2}$$

where the circular channel matrix, $\mathbf{H}_i$ is $N' \times N'$ matrix, and N' is equal to $(GI+N)$. This combining method does not need a computational operation for the cyclic reconstruction, but the symbol detection needs to be performed per subcarrier since the multiplication of $N' \times N$ IFFT matrix and its Hermitian matrix does not satisfy the identity matrix. The operation becomes very similar to TE in [3.7] and [3.8] so that the symbol replicas of the decision feedback in the iterative processing should be reliable enough not to cause the positive feedback due to the inclusion of the non-interfered received signal part. Accordingly, the way of cyclic reconstruction in Fig. 3.2 would not be favorable in OFDM with a large N-FFT size : N times IFFT per iteration only for ICI cancellation.

3.2.2 Combining Approach - II

The DWCC follows the second combining approach. This combining method can be implemented by taking a different look at Fig. 3.2. Figure 3.2 can be seen as Fig. 3.4 where the extended processing window consists of the two windows (Pre- and Post-windows) with N-point IFFT. The two windows can be taken from the beginning and the end of the symbol, respectively. In Fig. 3.4 both windows after pre- and post-ISI cancellation can be expressed in the matrix form as

$$\mathbf{r}_{i,pre} = \mathbf{H}_{i,pre}^{ici}\mathbf{x}_i + \mathbf{n}_{i,pre}^{res,isi} + \mathbf{n}_{i,pre} \tag{3.3a}$$

$$\mathbf{r}_{i,post} = \mathbf{H}_{i,post}^{ici}\mathbf{x}_i + \mathbf{n}_{i,post}^{res,isi} + \mathbf{n}_{i,post} \tag{3.3b}$$

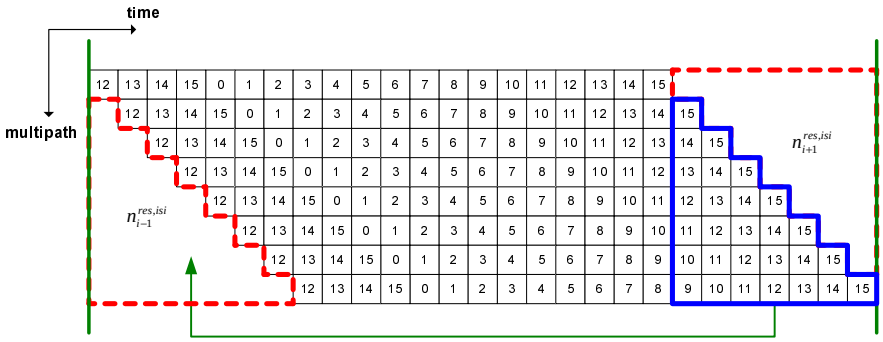

Figure 3.2: i^{th} symbol block after pre- and post-ISI cancellation.

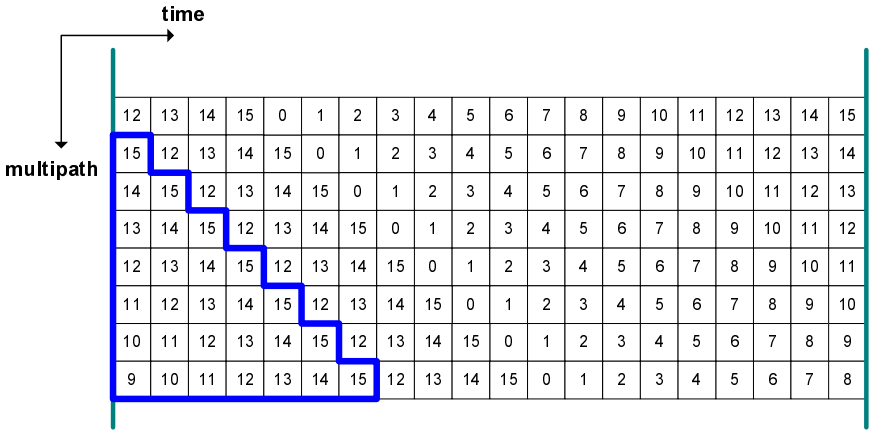

Figure 3.3: Cyclically reconstructed i^{th} symbol block.

where $\mathbf{n}_{i,pre}^{res,isi}$ and $\mathbf{n}_{i,post}^{res,isi}$ are the residual ISI at the i^{th} symbol for both windows. After cyclic reconstruction to (3.3a) and (3.3b) with the matrices of (2.28) and (2.29) is performed, the result is shown in Fig. 3.5. The cyclically reconstructed pre- and post-windows are individually given by

$$\begin{aligned} \mathbf{r}_{i,pre} &= (\mathbf{H}_{i,pre}^{ici}\mathbf{x}_i + \widetilde{\mathbf{H}}_{i,pre}^{isi}\widehat{\mathbf{x}_i}) \\ &\quad +\mathbf{n}_{i,pre}^{res,isi} + \mathbf{n}_{i,pre}^{res,ici} + \mathbf{n}_{i,pre} \qquad (3.4a) \\ \mathbf{r}_{i,post} &= (\mathbf{H}_{i,post}^{ici}\mathbf{x}_i + \widetilde{\mathbf{H}}_{i,post}^{isi}\widehat{\mathbf{x}_i}) \\ &\quad +\mathbf{n}_{i,post}^{res,isi} + \mathbf{n}_{i,post}^{res,ici} + \mathbf{n}_{i,post} \qquad (3.4b) \end{aligned}$$

where the vector, $\widehat{\mathbf{x}_i}$ denotes the IFFTed output of the i^{th} symbol replica, and $\widetilde{\mathbf{H}}_{i,pre}^{isi}$ and $\widetilde{\mathbf{H}}_{i,post}^{isi}$ are the estimated ISI channel matrices. The vectors of $\mathbf{n}_{i,pre}^{res,ici}$ and $\mathbf{n}_{i,post}^{res,ici}$ are the residual ICI at the i^{th} symbol for both windows.. Assuming that the the i^{th}

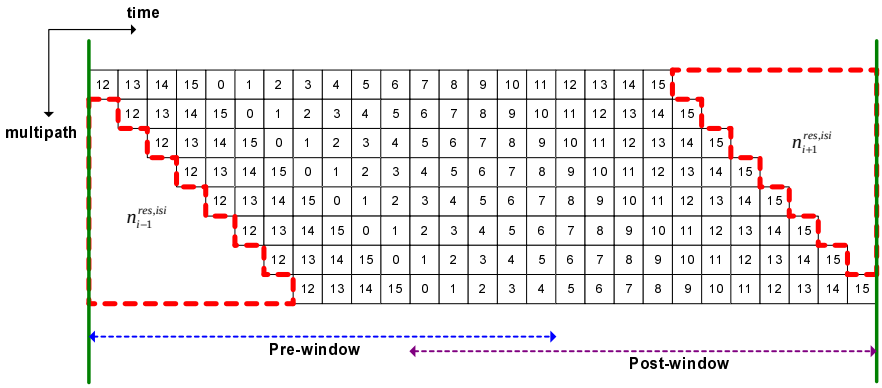

Figure 3.4: Double window in the i^{th} symbol block.

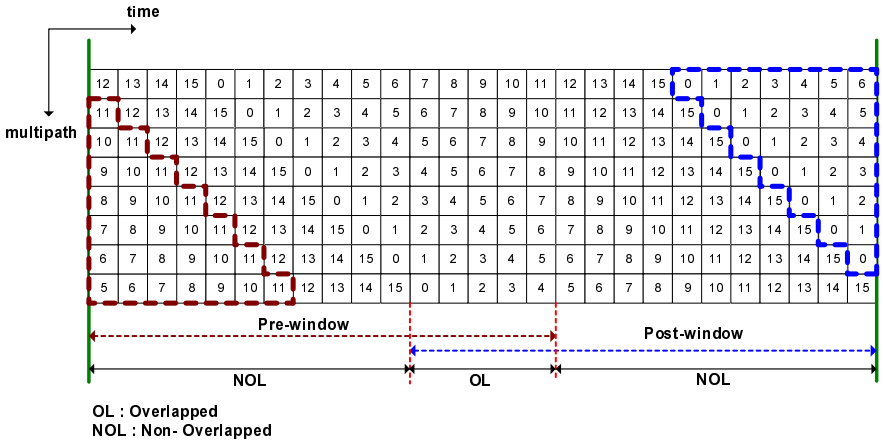

Figure 3.5: Double window after cyclic reconstruction to pre- and post-windows.

symbol replica and the pre- and post-ISI channel estimates are ideal in the brackets in (3.4a) and (3.4b), then $\mathbf{r}_{i,pre}$ and $\mathbf{r}_{i,post}$ are redefined as

$$\begin{aligned} \mathbf{r}_{i,pre} &= (\mathbf{H}_{i,pre}^{ici} + \mathbf{H}_{i,pre}^{isi})\mathbf{x}_i + \mathbf{n}_{i,pre}^{res,isi} + \mathbf{n}_{i,pre} \\ &= \mathbf{H}_{i,pre}^{circ}\mathbf{x}_i + \mathbf{n}_{i,pre}^{res,isi} + \mathbf{n}_{i,pre} \qquad (3.5a) \\ \mathbf{r}_{i,post}^{(1)} &= (\mathbf{H}_{i,post}^{ici} + \mathbf{H}_{i,post}^{isi})\mathbf{x}_i + \mathbf{n}_{i,post}^{res,isi} + \mathbf{n}_{i,post} \\ &= \mathbf{H}_{i,post}^{circ}\mathbf{x}_i + \mathbf{n}_{i,post}^{res,isi} + \mathbf{n}_{i,post} \qquad (3.5b) \end{aligned}$$

where $N \times N$ matrix, $\mathbf{H}_{i,pre}^{circ}$ can be defined by the cyclic shift of $\mathbf{H}_{i,post}^{circ}$. In this way the double windows are to be constructed.

In the meantime, the noise correlation ratio (NCR) between two windows can be defined as

$$NCR = 1 - \frac{(GI + MCD)}{N} \qquad (3.6)$$

where *MCD* denotes the maximum channel delay in sample.

As far as the cyclically reconstructed double windows are reliable enough, it is expected that the combining approach-II supply not a diversity effect but *SNR* gain depending on *NCR*. The relationship of *NCR* and the reliability of symbol replicas in the decision feedback would be inversely proportional since the large channel delay spread reduces the *NCR* but increases ISI and ICI.

3.3 Proposed Interference Canceller

The operations of DWCC-I and -II are described, and the computational complexity is evaluated with respect to the required number of the FFT operations. The processing window of DWCC is the entire i^{th} symbol and the large difference of both schemes can be found in the iterative processing. Meanwhile DWCC-I and -II can be defined as symbol-wise and group-wise canceller, respectively.

3.3.1 DWCC - I

The block diagram of DWCC-I is shown in Fig. 3.6. Figure 3.7 shows the pre- and post-cancellation and combining block in Fig. 3.6. The scheme proceeds as follows.

Step-1 The pre-ISI cancellation is performed to the i^{th} symbol, interfered by $(i-1)^{th}$ symbol where the processing window length is N.

Step-2 The TDE-MRC with ICI channel matrix, $\mathbf{H}_i^{ici}$ is performed to the result of Step-1.

Step-3 The Log-Likelihood Ratio (LLR), $\lambda(b_k)$ is calculated with the equalized i^{th} symbol vector, $\widetilde{\mathbf{p}}_i$. The LLRs of the coded bits are calculated by

$$\lambda(b_k) = \ln\left(\frac{\sum_{s^+\in\mathbf{S},b_k=+1}\exp(-|\widetilde{p}_{i,k}-\widetilde{\beta}_{i,k}s^+|^2)}{\sum_{s^-\in\mathbf{S},b_k=-1}\exp(-|\widetilde{p}_{i,k}-\widetilde{\beta}_{i,k}s^-|^2)}\right) \tag{3.7}$$

where the transmitted coded bit, b_k can be +1 or -1, and s^+ and s^- denote the modulated data symbol with $b_k = +1$ and $b_k = -1$ in a set of the constellation of the modulated symbols, $\mathbf{S}$, respectively. $\widetilde{p}_{i,k}$ and $\widetilde{\beta}_{i,k}$ denote the received data symbol and the channel estimate of the k^{th} sub-carrier in the i^{th} OFDM symbol, respectively.

Step-4 The obtained LLRs are mapped into the QPSK, 16QAM or 64QAM modulated symbols using a symbol mapper and the symbol vector mapped is used for the cyclic reconstruction with the IFFT matrix and ISI channel matrix. The first iteration ends with Step-4. Meanwhile, the cyclically reconstructed i^{th} time domain symbol is ready for the iterative processing.

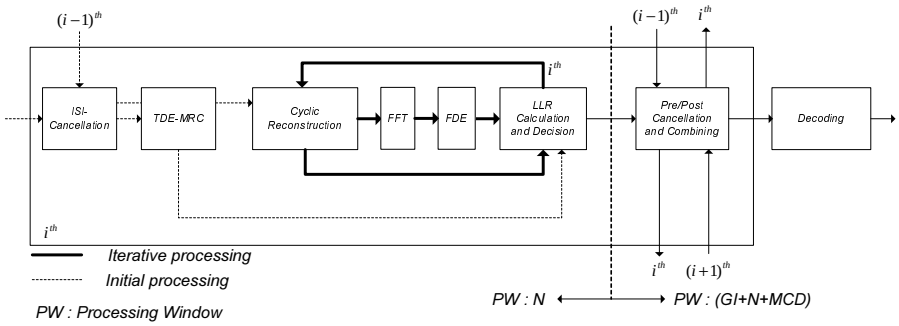

Figure 3.6: Block diagram of DWCC-I operation.

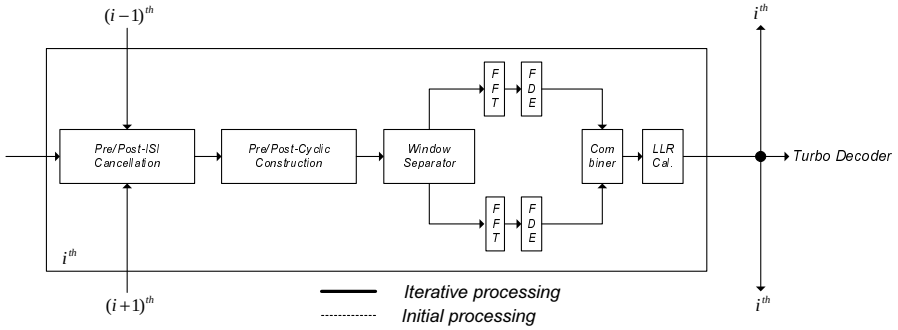

Figure 3.7: Block diagram of Pre- and post-window cancellation and combining in DWCC-I.

Step-5 In the iterative processing the one-tap FDE is applied to the output of Step-4, and the operations from Step-2 to Step-4 are repeated until the iteration ends.

Step-6 After the iteration is finished to the symbols within a packet, the processing window for each symbol is extended to the entire symbol, and the cancellation and cyclic reconstruction to the pre- and post-window are performed to design the double windows as shown in Fig. 3.5. The double windows are combined after one-tap FDE for each window.

In summary, DWCC-I takes the processing window length, N in the initial and iterative processing. Since the canceller processing is performed per symbol based, DWCC-I can be named as the symbol-wise canceller. It can be thought that the performance gain of DWCC-I would be originated from the matched filtering in the initial equalization with TDE-MRC, and from the coherent signal combining gain of the double windows which causes the channel coding gain to increase.

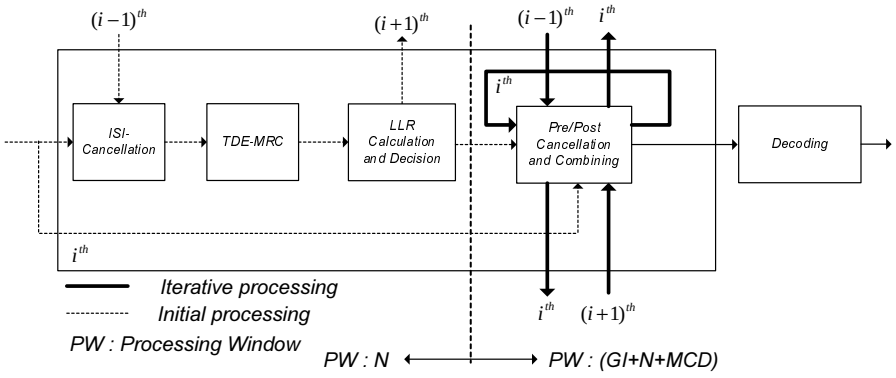

Figure 3.8: Block diagram of DWCC-II operation.

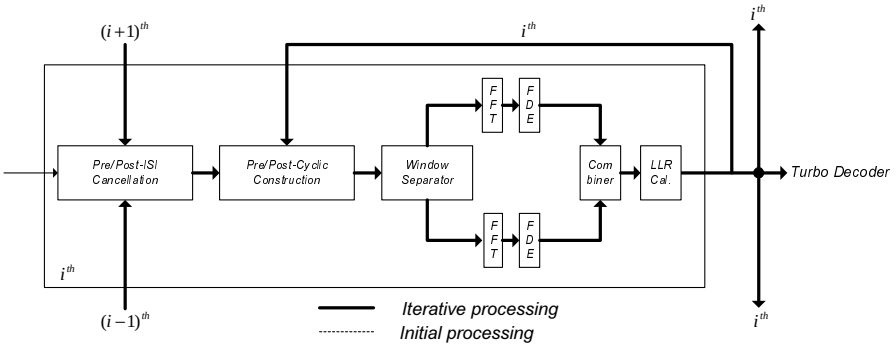

Figure 3.9: Block diagram of Pre- and post-window cancellation and combining in DWCC-II.

3.3.2 DWCC - II

The block diagram of DWCC-II is shown in Fig. 3.8. Figure 3.9 shows the pre- and post-cancellation and combining block in Fig. 3.8. The operation of DWCC-II is to use the double window combined output in the decision feedback. In other words, the difference of DWCC-II and DWCC-I can be found in the iterative processing, where the extended processing window is used. As shown in Fig. 3.8, since DWCC-II cooperates with the adjacent symbol blocks in the iterative processing, it can be named as the group-wise canceller. The initial processing of the scheme proceeds as follows.

Step-1 The pre-ISI cancellation is performed to the i^{th} symbol interfered by the $(i-1)^{th}$ symbol, where the processing window length is limited to N.

Step-2 Follow the Step-2 and Step-3 in DWCC-I operation.

Step-3 The Step-2 is performed to all the symbols within a packet. This is the end

Table 3.1: The required number of the FFT operations.

DWCC-I	2I+8
DWCC-II	6I+1

of the first iteration in DWCC-II.

The iterative processing proceeds as follows.

Step-4 The double window cancellation and combining to the i^{th} received symbol are performed as depicted in Figs. 3.4 and 3.5 using the module in Fig. 3.9.

Step-5 The LLRs for the coded bits are calculated with the combined output symbols.

Step-6 The Step-4 and Step-5 are repeated with the adjacent symbol blocks until the iteration ends.

By generating the symbol replica from the double window combined output, the reliable decision feedback could be achieved. Consequently, the processing window in DWCC-II takes the FFT and extended window length in the initial and iterative processing, respectively. The performance gain of DWCC-II can be obtained by matched filtering in the initial processing and by the reliable symbol detection resulted from the double window combining in the iteration.

3.3.3 Computational Complexity

The computational complexity of the proposed schemes is evaluated, where the criterion is the required number of the FFT operations per symbol. Table 3.1 summarizes the computational complexity. For example, if the number of iteration is set to three, the required number of FFT operations is fourteen and nineteen for DWCC-I and DWCC-II, respectively. However, the commercially available FFT processors such as Vertex-II pro Family can finish 1024 points FFT operation with 1024 clock cycles (3.36 μs) at 305 MHz maximum clock frequency, which is about the triple speed of the FFT processor, introduced in [3.6]. With the rapid advancements in the related field the computational complexity of DWCCs seems to be acceptable.

3.4 Analysis of Proposed Schemes

The basic concept of the double window cancellation and combining (DWCC) is to readily extend the canceller processing window to the entire symbol length and to exploit the coherent combining gain in the canceller operation. The DWCC-I and

DWCC-II have different processing window length in iterative canceller operation. The processing window length of DWCC-I is the N-FFT length (N) in both initial and iterative canceller operations. In contrast, the processing window length of DWCC-II is the N-FFT length in initial canceller operation while it is the entire symbol duration in iterative canceller operation. Meanwhile, DWCC-I performs the double window cancellation and combining once right before channel decoding, whereas DWCC-II performs the double window cancellation and combining in every iteration of iterative canceller operation. To help the understanding of the difference between the two schemes, the algorithmic features of DWCC-I and DWCC-II are summarized in Table 3.2.

In this section it is intended to investigate DWCC with respect to the *SINR* distribution under different delay spread channels. If the entire i^{th} received symbol duration is considered as a processing window, it can be divided into two parts; interfered and non-interfered part. The non-interfered signal part, $r_{i,n}^{free}$ is given by

$$r_{i,n}^{free} = \sum_{l=0}^{L-1} \beta_{i,l} x_{i,(n-l)_N} + \omega_{i,n} \tag{3.8}$$

where (L-G-1) $\leq n <$ N. Meanwhile, the interfered signal part with N-FFT length can be considered as two parts of pre- and post-window. For pre-window the interfered area, $r_{i,n}^{pre-isi}$ from the (i-1)th symbol is expressed by

$$\begin{aligned} r_{i,n}^{pre-isi} &= \sum_{l=0}^{G+n} \beta_{i,l} x_{i,(n-l)_N} + \\ &\quad \sum_{l=G+n+1}^{L-1} \beta_{i,l} x_{i-1,(n-l+G)_N} + \omega_{i,n} \end{aligned} \tag{3.9}$$

where -$G \leq n <$ L-G-1. The post-window, $r_{i,n}^{post-isi}$, interfered by the (i+1)th is given by

$$\begin{aligned} r_{i,n}^{post-isi} &= \sum_{l=0}^{n-N} \beta_l x_{i+1,(n-N-G-l)_N} + \\ &\quad \sum_{l=n-N+1}^{L-1} \beta_{i,l} x_{i,(n-l)_N} + \omega_{i,n} \end{aligned} \tag{3.10}$$

where $N \leq n <$ N+L-1. After all, the entire i^{th} symbol interfered by the adjacent symbols, $r_{i,n}^{ext,isi}$ is the sum of (3.8), (3.9), and (3.10) where -$G \leq n < (N + L - 1)$.

$$r_{i,n}^{ext,isi} = r_{i,n}^{free} + r_{i,n}^{pre-isi} + r_{i,n}^{post-isi} + \omega_{i,n} \tag{3.11}$$

Table 3.2: Algorithmic features of DWCC-I and DWCC-II

Feature	DWCC-I	DWCC-II
Processing window length in initial operation	N	N
Processing window length in iterative operation	N	N+G+MCD
Related symbol in iterative operation	(i-1)th	(i-1)th and (i+1)th
Number of DWCC operation	1	Number of Iterative operation

In case that MCD is within one symbol length, the i^{th} symbol is always relevant to the adjacent symbols of the (i-1)th and (i+1)th. If all three symbol replicas are available from tentative symbol decision, each ISI due to the (i-1)th and (i+1)th symbol can be subtracted in $r_{i,n}^{pre-isi}$ and $r_{i,n}^{post-isi}$, while ICI can be eliminated by cyclic reconstruction with the i^{th} symbol replica and hence and hence the individual result after ISI and ICI cancellations to (3.9) and (3.10) is expressed by (11) and (12).

$$r_{i,n}^{pre,res} = r_{i,n}^{pre-isi} + \sum_{l=G+n+1}^{L-1} \beta_{i,l} \left(\widetilde{x}_{i,(n-l)_N} - \widetilde{x}_{i-1,(n-l+G)_N} \right) \tag{3.12}$$

where $-G \leq n < L - G$-1, and $\widetilde{x}_i$ denotes the IFFT output to the i^{th} symbol replica.

$$r_{i,n}^{post,res} = r_{i,n}^{post-isi} + \sum_{l=0}^{n-N} \beta_{i,l} \left(\widetilde{x}_{i,(n-N-l)_N} - \widetilde{x}_{i+1,(n-N-G-l)_N} \right) \tag{3.13}$$

where $N \leq n < N$+L-1. Finally, the reconstructed i^{th} symbol can be separated into pre- and post-windows, where each window includes N samples and the overlapping length (M) is obtained by [N-(G+MCD)]. By taking FFT to each window, the pre- and post-windows are given by

$$R_{i,k}^{pre-win} = H_{i,k}^{pre} s_{i,k} + W_{i,k}^{pre} \tag{3.14}$$

$$R_{i,k}^{post-win} = H_{i,k}^{post} s_{i,k} + W_{i,k}^{post} \tag{3.15}$$

where $H_{i,k}^{pre}$ and $H_{i,k}^{post}$ are wireless channel coefficients at the k^{th} subcarrier, and $W_{i,k}^{pre}$ and $W_{i,k}^{post}$ include the thermal noise and the residual ISI and ICI at the k^{th} subcarrier

in each window. In a slow fading channel, the channel coefficient of each window per subcarrier can be approximated by (3.16).

$$H_{i,k}^{pre} \simeq H_{i,k}^{post} \cdot \left[\exp\left(j\frac{2\pi}{N}Mk\right)\right] \tag{3.16}$$

where M is the overlapped window length between double windows, noted by 'OL' in Fig. 3.5. After channel equalization, the combined output, $R_{i,k}^{comb}$ is given by (3.17).

$$\begin{aligned} R_{i,k}^{comb} &= \left(\left|H_{i,k}^{pre}\right|^2 + \left|H_{i,k}^{post}\right|^2\right)s_{i,k} \\ &+ \left(H_{i,k}^{pre}\right)^* W_{i,k}^{pre} + \left(H_{i,k}^{pre}\right)^* W_{i,k}^{post} \\ &= \widehat{H}_{i,k}s_{i,k} + \left(H_{i,k}^{pre}\right)^* W_{i,k}^{pre} + \left(H_{i,k}^{pre}\right)^* W_{i,k}^{post} \end{aligned} \tag{3.17}$$

$$\begin{aligned} \sigma_{i,k}^2 &= E[|R_{i,k}^{comb} - \hat{H}_{i,k}\tilde{s}_{i,k}|^2] \\ &= (\sigma_{i,k}^2)^{pre} + (\sigma_{i,k}^2)^{post} \end{aligned} \tag{3.18}$$

where it is assumed that $E[|H_{i,k}^{pre}|^2]$=$E[|H_{i,k}^{post}|^2]$=1, and $\sigma_{i,k}^2$ is the total variance of residual interference and thermal noise at the k^{th} subcarrier, where the increase of thermal noise at the k^{th} subcarrier due to the overlapping double windows, $NCR{\cdot}\sigma_{thermal}^2$ is included in $\sigma_{i,k}^2$ and the noise correlation ratio (NCR) is defined by 1-(G+MCD)/N. Finally, the average $SINR$ of the combined double windows per packet can be expressed as in (3.19) by using (3.17) and (3.18).

$$\begin{aligned} SINR_{packet} &= \frac{1}{N_S}\sum_{i=0}^{N_S-1} SINR_i \\ &= \frac{1}{N_S}\sum_{i=0}^{N_S-1}\left(\frac{1}{N_d}\sum_{k=0}^{N_d-1}\frac{2\left(\left|H_{i,k}^{pre}s_{i,k}\right|^2 + \left|H_{i,k}^{post}s_{i,k}\right|^2\right)}{\sigma_{i,k}^2}\right) \end{aligned} \tag{3.19}$$

where N_S is the number of OFDM symbols per packet and N_d is the number of data symbols per OFDM symbol.

The analysis of the $SINR$ distribution depending on PDBs defined in Fig. 2.7 is presented through the simulation in this paper. The average $SINR$ for 200000 packets and the packet error rate (PER) are shown in Figs. 3.10 and 3.11, respectively. From the results, it is found that DWCC outperforms the conventional canceller [3.6] in all PDBs. In particular, the PER performance of DWCC-II is better than those of the others even in the region where the average $SINR$ is lower than

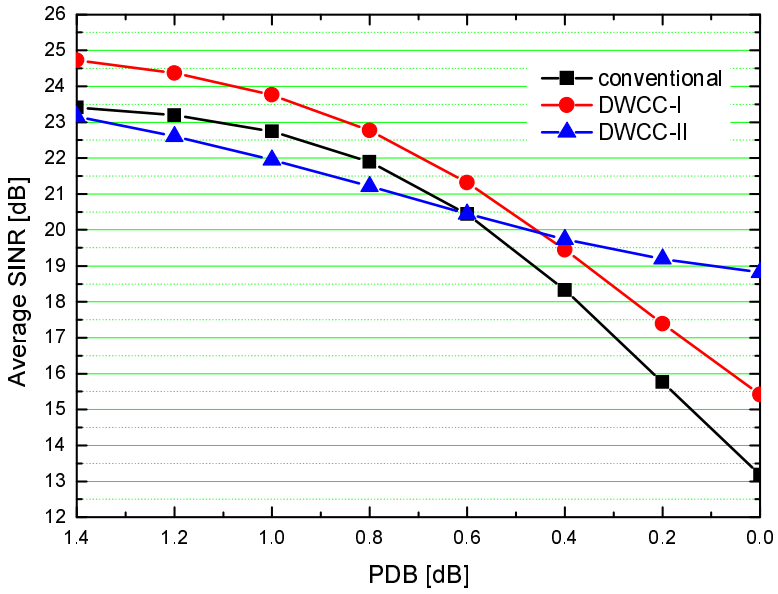

Figure 3.10: Comparison of the average *SINR* in 64QAM at the SNR of 24 dB.

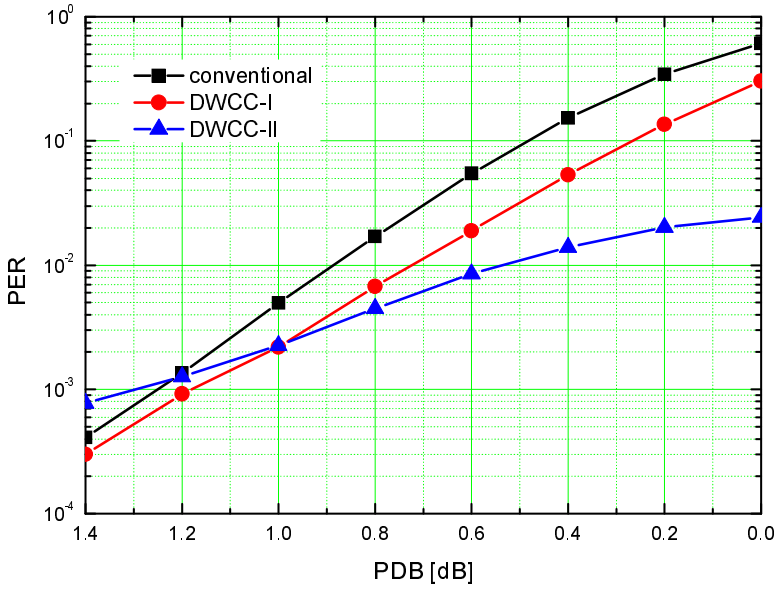

Figure 3.11: *PER* performance comparison in 64QAM at the *SNR* of 24 dB.

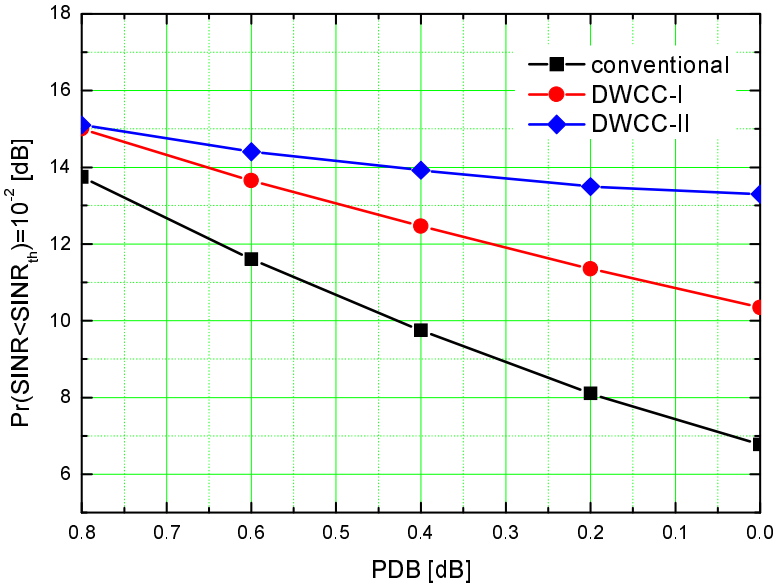

Figure 3.12: $SINR_{th}$ satisfying 10^{-2} *PER* of *CDF* in 64QAM at the *SNR* of 24 dB.

those of the others. For the verification of the fact, the $SINR_{th}$ that satisfies 1 % probability in the cumulative density function (*CDF*) is investigated in Fig. 3.12 where it explains the reason why DWCC-II shows the better performance even in the low average *SINR* region. In the meantime, the performance of DWCC-II is rather worse than that of DWCC-I up to the PDB of 1.0. The difference of DWCC-I and -II can be found in iterative canceller operation, where DWCC-I and -II take NFFT length and the entire symbol length as a processing window, respectively. In other words, the interference caused by extending a processing window in DWCC-II could dominate the combining gain in a non-interference dominant channel environment. Based on the analysis result, it is concluded that the interference adaptive operation of DWCC algorithms is advantageous for the performance.

3.5 Simulation Results and Discussion

For the evaluation of the proposed schemes, the simulation is performed in the turbo coded OFDM for low (QPSK) and high level modulations (16QAM, 64QAM), and compared in four different schemes (Conventional RISIC with FDE and TDE-MRC, DWCC-I and -II).

The system parameters are summarized in Table 3.3. The 10 MHz bandwidth

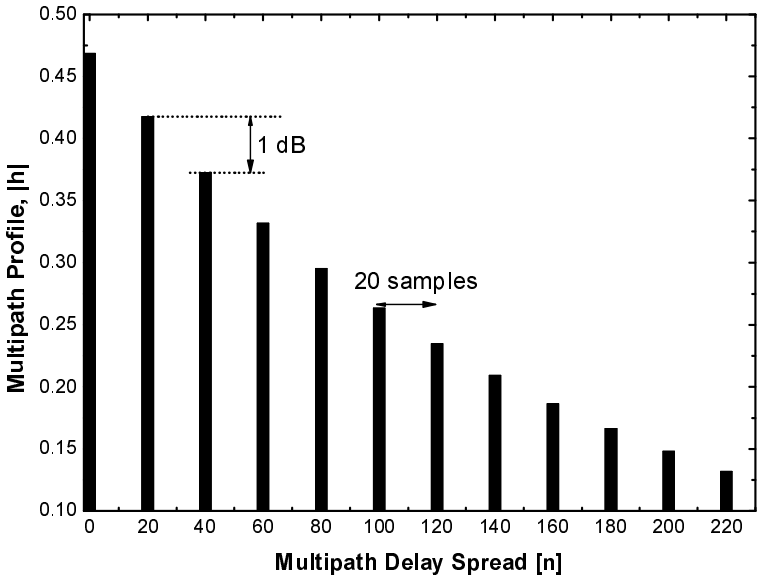

Figure 3.13: Minimum phase channel model.

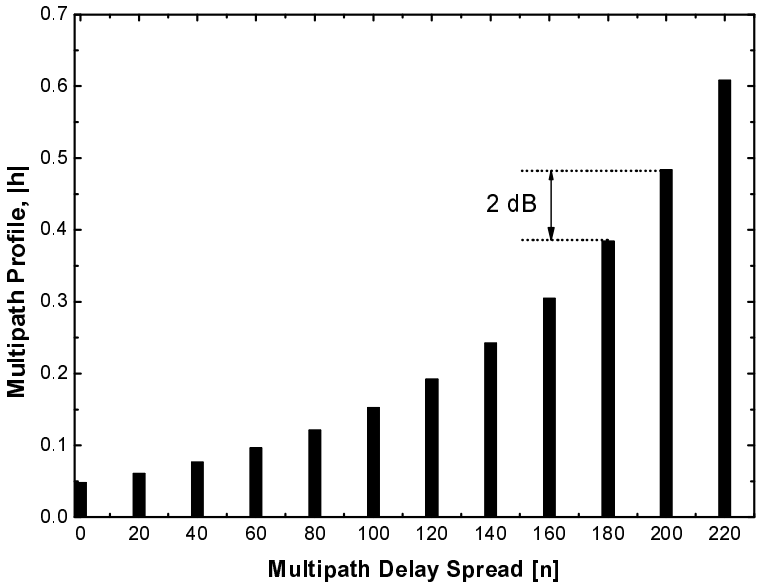

Figure 3.14: Non-minimum phase channel model.

Table 3.3: System parameters

System bandwidth	10 MHz
Number of IFFT/FFT	1024
Subcarrier spacing	15 kHz
Occupied bandwidth	9 MHz (10% guard band)
Sampling rate	15.36 MHz
Packet frame length	7 OFDM symbols (2 pilot symbols)
Data modulation	QPSK, 16QAM, 64QAM
Bit interleave	No
Channel coding / decoding	Turbo code (13,15,15) / Max-Log-Map (8 iterations)
Constraint length	4
Puncture	1/2 (RCPT)
Channel estimation	Perfect

is assumed and the guard band is 1 MHz. The number of data bearing subcarriers is 600, and the sampling time is about 65 ns. When there is no ISI and ICI in a time-invariant channel, the GI is assumed as 256 samples (16.7 μs). The Max-Log-Map for turbo decoding is applied, where the maximum number of iterations in the turbo decoder is set to 8.

For the wireless channel model, the minimum phase channel (MPC) and non-minimum phase channel (NMPC) are assumed. The minimum phase channel model implies that the energy of the leading part of the channel profile is greater than that of the lagging part. The non-minimum phase channel model implies the opposite case of the minimum phase channel. Each multipath profile is shown in Figs. 3.13 and 3.14. In a fixed guard interval length the interference level in non-minimum phase channel is larger than that of the minimum phase channel". In the meantime, the simulation in the non-minimum phase channel is performed only in the turbo coded 64QAM since the 64QAM is very susceptible to ISI and ICI. The multipath model is designed by a finite impulse response (FIR) filter where the number of the filter taps and tap delay are 12 and 20 samples delay, respectively, while the tap weights are independent and identically distributed Rayleigh fading random variables, generated with [3.17]. The ratio of the maximum channel delay to the symbol duration assumed is about 0.199 (19.9 %), and 0.207 (20.7 %) for the simulation. To see the effects of the interference on the system performance, the guard interval length is controlled while the multipath delay spread is fixed. In other words, the GI length is set to 40 (2.6 μs) and 80 (5.2 μs) samples, where ISI power over GI to the total transmit power (=1) is about -14.9, -17.8 and -8.4, -9.8 dB in the minimum and non-minimum phase channel, respectively. The normalized Doppler frequency ($f_d T_s$) is about 0.0012 in both channel scenarios.

Finally, it is assumed that the timing synchronization is ideal and the channel estimates are perfectly known at the receiver. The mismatch of the former can cause the residual ISI and the latter is dependant on the pilot structure and the applied algorithm. For example, it can be found that the channel estimation in the static ISI channel and slowly fading ISI channel does not degrade the canceller performance excessively [3.6], where the cancellation is similar to the DWCC. Meanwhile, the research on the channel estimation and the channel aliasing in ISI channel can be found in [3.8]. For more precise analysis in the DWCC, those detrimental effects need to be investigated as a further study.

3.5.1 Evaluation of DWCC

To evaluate the effect due to the initial equalization in the proposed schemes, the simulation is performed in the turbo coded OFDM for 16QAM in 'GI40'. The number of iteration for the DWCC-II is four times including the initial processing, while three times for the DWCC-I are performed since the DWCC-I does not need the separate operation for the initial processing. From Fig. 3.15, the DWCC-II shows almost the same performance in both FDE and TDE-MRC while the DWCC-I shows the large difference. Accordingly, it can be seen that the interference difference, incurred by applying FDE and TDE-MRC does not seriously affect the performance of the DWCC-II, which results from the double window combined output in the decision feedback. It implies that the DWCC-II is not sensitive to the initial equalization so that the computational complexity can be reduced. The lower bound hereafter denotes the performance without interference, and the SNR implies the Es/No. In addition, the simulation is performed with 40000 packets.

The simulation results in Figs. 3.16 and 3.17 are performed with and without ISI in the turbo coded OFDM for 16QAM and 64QAM, respectively. In other words, ISI free channel implies that the pre- and post-ISI are perfectly cancelled out in the specific symbol processing, but there still exist ICI and thermal noise. From the results, it can be seen that the DWCC-II can effectively suppress the residual ICI by combining the double windows in the iteration which results in the less ISI to the adjacent symbol processing.

Figure 3.18 shows the performance in the turbo coded OFDM for 64QAM in the minimum (MPC) and the non-minimum phase channel (NMPC), where the high level modulation such as 64QAM is expected to be susceptible to ISI fading channel. From the result, it can be seen that the performance of DWCC-I is severely degraded in the given non-minimum phase channel, but DWCC-II is not much susceptible since it takes advantage of the double window combing gain in the iterative canceller processing. Even if the given non-minimum phase channel is extreme case, Fig. 3.18 is a good example to describe the sensitivity to ISI in both DWCC-I and DWCC-II. From the following subsections, the simulations are performed only in the minimum channel model that can often be encountered in

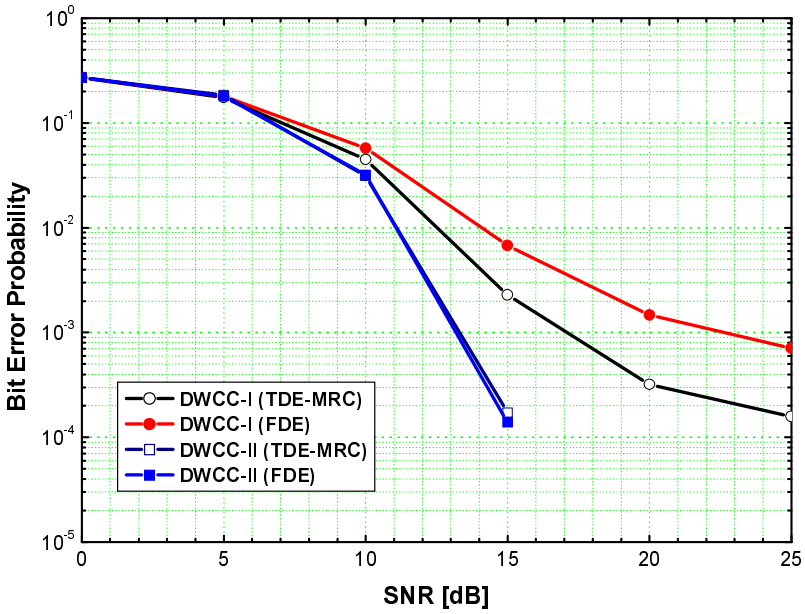

Figure 3.15: Sensitivity of DWCC to initial equalization in turbo coded OFDM for 16QAM in 'GI40'(=2.6μs).

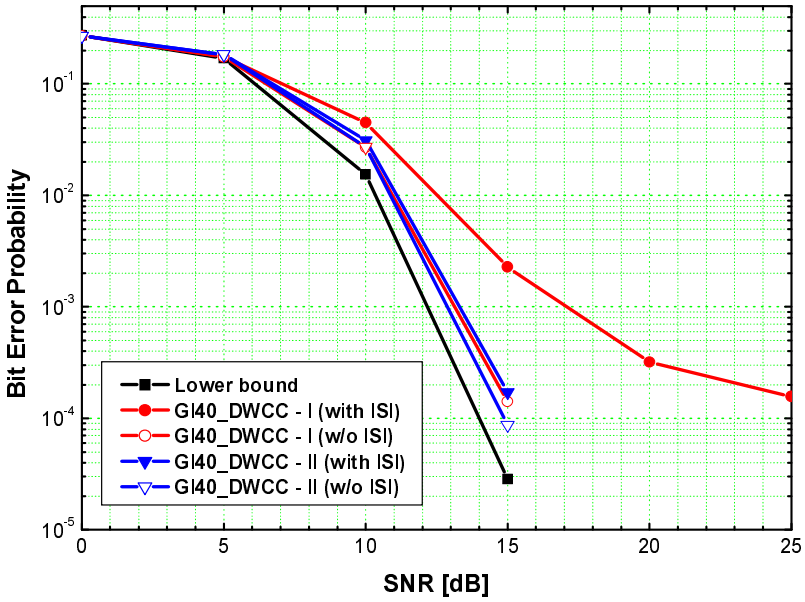

Figure 3.16: Performance comparison of the proposed schemes against ICI and thermal noise in turbo coded OFDM for 16QAM in 'GI40'(=2.6μs).

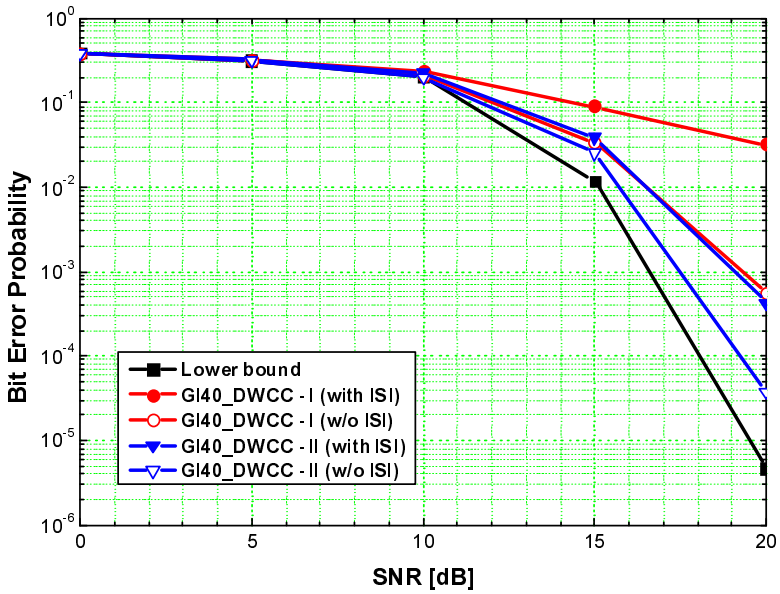

Figure 3.17: Performance comparison of the proposed schemes against ICI and thermal noise in turbo coded OFDM for 64QAM in 'GI40'(=2.6μs).

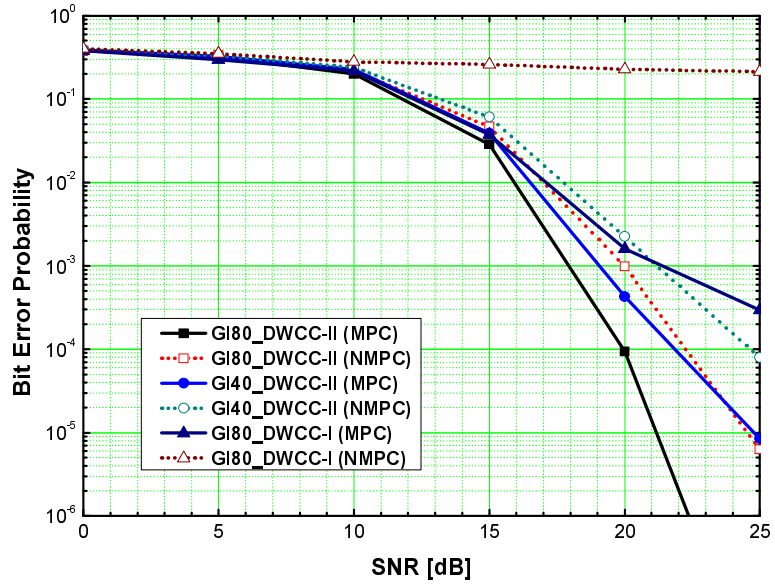

Figure 3.18: Performance of DWCC in turbo coded OFDM for 64QAM in the minimum and non-minimum phase channels.

the real environment.

3.5.2 Performance Evaluation in Turbo-Coded OFDM

Performance in Turbo-Coded QPSK/OFDM

Figure 3.19 shows the turbo coded BER without a canceller for QPSK, and the results implies the lower and upper bound in the proceeding results for QPSK. The BER results not shown in the proceeding figures denote no error during the simulation with 2800 bits per packet. In 'GI40' and 'GI80' the results show no error floor in turbo coded QPSK which means the channel coding itself plays a role as a canceller in low level modulation [3.18]. However, the difference from the lower bound (when there are no ISI and ICI) still needs to be reduced.

In Fig. 3.20 the BER performances of the four schemes are shown. For simplicity, the 'FDE' and the 'TDE-MRC' denote the conventional RISIC and the conventional RISIC with TDE-MRC, respectively, where both have the processing window with FFT length. The 'TDE-MRC' outperforms the 'FDE' about 0.5 dB at 10^{-4}. The matched filtering to the symbol after ISI cancellation is performed not with one-tap FDE but with TDE-MRC, using ICI channel matrix, $\mathbf{H}^{ici}$, so the BER performance in 'TDE-MRC' is better than that of 'FDE'. The proposed schemes show the improved performances about 1.4 dB gain at 10^{-4} to the 'No canceller' and they show almost the same results. It reflects that the low level modulation is not much sensitive to ISI and ICI with the turbo channel coding.

In Fig. 3.21 the BER performances of the cancellers in 'GI40' are shown. The BER difference between 'FDE' and 'TDE-MRC' is similar to that in Fig. 3.20. On the other hand, the BER difference between the DWCC-I and -II in Fig. 3.21 is larger than that in Fig. 3.20. In a severe frequency selective channel the decision feedback of the double window combined output in the DWCC-II results in the performance gain, compared to the DWCC-I. The proposed schemes show the improved performance even in 'GI40' compared with other cancellers.

The turbo coded QPSK/OFDM in the given channel scenarios is not much sensitive to ISI and ICI, but it is proved that the proposed canceller, particularly DWCC-II could achieve the maximum gains of 1.5 dB and 2 dB at 10^{-4} in 'GI80' and 'GI40', respectively, compared with 'No canceller'.

Performance in Turbo-Coded 16QAM/OFDM

Figure 3.22 shows the BER performance of the turbo coded OFDM without a canceller in a 16-ary quadrature amplitude modulation (16QAM). The total number of the transmit bits per packet is 5500 bits. Unlike QPSK, 16QAM shows an error floor in the assumed channel scenarios. From the results, the turbo channel coded OFDM for 16QAM without a canceller can not efficiently cope with ISI and ICI.

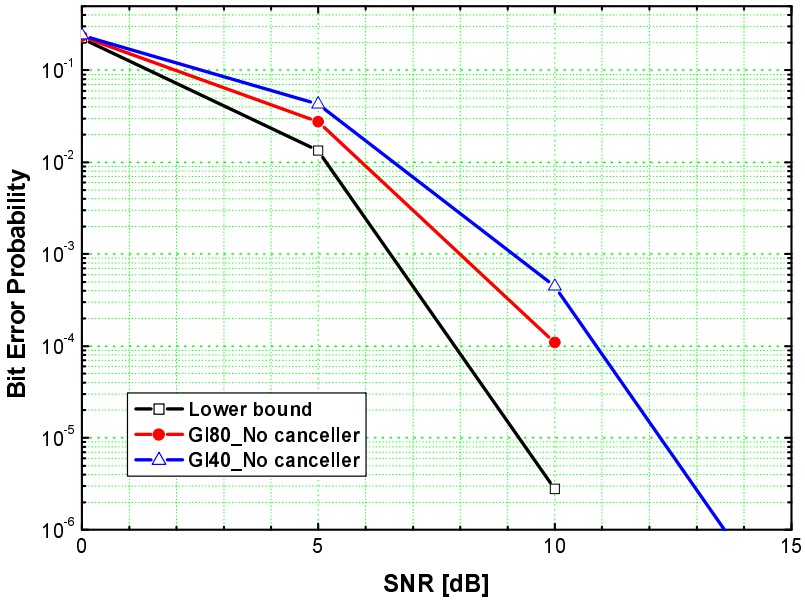

Figure 3.19: BER performance without canceller in turbo coded OFDM for QPSK in 'GI80'(=5.2 μs)*and*'*GI*40'(=2.6μs).

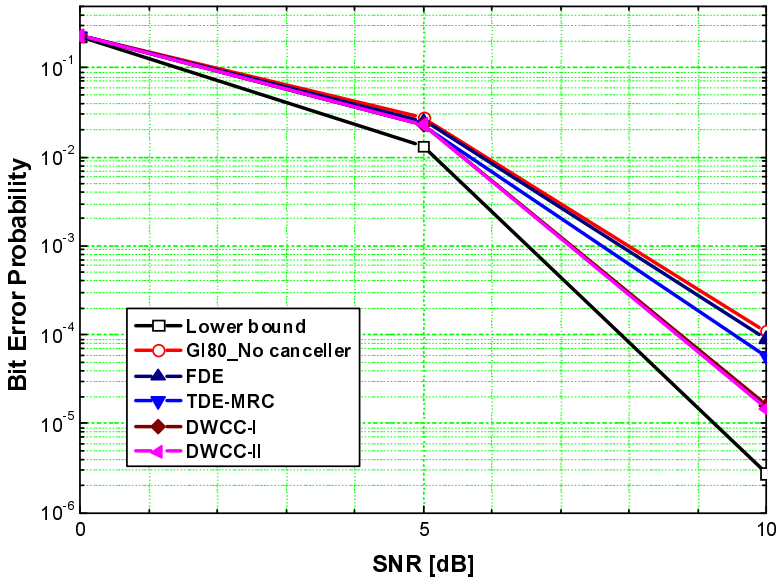

Figure 3.20: BER performance of the cancellers in turbo coded OFDM for QPSK in 'GI80'(=5.2 μs).

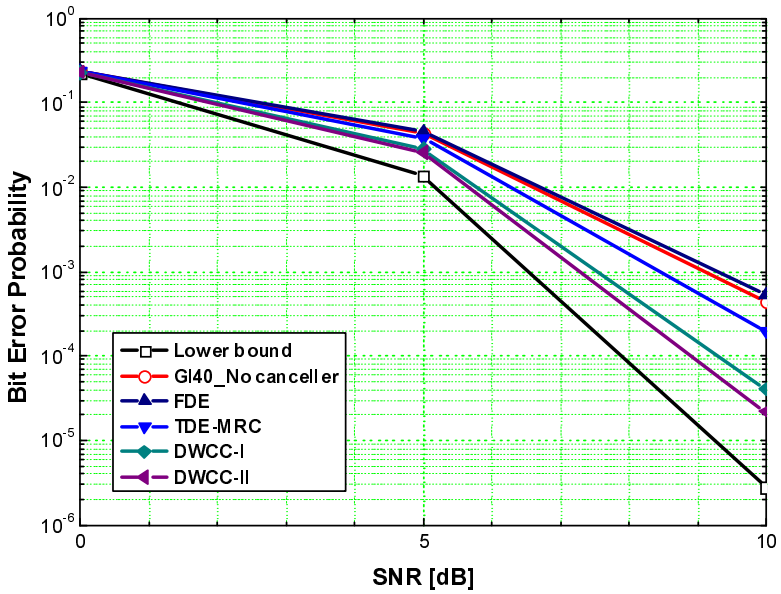

Figure 3.21: BER performance of the cancellers in turbo coded OFDM for QPSK in 'GI40'(=2.6μs).

Figures 3.23 and 3.24 show the BER performance of the cancellers in turbo coded OFDM for 16QAM in 'GI80' and 'GI40', respectively. The effect of DWCC shows the noticeable difference from the performances of other cancellers. In addition, the obtainable gain from 'TDE-MRC' is not negligible even for 16QAM in the given channel scenarios. The conventional RISIC with FDE or with TDE-MRC is seriously deteriorated in Fig. 3.24 since the strong interference causes the error propagation. On the other hand, the BER performance of the DWCC-I is acceptable in 'GI80', but the error floor is shown in 'GI40'. However, the performance of the DWCC-II is still close to the lower bound even in 'GI40'. From the result, the DWCC-II effectively suppresses the residual ISI and ICI by using double window combining gain, where the noise correlation ration (NCR) is about 74 % and 70 % in 'GI40' and 'GI80', respectively.

The DWCC-II makes use of the double window combined output in the decision feedback, the SNR gain from the non-overlapped signal part of the double windows can result in the reliable symbol detection while the residual noise is suppressed. On the other hand, the BER performance of the DWCC-I which does combine the double windows once after the canceller operation is finished, shows an error floor for the less computational complexity in Fig. 3.24.

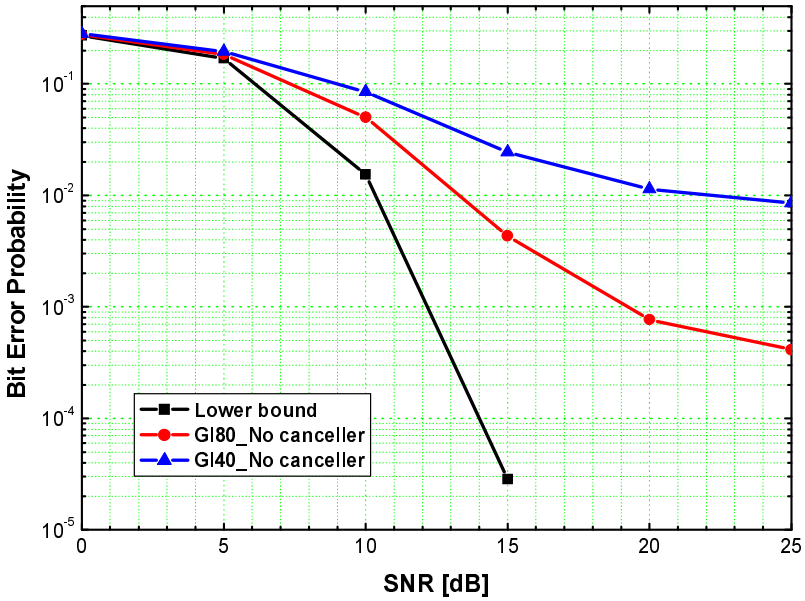

Figure 3.22: BER performance without canceller in turbo coded OFDM for 16QAM in 'GI80'(=5.2 μs)*and*'*GI*40'(=2.6μs).

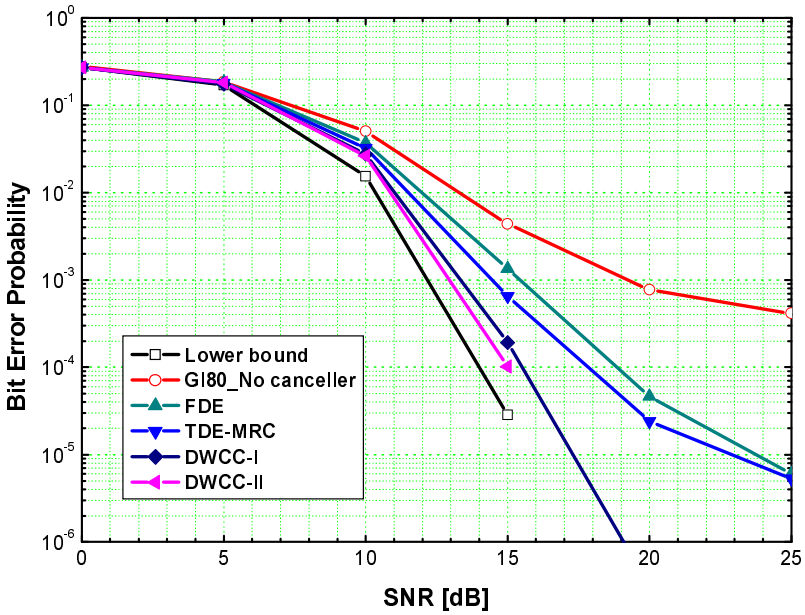

Figure 3.23: BER performance of the cancellers in turbo coded OFDM for 16QAM in 'GI80'(=5.2 μs).

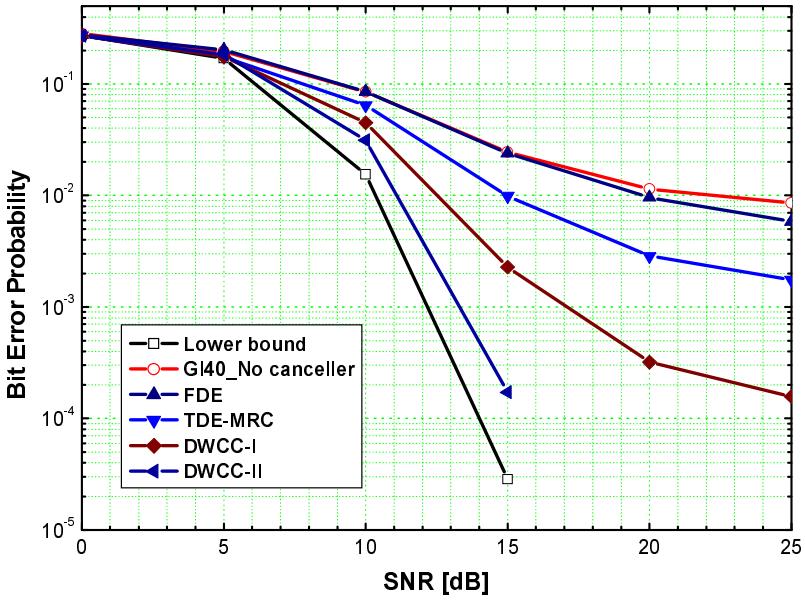

Figure 3.24: BER performance of the cancellers in turbo coded OFDM for 16QAM in 'GI40'(=2.6μs).

Performance in Turbo-Coded 64QAM/OFDM

Figure 3.25 shows the BER performance of the turbo coded OFDM without a canceller in a 64-ary quadrature amplitude modulation (64QAM). The total number of the transmit bits per packet is 8000 bits. It shows an unacceptable BER performance. Figures 3.26 and 3.27 show the performances of the cancellers for 64QAM in 'GI80' and 'GI40', respectively. The overall BER performance is worse than that of 16 QAM. However, the DWCC-II does not show an error floor even for 64QAM in the given channel scenarios, while the performance of the DWCC-I begins to show the error floor even in 'GI80', and becomes an unacceptable in 'GI40'. The results show that the performance difference between the conventional RISIC with FDE and with TDE-MRC becomes negligible in the given channel scenarios. It can be thought that ISI and ICI interference level in 64QAM becomes higher than the obtainable gain from TDE-MRC.

3.6 Summary

In this Chapter the new canceller scheme, named as Double Window Cancellation and Combining (DWCC) has been proposed. The performance of the DWCC has

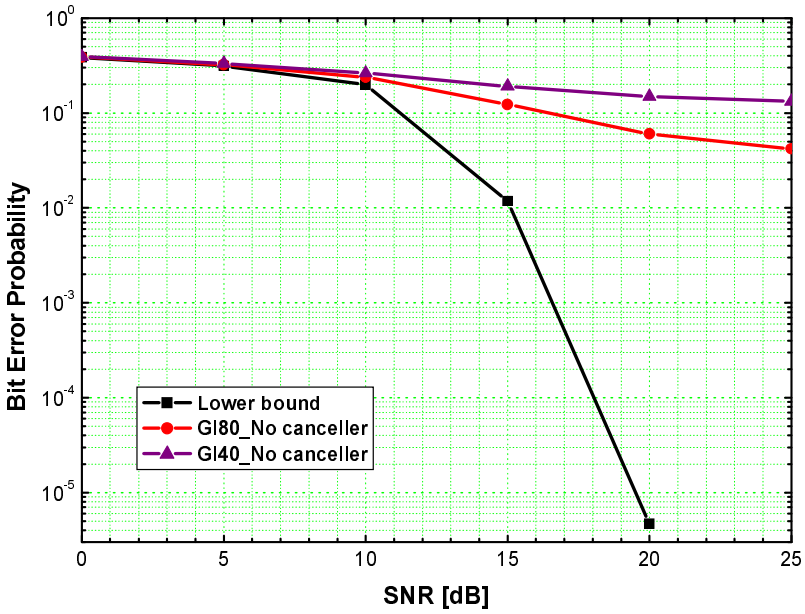

Figure 3.25: BER performance without canceller in turbo coded OFDM for 64QAM in 'GI80'(=5.2 μs)*and*'*GI*40'(=2.6μs).

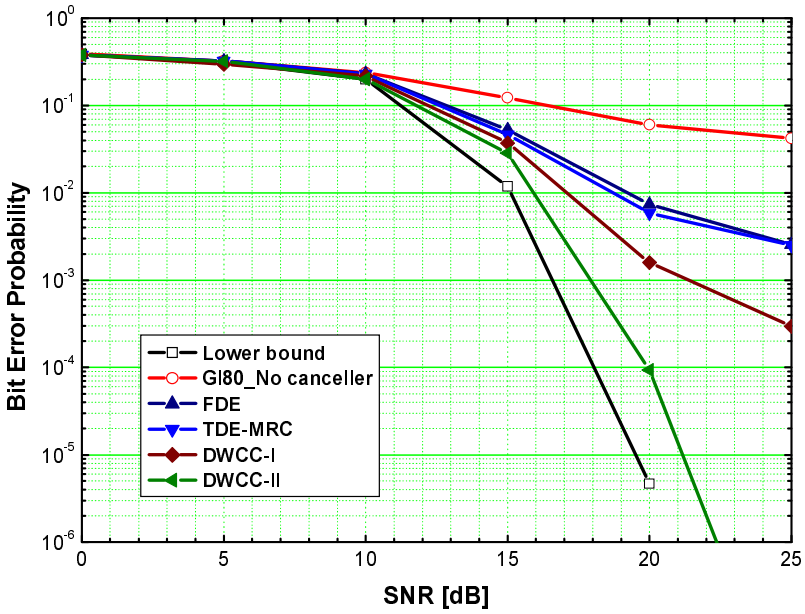

Figure 3.26: BER performance of the cancellers in turbo coded OFDM for 64QAM in 'GI80'(=5.2 μs).

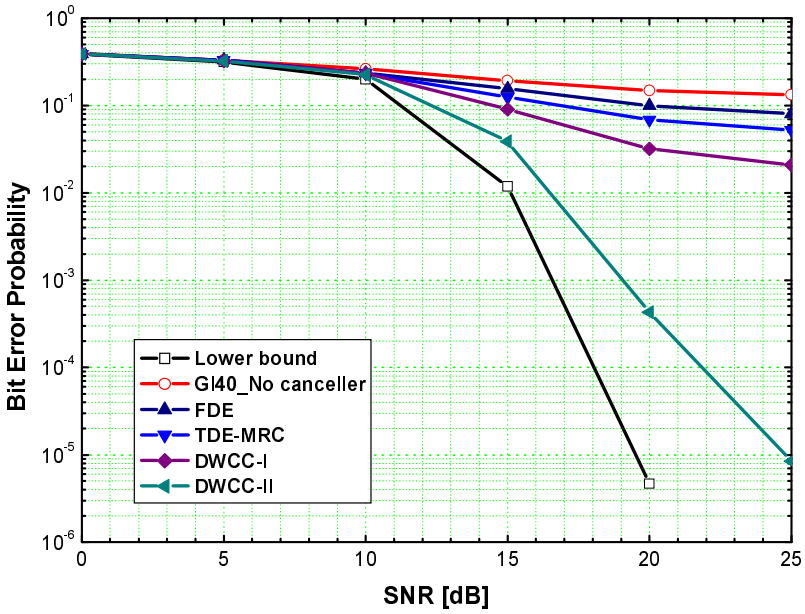

Figure 3.27: BER performance of the cancellers in turbo coded OFDM for 64QAM in 'GI40'(=2.6μs).

been compared with the conventional canceller and the computational complexity was presented. Regarding the performance and computational complexity, the schemes adopt the time and frequency domain equalization in the initial and the iterative processing, respectively. In the slowly fading ISI channel, it can be seen that the turbo channel coding itself could play a role as a canceller in low level modulation, but the performance is severely deteriorated in high level modulations. On the other hand, the proposed schemes with turbo channel coding can be tolerable even in high level modulations and achieve the larger performance gain than the conventional canceller. Consequently, the proposed schemes are expected to be a countermeasure in Single Frequency Network (SFN) where the limited insertion of the guard interval can not prevent ISI and ICI due to the large channel delay spread.

3.7 References

[3.1] T. Ue, S. Sampei, and N. Morinaga, "Symbol rate and modulation level-controlled AM/TDMA/TDD system for high-bit-rate wireless data transmission," IEEE Trans. Vehicular Technol., vol. 47, no. 4, pp. 1134–1147, Nov. 1998.

[3.2] T. Keller, and L. Hanzo, "Adaptive modulation techniques for duplex OFDM transmission," IEEE Trans. Vehicular Technol., vol. 49, no. 5, pp. 1893–1906, Sept. 2000.

[3.3] N. Kawai, S. Namba, and S. Yamazaki, "Performance of multimedia broadcasting through ISDB transmission system," IEEE Trans. Broadcast., vol. 42, no. 3, pp. 151–158, Sept. 1996.

[3.4] U. Reimers, "Digital video broadcasting," IEEE Commun. Mag., vol. 36, no. 6, pp. 104–110, June 1996.

[3.5] G. Malmgren, "Impact of carrier frequency offset, doppler spread, and time synchronization errors in OFDM based single frequency network," IEEE Proc. GLOBECOM, vol. 1, pp. 729–733, Nov. 1996.

[3.6] D. Kim and G.L. Stber, "Residual ISI cancellation for OFDM with applications to HDTV broadcasting," IEEE J. Sel. Areas Commun., vol. 16, no. 8, pp. 1590–1599, Oct. 1998.

[3.7] S. Suyama, S. Suzuki, and K. Fukawa, "An OFDM receiver employing turbo equalization for multipath environments with delay spread greater than the guard interval," IEEE Proc. Vehicular Technol., vol. 1, pp. 632–636, Apr. 2003.

[3.8] Y. Sagae, S. Suyama, H. Suzuki, and K. Fukawa, "An OFDM turbo equalizer for scattered pilot signals in multipath environments with delay difference greater than guard interval," IEEE Proc. Vehicular Technol., vol. 1, pp. 425–429, May 2004.

[3.9] M. Uesugi, "An interference cancellation scheme for OFDM using adaptive algorithm," IEICE Trans. Commun., vol. E86-B, no. 11, pp. 3182–3191, Nov. 2003.

[3.10] H. J. Yu, M. S. Kim, T. H. Jeon, and S. K. Lee, "Equalization scheme for OFDM systems in long delay spread channels," IEEE Proc. PIMRC, vol. 2, pp. 1297–1301, Sept. 2004.

[3.11] N. Suzuki, H. Uehara, and M. Yokoyama, "A new OFDM demodulation method with variable-length effective symbol and ICI canceller," IEICE Trans. Fundamentals, vol. E85-A, no. 12, Dec. 2002.

[3.12] N. Suzuki, T. Shibata, N. Itoh, and M. Yokoyama, "OFDM demodulation method with variable effective symbol duration," IEICE Trans. Fundamentals, vol. E85-A, no. 7, July 2002.

[3.13] M. Itami, H. Takano, H. Ohta, and K. Itoh, "A method of equalization of OFDM signal with inter-symbol and inter-channel interferences," IEEE Proc. ICCS, vol. 1, pp. 109–113, pp. 14-18, Nov. 1994.

[3.14] C. J. Park, and G. H. Im, "Efficient cyclic prefix reconstruction for coded OFDM systems," IEEE Commun. Lett., vol. 8, no. 5, pp. 274–276, May 2004.

[3.15] G. R. Parsace, A. Yarali, and H. Ebrahimzad, "MMSE-DFE equalizer design for OFDM systems with insufficient cyclic prefix," IEEE Proc. VTC2004-fall, vol. 6, pp. 3828–3832, Sept. 2004.

[3.16] N. Pulimamidi, J. Nulu, and M. M. Tahernezhadi, "Development of a New OFDM transceiver without guard interval," IEEE Proc. EIT-2007, pp. 300–305, May 2007.

[3.17] P. Dent, G. E. Bottomley, and T. Croft, "Jakes fading model revisited," IEE Electron., Lett., vol. 29, no. 13, pp. 1162–1163, June 1993.

[3.18] E. Viterbo, and K. Fazel, "How to combat long echoes in OFDM transmission schemes: Sub-channel equalization or more powerful channel coding," IEEE Proc. GLOBECOM, vol. 3, pp. 2069–2074, Nov. 1995.

Chapter 4

Optimal Incorporation Method in Turbo Equalized Double Window Cancellation and Combining

In orthogonal frequency division multiplexing (OFDM) the multipath exceeding the guard interval (GI) causes inter-symbol interference (ISI) and inter-carrier interference (ICI), thereby making it difficult to achieve high data rate transmission. In this proposal, the optimal combining of DWCC and turbo equalization (TE), named TE-DWCC, is investigated by varying the iterative cancellation procedure between DWCC and channel decoder and the decision feedback type such as hard decision feedback (HDF) or soft decision feedback (SDF). Finally, by changing interference level, code rate, and decision feedback type, the performance of TE-DWCC is compared with the conventional canceller that adopts turbo equalization in the exponentially distributed slow fading channel.

4.1 Background of Proposal

The proposed canceller in this Chapter is based on Double Window Cancellation and Combining (DWCC) whose basic concept was proposed by the authors [4.1]. The intent of DWCC is to enjoy the coherent combining gain in canceller operation by readily extending the processing window to entire symbol length. However, since the canceller operation of DWCC is performed before channel decoding, it is still susceptible to deep fading. To overcome the drawback in DWCC, the DWCC combined with channel coding gain, named TE-DWCC, is proposed. Under different delay spread channels, assumed in [4.2], it is found that TE-DWCC is more robust to ISI and ICI than the conventional canceller [4.2] [4.3] that adopts turbo equalization [4.4]– [4.6]. In the meantime, it is found that the performance of TE-DWCC relies on the iterative cancellation procedure involving DWCC and channel decoder, and TE-DWCC is more compatible with hard decision feedback (HDF)

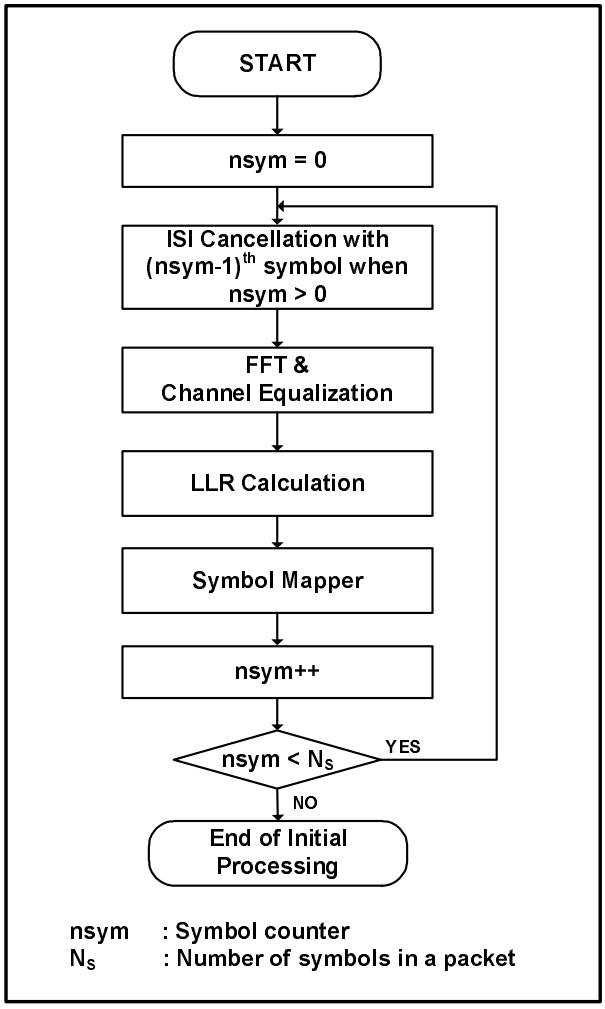

Figure 4.1: Algorithm flow in the initial processing.

than with soft decision feedback (SDF) due to the characteristic of the canceller operation.

4.2 Proposed Turbo Equalized Interference Canceller

The optimal combining method of DWCC-II and turbo equalization is presented by investigating the iterative cancellation procedure between DWCC and channel decoder and the required number of iterations in DWCC and turbo equalization. In addition, it is explained that TE-DWCC is combined well with hard decision feedback (HDF) rather than with soft decision feedback (SDF).

4.2.1 Basic Operations of TE-DWCC

Initial Canceller Operation

Figure 4.1 shows the algorithm flow chart of TE-DWCC in initial canceller operation. The processing window in initial canceller operation is restricted to N-FFT length and the operation is summarized as follows.

Step-1 Conventional one-tap frequency domain equalization is taken to the (i-1)th interfered symbol with N-FFT length and its symbol replica is determined.

Step-2 When the i^{th} symbol is input, ISI cancellation is performed with the (i-1)th symbol replica and the result follows the first step (S-1). These two steps are executed to all the symbols in a packet and initial canceller operation ends.

Iterative Canceller Operation

- MAP Detector Symbol Mappter

In iterative canceller operation of Fig. 4.2, the data symbol replicas from initial canceller operation are applied in the first iterative canceller operation. The output of DWCC for each symbol is used to calculate the Log-Likelihood Ratio (*LLR*) for coded bits by using the MAP detector [4.7]– [4.9]. The *LLRs* from MAP detector is calculated by (4.1).

$$LLR_{\mathrm{n}} = \ln \frac{\max\limits_{s^+ \in \mathbf{S}|b_n=1} \exp\left\{-\frac{\left|R_{i,k}^{comb} - \widehat{H}_{i,k}s^+\right|^2}{2\sigma_{i,k}^2}\right\}}{\max\limits_{s^- \in \mathbf{S}|b_n=-1} \exp\left\{-\frac{\left|R_{i,k}^{comb} - \widehat{H}_{i,k}s^-\right|^2}{2\sigma_{i,k}^2}\right\}}$$
$$\approx \frac{1}{2\sigma_{i,k}^2}\left[\min_{s^+ \in \mathbf{S}|b_n=1}[|R_{i,k}^{comb} - \hat{H}s^+|]^2 - \min_{s^- \in \mathbf{S}|b_n=1}[|R_{i,k}^{comb} - \hat{H}s^-|]^2\right] \quad (4.1)$$

where the transmit coded bit, b_n is +1 or -1, and s^+ and s^- denote the modulated data symbols with b_n=+1 or b_n=-1 in a set (**S**) of the constellation of the modulated symbols, respectively, and $\widehat{H}_{i,k}$, $\sigma_{i,k}^2$ and $R_{i,k}^{comb}$ are referred to (3.17) and (3.18).

Meanwhile, the symbol mapping is performed in DWCC with the *LLRs* from DWCC combined output and channel decoder in turbo equalization. The channel decoder output consists of the updated systematic bit and two parity bits from the final iteration of turbo decoder, and the parity bits from turbo decoder are also updated with the final systematic bits from turbo decoder [4.10]. In other words, likewise in the update of the systematic bits, the update of the parity bits can be calculated by the forward state probability, α_{k-1}, the transition probability, γ_k and the backward state probability, β_k at time k. The state transition information to the

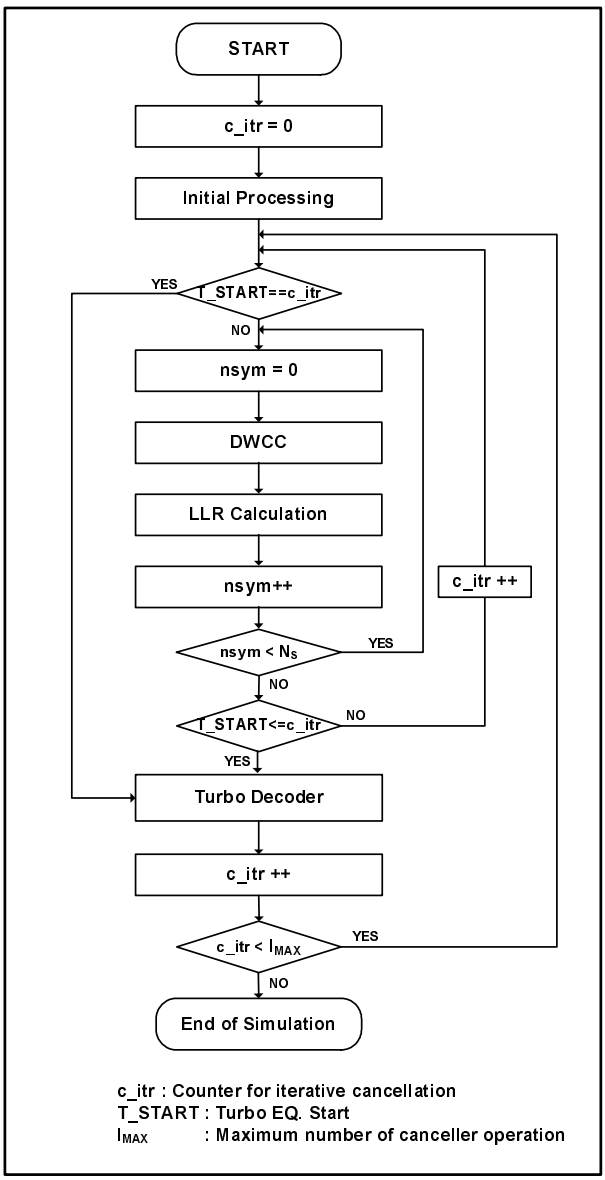

Figure 4.2: Comparison of the average *SINR* in 64QAM at the SNR of 24 dB.

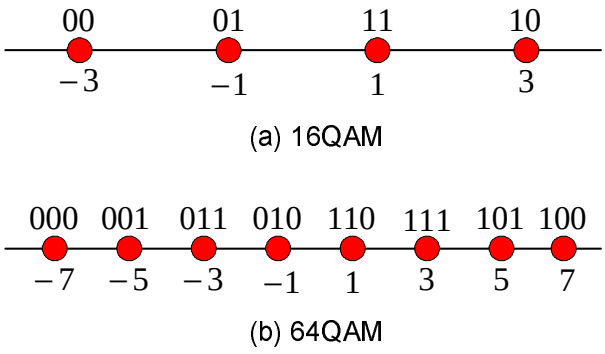

Figure 4.3: Gray mapping in 16QAM and 64QAM.

input bit is already known in the channel decoder and a posteriori *LLRs* for the parity bits can be obtained by (4.2).

$$LLR(p_k) = \ln\left(\frac{\sum_{p_k=+1,(\bar{s},s)} \alpha_{k-1}(\bar{s})\gamma_k(\bar{s},s)\beta_k(s)}{\sum_{p_k=-1,(\bar{s},s)} \alpha_{k-1}(\bar{s})\gamma_k(\bar{s},s)\beta_k(s)}\right) \tag{4.2}$$

where ($\bar{s}$,s) is the state transition set from the previous state, $\bar{s}$ to the present state, s, and α, β, and γ denote forward state, backward state, and transition probability, respectively. The calculations of those parameters are well described in [4.9] [4.10] so that the detail explanation is omitted in this paper. The updated systematic and parity bits are converted to data symbols with symbol mapper for ISI and ICI cancellation in DWCC block. There are two types of symbol mapping, and particularly the soft symbol mapping requires some manipulation depending on the Gray mapping rule in the transmitter. The Gray mapping used in this paper is shown in Fig. 4.3. In [4.11] and [4.12], the soft symbol mapping rule can be found by using the definition of *LLR* and (4.3).

$$\begin{aligned} \widehat{s_n} &= E\{s_n(\mathbf{b}_n)|r(t)\} \\ &= \sum_{\mathbf{b}_n} s_n(\mathbf{b}_n) \prod_{j=1}^{m} \Pr\left\{b_{n,j}(\mathbf{b}_n)|r(t)\right\} \end{aligned} \tag{4.3}$$

where $r(t)$ and $s_n(\mathbf{b}_n)$ denote the received symbol at time t and the modulated symbol, respectively, where $\mathbf{b}_n$ is the set of the bits composing the n^{th} symbol, and m implies $\log_2(\sqrt{M})$ and $b_{n,j}$ is the j^{th} bit in the n^{th} symbol in $s_n(\mathbf{b}_n)$. The soft symbol mapping rule in (4.4) is applied.

$$\begin{aligned} \widetilde{\mathbf{P}}_{i,16QAM} &= \frac{1}{\sqrt{10}}\left[\tanh(\frac{\lambda_0}{2})(2-\tanh(\frac{\lambda_1}{2}))\right] \\ &\quad + \frac{j}{\sqrt{10}}\left[\tanh(\frac{\lambda_0}{2})(2-\tanh(\frac{\lambda_1}{2}))\right] \\ \widetilde{\mathbf{P}}_{i,64QAM} &= \frac{1}{\sqrt{42}}\left[\begin{array}{c}\tanh(\frac{\lambda_0}{2})(4-2\tanh(\frac{\lambda_1}{2})) \\ +\tanh(\frac{\lambda_1}{2})\tanh(\frac{\lambda_2}{2})\end{array}\right] \\ &\quad + \frac{j}{\sqrt{42}}\left[\begin{array}{c}\tanh(\frac{\lambda_0}{2})(4-2\tanh(\frac{\lambda_1}{2})) \\ +\tanh(\frac{\lambda_1}{2})\tanh(\frac{\lambda_2}{2})\end{array}\right] \end{aligned} \tag{4.4}$$

where λ_k denotes the *LLR* of the k^{th} bit for the real and imaginary part of a data symbol.

4.2.2 Optimal Combining Method

In [4.13], the effectiveness of the equalizer and channel coder against the interference was discussed and it was emphasized that the powerful channel coder can be

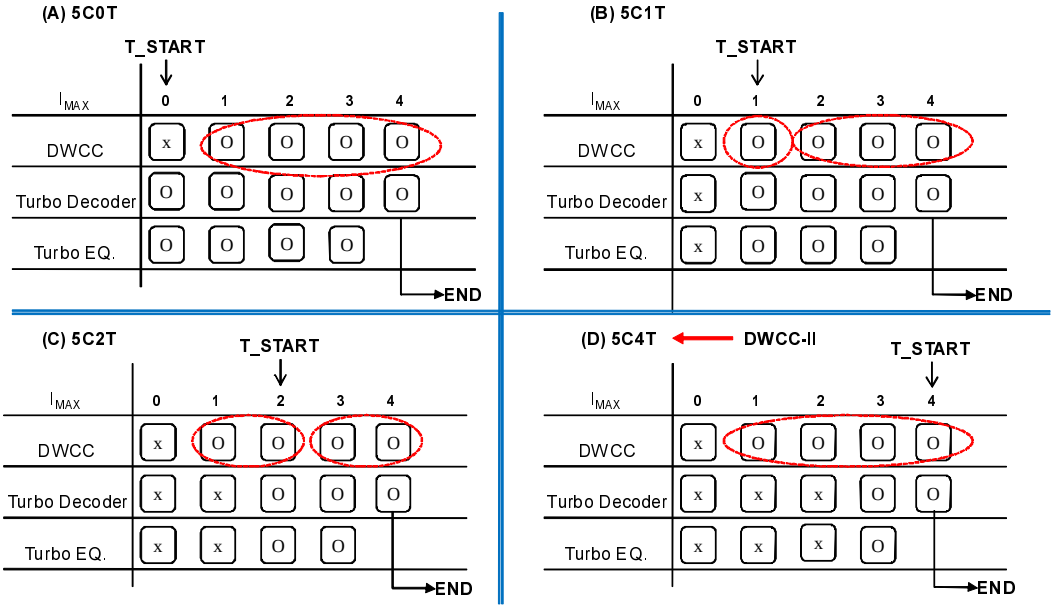

Figure 4.4: Required number of DWCC and turbo equalization and symbol update at 'xCyT'.

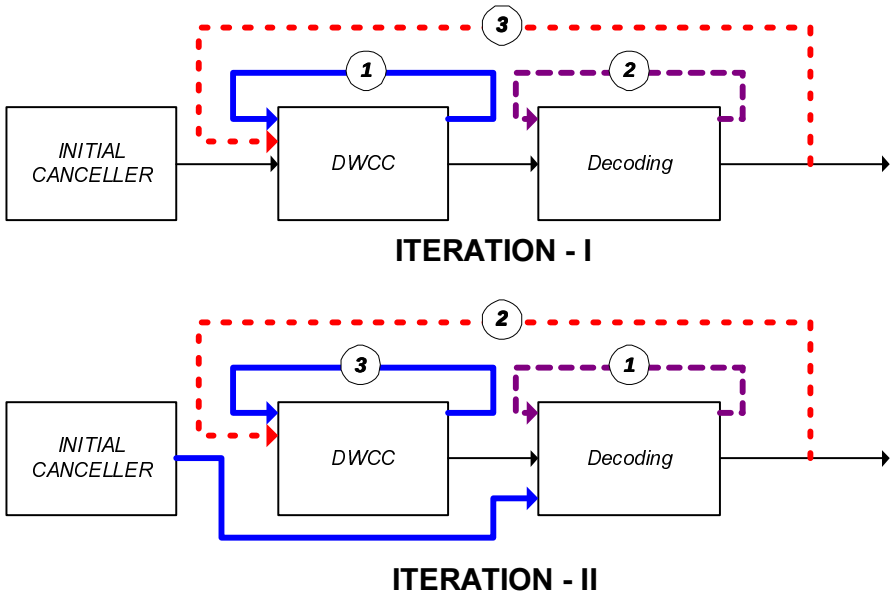

Figure 4.5: TE-DWCC with different processing order.

one of solutions to mitigate ISI and ICI. From [4.13], it can be inferred that there is a priority between the coherent combining gain from DWCC and channel coding gain from channel coder, and the effects of two different operating modes on the performance of TE-DWCC are investigated. One is the canceller operation after channel decoding (COAD) and the other is the canceller operation before channel decoding (COBD). The selection between the two modes can be controlled by setting the parameter 'T_START' in Fig. 4.2 and the corresponding number of DWCC and turbo equalization is shown in Fig. 4.4. For example, 'T_START' equal to '0' implies the COAD. Otherwise, it implies the COBD where DWCC is performed first before turbo equalization with a different number of DWCC and turbo equalization. In other words, when 'T_START' is set to '0', the channel decoding is firstly operated to the interfered data symbols and then DWCC is proceeded with the symbol replicas mapped with the updated LLRs by channel decoder. After all, the selection between the COAD and COBD is controlled by the priority between DWCC and turbo equalization, and TE-DWCC with different processing order is shown in 4.5.

The performance of COAD and COBD on the iterative processing procedure and the optimum number of iterations in DWCC and turbo equalization are investigated through simulations. Figure 4.6 shows the minimum required *SNRs* satisfying the packet error rate (*PER*) of 10^{-3} and 10^{-2} in 16QAM and 64QAM, respectively, where, for example, '5C2T' implies that turbo equalization starts when 'c_itr' equals 2 with 'I_{max}' set to 5, and '5C4T' implies the pure DWCC-II operation without turbo equalization. From the simulation results, it is found that the COBD has a lower minimum required *SNR* than the COAD in the given channel conditions. In the meantime, the optimum number of iterations in COBD can be found at '5C2T' or '5C3T' where the required number of turbo equalization is two and one, respectively. Figure 4.7 shows the performance dependence of COBD on the number of iterations in DWCC and turbo equalization for 64QAM at the *SNR* of 24 dB. It is found that the optimal number of DWCC and turbo equalization is two and one, respectively, and the performance does not severely depend on the number of turbo equalization. Consequently, the performance of TE-DWCC is largely affected by the priority between coherent combining gain and channel decoding gain in the interference dominant channel. In addition, it is also found that the powerful channel coder such as turbo coder by itself is not efficient for suppressing the large interference.

Regarding computational complexity and latency, the required number of FFT operation and turbo equalization in TE-DWCC is comparable to the conventional canceller in [4.2] [4.3], i.e., the required number of FFT operation in the conventional canceller is proportional to the number of data symbols in an OFDM symbol, and the required number of turbo equalization is larger than two (See Table 1 in [4.1] and Fig. 6 in [4.3]).

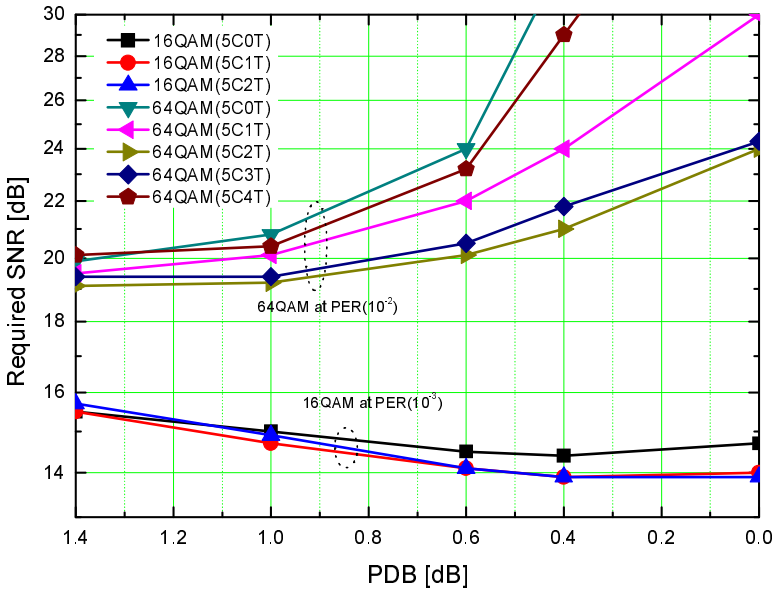

Figure 4.6: Performace dependence of TE-DWCC on the iterative processing procedure.

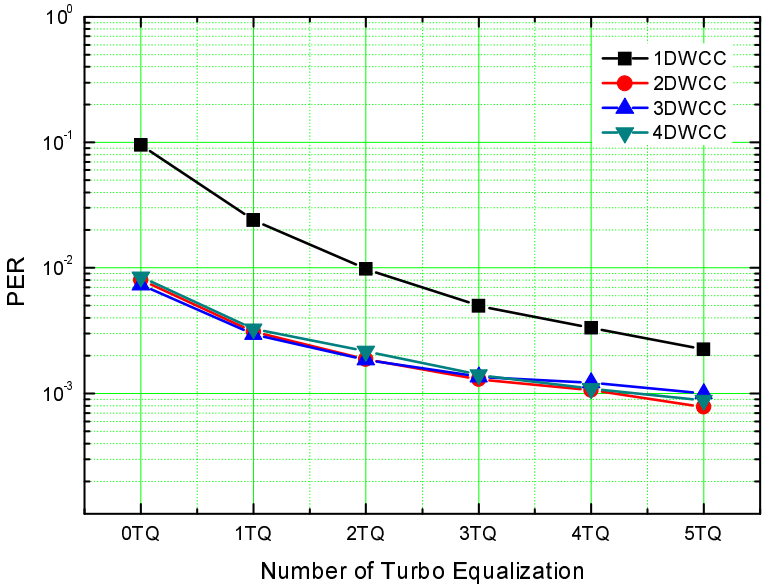

Figure 4.7: Optimum number of iteration in TE-DWCC at PDB of 0.6.

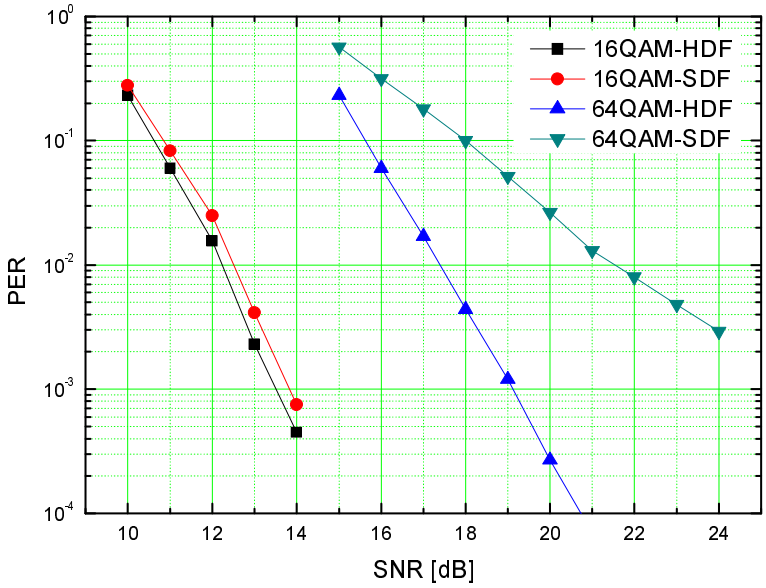

Figure 4.8: *PER* performance comparison of HDF and SDF in 16QAM and 64QAM at PDB of 0.6 dB.

4.2.3 Compatibility with SDF and HDF

In Fig. 4.8 the performance of TE-DWCC is compared in both HDF and SDF, where PDB is set to 0.6 dB. In the simulation it is assumed that ISI is perfectly eliminated since ISI, particularly in 64QAM, is severe and it is hard to investigate the compatibility of HDF and SDF in TE-DWCC in the presence of ISI. The result implies that HDF is more suitable for TE-DWCC than SDF in both 16QAM and 64QAM. This is because TE-DWCC mitigates ICI by using cyclic reconstruction in the time domain and hence the symbol replicas, generated by unreliable *LLRs* could cause variation in the signal within an OFDM symbol, resulting in the increased ICI in the frequency domain. The performances of the conventional canceller in HDF and SDF are presented in the following sub-chapter, where SDF is more suitable for TE than HDF.

4.3 Simulation Results and Discussion

In this section the *PER* performance of TE-DWCC is compared with the previous canceller in [4.2] [4.3]. The system parameters for the simulation are listed in Table

Table 4.1: System parameters.

System bandwidth	20 MHz
Number of IFFT/FFT	64
Subcarrier spacing	312.5 kHz
Packet frame length	10 OFDM symbols (pilot : 2, data : 8)
Data modulation	16QAM, 64QAM
Channel coding / decoding	RSC (13,15,15) Max-Log-MAP (8 iterations)
Constraint length	4
Puncture	1/2 , 2/3 (RCPT)
Channel estimation	Perfect

Table 4.2: rms delay spread depending on PDB.

PDB [dB]	*rms* delay [ns]
1.4	292.5
1.2	327.8
1.0	367.1
0.8	408.9
0.6	450
0.4	485.5
0.2	510
0.0	518.8

4.1 where the system parameters are different from those in Chapter 3. The Chapter 4 mainly focuses on the error performances of TE-DWCC and conventional turbo equalized canceller. The conventional turbo equalized canceller with a large-point of FFT operation requires the heavy computational complexity in ICI cancellation, therefore the small-point of FFT operation is assumed unlike the system parameters in Chapter 3. The total bandwidth is 20 MHz and all the subcarriers bear data symbols. The sampling time is 50 ns. The Max-Log-MAP for turbo decoding is applied and the maximum number of iterations in turbo decoder is set to 8. For the wireless channel model, the exponentially distributed 18 multipath delay profile in [4.2] is assumed as already shown in Fig. 2.7, where the number of taps and tap delay are 18 and 2 samples delay, respectively.The tap weights are independent and identically distributed Rayleigh fading random variables referring to [4.14]. The *rms* delay spread is controlled by the multipath power difference in dB scale (PDB) with the maximum channel delay fixed. Table 4.2 describes the *rms* delay depending on PDB. The smaller PDB is, the larger ISI and ICI are, whereas the

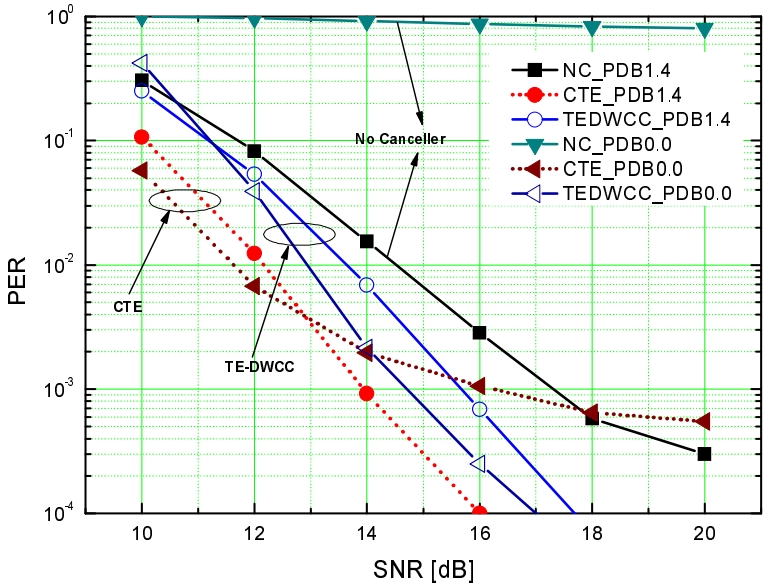

Figure 4.9: *PER* performance comparison of TE-DWCC with the conventional TE (CTE) at 1/2 code rate.

channel coding gain by the multipath increases. Meanwhile, the channel impulse response is assumed to be static during a packet since the simulation is performed in a slow fading channel with Doppler frequency is 18 Hz and its coherent time is about 0.056 sec. Compared with the single packet duration of 40 μs, the coherent time is long enough so that the assumption of the static fading channel during a packet is reasonable, while the fading coefficients are generated by changing an initial phase seed per packet to obtain the converged simulation results. For the fair comparison, the perfect timing synchronization and ideal channel estimation are also assumed in the simulation.

4.3.1 Performance Comparison in 16QAM/OFDM

In Fig. 4.9 the simulation is performed in the code rate of 1/2 and the PDB at 1.4 dB and 0.0 dB, where 'NC' and 'CTE' denote 'no canceller' and 'conventional TE' of [4.2] [4.3], respectively. In 'CTE' the soft decision feedback is applied. The number of transmit bits is 1000 bits per packet. For simplicity, PDB at 1.4 dB is written by PDB1.4, hereafter. The number of turbo equalization is set to 3 in 'CTE' and 2 in TE-DWCC ('5C2T'), respectively. The PDB1.4 and PDB0.0

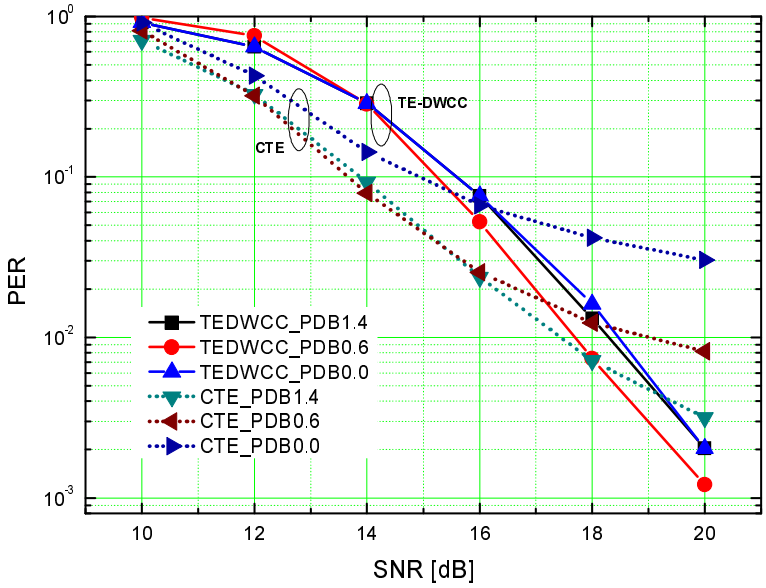

Figure 4.10: *PER* performance comparison of TE-DWCC with the conventional TE (CTE) at 2/3 code rate.

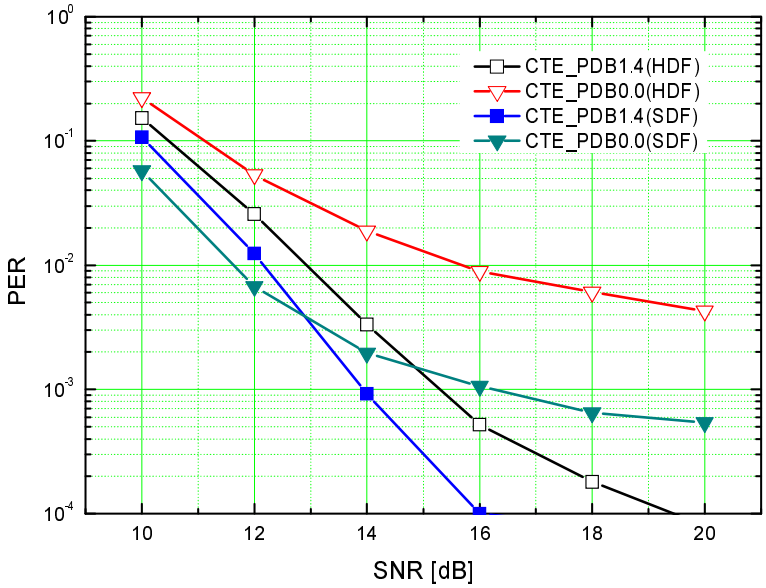

Figure 4.11: *PER* performance comparison of the conventional TE (CTE) with HDF and SDF.

in 16QAM implies the noise dominant and interference dominant environments, respectively. From the result, 'CTE' shows the best *PER* performance in the noise dominant region, whereas its performance is severely degraded when it goes into the interference dominant region. Even though the *PER* performance of the TE-DWCC is worse than that of 'CTE' about 1.7 dB in PDB1.4, it is not dominated by ISI and ICI even in PDB0.0. In the meantime, the *PER* performance of the TE-DWCC in the PDB0.0 is better than that in the PDB1.4 due to the channel decoding gain from the frequency diversity. In Fig. 4.10 the *PER* performance comparison of each scheme is shown in the code rate of 2/3. Since the 'CTE' largely depends on the channel decoding gain, the performance shows the floor even at PDB0.6, whereas the TE-DWCC with the double window combining gain is still tolerable against the severe ISI and ICI. Consequently, it is proved that the TE-DWCC with the coherent combining and the channel decoding gain is more robust to the interference dominant channel environment. In Fig. 4.11 the *PER* performances in the soft decision feedback (SDF) and hard decision feedback (HDF) are evaluated in 'CTE'. Unlike the result in Fig. 14, the canceller like 'CTE' is compatible with SDF, which is generally known in turbo equalization [4.10]. On the other hand, the canceller that performs the cyclic reconstruction in the time domain to suppress ICI with symbol replica, generated by soft symbol mapper can cause the variation within OFDM symbol which results in the increased ICI in the frequency domain.

4.3.2 Performance Comparison in 64QAM/OFDM

In Fig. 4.12 the *PER* performance of the TE-DWCC and 'CTE' is compared in 64QAM at the *SNR* of 24 dB since the minimum required *SNR* to satisfy the *PER* of 10^{-2} is about 24 dB in all PDBs as shown in Fig. 4.5. The number of transmit bits is 1500 bits per packet. In Fig. 4.12, the frequency diversity gain is not found in 64QAM since ISI in the operating range of 64QAM becomes dominant even with the same interference as in 16QAM. The performance difference between two algorithms is due to the following reason. The canceller, 'CTE' mainly depends on the channel decoding gain and the guard interval combining gain in iterative canceller operation, while its operation includes not only the interfered signal part but also the non-interfered signal part to eliminate ICI. Unfortunately, however, the tentative symbol replica is not much reliable in 64QAM even under the small ISI environment comparing to 16QAM so that the interference from the non-interfered signal part becomes greater than the guard interval combing gain. Accordingly, the overall performance in TE-DWCC is better than that of 'CTE'.

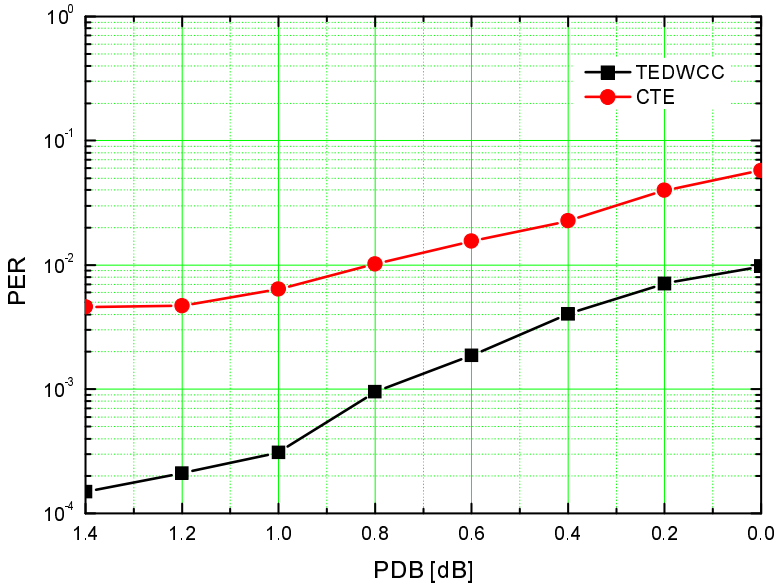

Figure 4.12: *PER* performance comparison of TE-DWCC and the conventional TE (CTE) under different delay spreads.

4.4 Summary

In conclusion turbo equalized DWCC is introduced, and it is found that the coherent combining gain due to DWCC prior to channel coding gain brings the large performance gain and thus the canceller that largely relies on the channel decoding gain is not efficient in interference dominant channels, particularly for 64QAM. In addition, it is also found that the cancellers which eliminate ICI by using the cyclic reconstruction, are compatible with hard decison feedback since soft decision feedback may cause the abrupt change within an OFDM symbol duration resulting in the increased ICI. Finally, the optimally incorporated TE-DWCC is shown to be more robust to the ISI and ICI with reduced computational complexity and less susceptible to code rate, compared with the conventional canceller that adopts turbo equalization in the canceller operation.

4.5 References

[4.1] J. H. Lee, Y. Kishiyama, T. Ohtsuki, and M. Nakagawa, "Double window cancellation and combining for OFDM in time-invariant large delay spread channel," IEICE

Trans. Fundamentals, vol. E90-A, no. 10, pp. 2066–2078, Oct. 2007.

[4.2] S. Suyama, S. Suzuki, and K. Fukawa, "An OFDM receiver employing turbo equalization for multipath environments with delay spread greater than the guard interval," IEEE Proc. Vehicular Technol., vol. 1, pp. 632–636, Apr. 2003.

[4.3] Y. Sagae, S. Suyama, H. Suzuki, and K. Fukawa, "An OFDM turbo equalizer for scattered pilot signals in multipath environments with delay difference greater than guard interval," IEEE Proc. Vehicular Technol., vol. 1, pp. 425–429, May 2004.

[4.4] M. Tuchler, R. Koetter, and A. C. Singer, "Turbo equalization: principles and new results," IEEE Trans. Commun., vol. 50, no. 5, pp. 754–767, May 2002.

[4.5] R. Koetter, A. C. Singer, and M. Tuchler, "Turbo equalization," IEEE Signal Processing Mag., vol. 21, no. 1, Jan. 2004.

[4.6] I. Marsland, "An introduction to turbo equalization," BCWS Seminar Series, Mar. 2001.

[4.7] A. Burr, "Turbo-codes: the ultimate error control codes?," Electron. Commun. Engineering Journal, vol. 13, no. 4, pp. 155–165, Aug. 2001.

[4.8] B. Sklar, "A primer on turbo code concepts," IEEE Commun. Mag., vol. 35, no. 12, pp. 94–102, Dec. 1997.

[4.9] P. Jason, and L. Hanzo, "Comparative study of turbo decoding techniques: An overview," IEEE Trans. on Vehicular Technol., vol. 49, no. 6, pp. 2208–2233l, Nov. 2000.

[4.10] X. Wang, and H. V. Poor, "Iterative (turbo) soft interference cancellation and decoding for coded CDMA," IEEE Trans. on Commun., vol. 47, no. 7, pp. 1046–1061, July 1999.

[4.11] C. Laot, A. Glavieux, and J. Labat, "Turbo equalization: Adaptive equalization and channel decoding jointly optimized," IEEE J. Sel. Areas Commun., vol. 19, no. 9, pp. 1744–1752, Sept. 2001.

[4.12] F. Tosato, and P. Bisaglia, "Simplified soft-output demapper for binary interleaved COFDM with application to HIPERLAN/2," IEEE Proc. ICC, vol. 2. pp. 664–668, 2002.

[4.13] E. Viterbo, and K. Fazel, "How to combat long echoes in OFDM transmission schemes: Sub-channel equalization or more powerful channel coding," IEEE Proc. GLOBECOM, vol. 3, pp. 2069–2074, Nov. 1995.

[4.14] P. Dent, G. E. Bottomley, and T. Croft, "Jakes fading model revisited," IEE Electron., Lett., vol. 29, no. 13, pp. 1162–1163, June 1993.

Chapter 5

Conclusion

OFDM technology has been applied in many applications because of flexible usage of the restricted resource and the simplified receiver structure in broadband communication systems. Meanwhile, the shortage of frequency band and the transition of spectral band to upper-band may change the traditional network concept from point-to-point (PTP) to point-to-multi (PTM) since the current research trends of cooperative communication network is getting popular rather than the conventional competitive communication network. In addition, the world-wide propaganda toward the implementation of green IT network leads to the change of the conventional network topology. For example, the centralized cellular based network is evolving toward the distributed network, and the paradigm shift both in homogeneous and heterogeneous networks is indispensable. In accordance with the emerging requirements for future communication networks, it is no doubt that OFDM is still very attractive transmission technology for further evolving cellular based network (WAN), local area network (WLAN), and metropolitan area network (WMAN) and so on. On the other hands, the performance of multicarrier transmission systems are prone to be affected by several impairments, generated by the system itself such as oscillator mismatch and the wireless/wired channel environments such as fast fading and large delay spread over guard interval. Since those impairments bring about the destruction of orthogonality among subcarriers, the simplified receiver structure is no longer effective to cope with those detrimental effects.

In particular, the multipath exceeding a guard interval causes the severe performance degradation by intersymbol and intercarrier interferences. The best possible way to prevent the performance from being deteriorated is to insert a guard interval, long enough to cover the large channel delay, but the guard interval insertion is directly relevant to the power and frequency efficiency losses. Accordingly, the adoption of the interference canceller has been considered. In this thesis, we introduced the interference canceller which is robust to the large channel delay by readily combining a guard interval as a canceller processing window, considering the selection of the processing window and the channel equalization, and proved

Table 5.1: Basic operations of the interference cancellers.

Canceller	Type	Main Operations
RISIC	COBD	- ISI cancellation - Cyclic Reconstruction for ICI cancellation
CTE	COAD	- Turbo equalized ISI cancellation - Turbo equalized ICI cancellation per sub-carrier
DWCC-I	COBD	- Pre/Post-ISI cancellation - Pre/Post-cyclic reconstruction for ICI cancellation
DWCC-II	COBD	- Pre/Post-ISI cancellation - Pre/Post-cyclic reconstruction for ICI cancellation
TE-DWCC	COABD	- DWCC - Turbo equalization

the superiority of the proposed interference cancellers in error performances of *BER* and *PER* through the comparison with the representative previous cancellers.

In Chapter 1 the general introduction of OFDM is presented, and the prospective of evolving 4G cellular based networks are briefly introduced. By investigating the research trends for 4G networks, the cooperative heterogeneous networks will be the forthcoming cellular based networks in a distributed manner. In addition, the impairments in OFDM system are described. In Chapter 2 it is verified that the variance of interferences due to the large channel delay is analyzed and it is manifested that ICI from adjacent subcarriers are dominant in the targeted subcarrier, and the thermal noise-like interference characteristic is also analyzed. Meanwhile, the design methodology of the interference canceller is introduced with respect to how to mitigate interferences of ISI and ICI and how to equalize the channel distortion. From that, it can be seen that the computational complexity is largely affected by ICI cancellation methods by exemplifying the several canceller design approaches.

In Chapter 3 the two different canceller schemes are introduced by investigating the double window cancellation and combing (DWCC) which is one of processing window extending methods to readily combine the entire symbol duration in the canceller operation. One is DWCC-I as symbol-wise canceller, and the other is DWCC-II as group-wise canceller. The proposed canceller operates with the decision feedback of tentative symbol replicas and the improved reliability of the symbol replicas can be pursued by combining the guard interval and coherent combining gain of double windows. In the meantime, the analysis results depending on different delay spread channels say that the adaptive operation of DWCC-I

Table 5.2: Algorithm characteristics of the interference cancellers.

Canceller	Advantage	Disadvantage
RISIC	-Less computational complexity	-Vulnerable to the amount of interference and frequency selectivity
CTE	-Enjoying channel coding gain -Including the gain from guard interval	-High computational complexity -Bad performance in high order modulation such as 64QAM
DWCC-I	-Enjoying coherent combining gain -Including the gain from guard interval	-Susceptible to deep fading -Still vulnerable to the amount of interference and frequency selectivity
DWCC-II	-Enjoying coherent combining gain -Including the gain from guard interval -less sensitive to large interference	- Vulnerable to the frequency selectivity
TE-DWCC	-Enjoying coherent combining gain -Including the gain from guard interval -Enjoying channel coding gain -Robust to large interference even in high order modulation	- Still high computational complexity but CTE > TE-DWCC

and -II is favorable in terms of the error performance, and hence it is concluded that extending the processing window in iterative canceller operation is not always beneficial to the error performance. Summarizing all the simulation results, it is concluded that DWCC-II is more robust algorithm than DWCC-I against ISI and ICI due to large delay spread channels over a guard interval.

The proposed cancellers, DWCCs in Chapter 3 operates before channel decoding, and it still susceptible to deep fading since the data symbol in deep fading is difficult to be reliably detected in the decision feedback operation. Regarding the drawbacks in DWCC, turbo equalized DWCC (TE-DWCC) is introduced in Chapter 4. To find the optimal incorporation of DWCC and turbo equalization, TE-DWCC, it is investigated by varying the iterative cancellation procedure between DWCC and channel decoder. In addition, it is also found that the hard decision feedback (HDF) is more compatible than the soft decision feedback (SDF) in TE-DWCC. After all, it is concluded that the cancellers operated by cyclic re-

construction for ICI cancellation in time domain could cause variation within an OFDM symbol resulting in the increased ICI in frequency domain. To investigate the efficient way of ICI cancellation in terms of the error performance, the proposed canceller, TE-DWCC and the conventional turbo equalized canceller are also evaluated with respect to the error performance under different delay spread channels and different code rates. Finally, optimally incorporated TE-DWCC is proved to be superior to the conventional turbo equalized canceller with reduced computational complexity in the large interference channels. In Table 5.1 and Table 5.2 the basic operations and the algorithm characteristics of the cancellers, investigated in this thesis, are summarized where the cancellers can be classified into three types such as COBD (Canceller Operation Before Channel Decoding), COAD (Canceller Operation After Channel Decoding), and COABD (Canceller Operation After and Before Channel Decoding).

As a further research, the effects of timing synchronization and channel estimation errors on the cancellers operating in the time domain needs to be investigated.

Acknowledgments

Above anything else, I would like to glorify the lord of my Jesus and thank for his everlasting love in my whole life.

There are many people around me that I would like to appreciate for their advices, encouragement, and assistance throughout my Ph.D course in Japan. First and foremost, I would like to deeply thank to my professor, Masao Nakagawa, for this incessant encouragement and support since I joined in the Nakagawa laboratory.

I would also like to thank my technical adviser, professor Tomoaki Ohtsuki, and thesis committee members, professor Iwao Sasase, Yukitoshi Sanada of Keio University for their invaluable technical comments and review my dissertation.

I am also greatly indebted to Arita Takemi and his wife for their warm heart, encouragement and assistance during my staying in Japan.

I am pleased to acknowledge many individuals who helped me constantly in my research and student life in Nakagawa Laboratory: in particular, Dr. Incheol Jeong, Dr. Toshihiko Komine, and many others for their discussions and help.

I am also very grateful to the members of NTT DoCoMo project and korean colleagues who have shared enjoyable time at Keio University: Dr. Osamu Takyu, Dr. Koichi Adachi, Dr. ChiHong, Cho, Mr. KiMin, Kim, Mr. YoungWoon, Kim, and many others.

Besides, I want to share this honor with my colleagues in ETRI, Korea, particularly the department managers of Dr. JeeHwan Ahn, Dr. YeongJin Kim, Dr. HyunKyu Chung, and Dr. SeungChan Bang, and the team leaders of Dr. YoungHoon Kim, Dr. SokKyu Lee, Dr. ByungHan Ryu, Dr. HyeongJun Park, YounOk Park, Dr. InKyeong Choi, Dr. KwangChun Lee, Dr. AeSoon Park, Dr. IlGyu Kim, and my intimate seniors and friends of Dr. YoungSeog Song, Dr. MoonSik Lee, Dr. YoungJo Ko, Dr. HyeongGeun Park, Mrs. HyeKyung Jwa, Mrs. EunJeong Shin, Mr. YangGi Kang, and finally many others for their valuable discussions and encouragement.

Last, but no means last, this work is dedicated to my family members; my parents, my wife's parents, and my four elder sisters who always encouraged me, and to my wife for her support with love, and to my first son, KyuHo, who always cheers me up, and finally to my second son, KyuHyun, an invaluable present from God on 15th of February this year.

List of Papers

Transaction Papers

[1] JunHwan Lee, Yoshihisa Kishiyama, Tomoaki Ohtsuki, Masao Nakagawa, "Double Window Cancellation and Combining for OFDM in Time-Invariant Large Delay Spread Channel," IEICE Transactions on Fundamentals, vol. E90-A, no. 10, pp. 2066-2078, October 2007.

[2] JunHwan Lee, Tomoaki Ohtsuki, Masao Nakagawa, "Turbo Equalized Double Window Cancellation and Combining Robust to Large Delay Spread Channel," IEICE Transactions on Communications, vol. E92-B, no. 2, pp. 517–526, Feb. 2009.

[3] T. Komine, JunHwan Lee, S. Haruyama, M. Nakagawa, "Adaptive Equalization System for Visible Light Communication utilizing Multiple White LED Lighting Equipment," IEEE Trans. on Wireless Commun., vol. no. June 2007 (Accepted).

International Conferences

[1] JunHwan Lee, Masao Nakagawa, "Pre-Rake System Applied with Frequency Domain Equalization in Multi-Code TDD-CDMA," IEEE PIMRC, vol. 1, pp. 447–451, Sept. 2005.

[2] JunHwan Lee, Masao Nakagawa, "Cyclic Prefix Controlled Prerake System with Frequency Domain Equalizer," WPMC, pp. IV644–IV648, Sept. 2005.

[3] JunHwan Lee, Masao Nakagawa, "LED Panel Lighting Communication with Delay Feedback Control for High Data Rate Downlink Transmission," 9th World Multiconf. Systemics, Cybernetics, and Informatics, July 2005.

[4] T. Komine, JunHwan Lee, Masao Nakagawa, "Adaptive Equalization for Indoor Visible-Light Wireless Communication Systems," IEEE Asia-Pacific Conference on Commun., pp. 294–298, 2005.

Technical Reports

[1] JunHwan Lee, Yoshihisa Kishiyama, Tomoaki Ohtsuki, Masao Nakagawa, "New Canceller Scheme with Double Window Cancellation and Combining in Large Delay Spread Channel," IEICE Technical Report, vol. 106, no. 305, pp. 101–106, Oct. 2006.